Ph.D. Thesis

Doctoral Program in Aerospace Science & Technology

Improvements in autonomous GPS navigation of Low Earth Orbit satellites

Pere Ramos-Bosch

Advisors:
Dr. Manuel Hernández Pajares [1]
Dr. J.Miguel Juan Zornoza [1]
Dr. Oliver Montenbruck [2]

[1] Research group of Astronomy and Geomatics (gAGE)
Depts. of Applied Mathematics IV and Applied Physics
Universitat Politècnica de Catalunya (UPC), Spain

[2] German Space Operations Center (DLR), Germany

September 10, 2008

Acknowledgements

Mai hauria sigut capaç de portar aquesta tesi a terme sense el suport incondicional dels meus pares, que sempre han estat quan els he necessitat, moltes gracies per tot.

Mari, ja portes més d'un any compartint amb mi els millors mo- ments i les coses que realment importen. Gracies per aguantar les meves

explicacions i sofrir la meva falta de temps en les etapes finals de l'escriptura.

M'agradaria agrair també a la colla *de sempre* distribuits entre l'Hospitalet, Martorell i *ses illes* que sempre m'han aguantat les neures i les divagacions mentals, així com altres coses que no posare aquí! Un record per tots vosaltres Isra, Jordi, Jorge, Mar, Martin, Nahia, Oriol, Oscar, Ramon, Silvia i Sonia.

I com no, no oblidar els molts anys de carrera amb en Dani, Maria, Rodri, Alfredo, Xavi (Tabo) i Pasca. Bons moments d'estudi i de bar (perquè a les classes tampoc ens veiem massa que diguem!), recordo grans partides de mus, d'escacs i del que fos necessari. Així com d'antigues històries de *boles de foc...*

També vui agrair els cafes, esmorzars, dinars, sopars i de tot (incloent *Los Lunes al Sol*) amb els *criptos*, records a Marc i Carla.

Per acabar m'agradaria recordar les *rambletes* amb Alfredo, Ainhoa i Alba amb les infinites discusions sobre Phobos, sempre genials per relaxarse al acabar el dia.

Contents

Introduction

The Global Positioning System (GPS) is the most widely known and used satellite navigation system. It consists in a network of at least 24 satellites orbiting at 20200 km over the Earth's surface continuously transmitting dual-frequency signals which are processed by the receivers. GPS was designed from the military for the military, and the first vehicle was launched the 22nd of February of 1978 by the US Department of Defense (DoD), but it was not until 1995 when GPS reached the Full Operation Capability (FOC). Its public use has widely spread due to two key milestones: one in 1983, when the system (the first probing satellites) was made available to the general public, and the other in 2000, when the DoD disabled the Selective Availability (S/A), which was an intentional degradation of the signal for civil users and had been decreasing their accuracy from about 10 m to more than 100 m.

Satellite navigation is getting an increasing importance in many fields. Nowadays new satellite systems are being developed, such as the European initiative GALILEO, which is expected for 2014 and the Chinese COMPASS, and the existing ones are being extended and modernized (GLONASS and GPS). Global Navigation Satellite Systems (GNSS) provide a highly available and cheap solution for precise positioning and timing, and its use has proven to be valuable in a wide spectrum of fields, such as Low Earth Orbiters (LEO) navigation, among others.

Heading image: Representation of the GPS constellation.

In this sense, LEO positioning has received great benefits from GPS measurements, using them to extract a posteriori orbit of the satellite in ground processing. New trends in LEO navigation are more focused in the attempt to move the positioning computation from ground stations to the own spacecraft, trying to achieve a precise and cheap autonomous real-time navigation.

This doctoral thesis will deeply study the LEO autonomous real-time navigation based on GPS data as the main source of information: it will focus in the exploration of new techniques and algorithms to contribute in this topic.

LEO satellites

Satellites in low Earth orbits are generally defined to be up to an altitude of 2000 km above Earth's surface. Given the rapid decay of objects on the lower altitude range due to the atmospheric drag, it is commonly accepted that a typical LEO height lies between 200 an 2000 km. The first LEO was launched in 1957 (Figure 1) and nowadays these kind of satellites are used in a wide range of missions, such as communication applications, remote sensing, gravimetric and magnetometric sounding, ocean altimetry, atmospheric retrieval and Search and Rescue alarm operations. Its accurate positioning is of great importance for the successful accomplishment of their objectives.

Several of these applications are satisfied by a postprocessed on-ground positioning, but some of them could benefit from an autonomous positioning independent from ground and available in real-time, allowing the satellite to make autonomous decisions based on its precise trajectory. The specific requirements for real-time or near real-time greatly vary from one mission to the other, but most of them have a position and velocity accuracy requirement in the order of 10-20 m and 0.1 mm/s of 3D RMS respectively. In this sense, the near real-time position requirement of the future Sentinel-3 will be of 10-20 cm [Drinkwater and Rebhan, 2007], and for Jason-2 mission (launched on June, 2008) was of 10 cm [CNES, 2006]. Coping the position and velocity requirements in real-time allows a fast delivery of science products. Besides that, autonomous spacecraft operations clearly benefits from a precise knowledge of its position and velocity. That would provide valuable information in some satellite maneuvers, such as Autonomous Formation Flying (AFF) and Space Rendezvous and Docking (RVD).
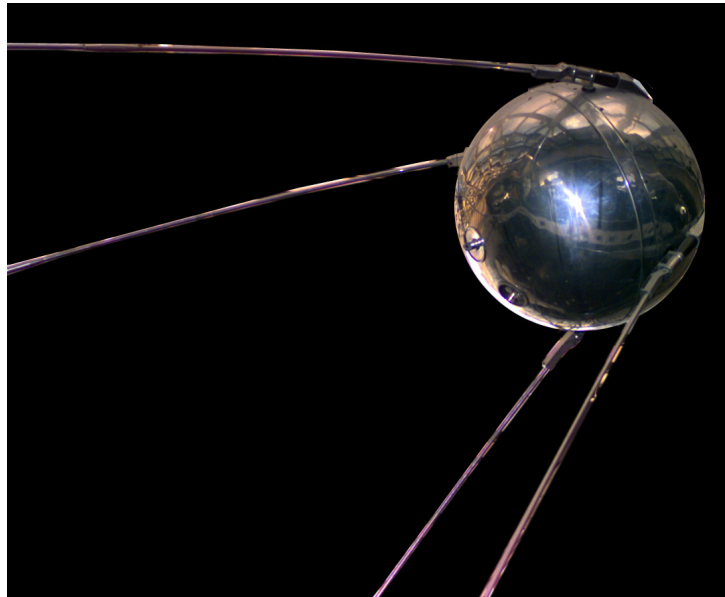
Figure 1: *Image of Sputnik 1, the first artificial satellite. It was launched in 1957 by the Soviet Union.*

State-of-the-art of LEO real-time positioning

Following the trend for satellite autonomy, LEO real-time positioning is becoming more important as it is progressively being able to accomplish the position and velocity requirements for the missions. In this sense, several works have done an approximation to absolute autonomous positioning after deactivating the S/A, such as [Reichert et al., 2002] with an inflight demonstration of GPS-based real-time navigation which achieved 3D positioning errors of 1.5m with broadcast ephemerides for SAC-C satellite; or [Gill et al., 2004] for X-SAT, which was able to prove a real-time position accuracy of 1-2 m with a single-frequency receiver (a requirement for the mission, which still has to be launched). [Zhou and Feng, 2002] used a short-arc batch estimation approach to attain accuracies of 2-4 m for TOPEX/Poseidon, SAC-C and CHAMP. An approximation to autonomous positioning in a microsatellite was done on [Montenbruck and Leung, 2002], with PCSat, a 10 kg satellite with a single-frequency GPS receiver, which obtained a 20 m 3D RMS accuracy (due to large and continuous outliers). [Gill et al., 2001] obtained a 5 m accuracy on the single-frequency receiver inside the BIRD mission.

On the other hand, real-time relative navigation has been explored in several works, such as [Leung and Montenbruck, 2005] for AFF (attaining

position and velocity accuracies of 1.5 mm and 5 μm/s respectively) or [Kroes, 2005] (obtaining 1 mm of position accuracy). An approach to space-craft rendezvous was done by [Ebinuma et al., 2003] (achieving 3.5 cm and 1 mm/s position and velocity accuracies), and [Edward, 2003] studied the RVD maneuvers in the International Space Station, where GPS measurements suffer from high multipath and signal blockage, and achieved one meter relative navigation accuracy by the integration of inertial sensors and GPS data.

Other approaches on autonomous navigation used real-time estimations of GPS orbits and clocks, in this sense, the NASA's GDGPS ([NASA/JPL, 2008] and [Bar-Sever et al., 2002]) provides a real-time stream with precise GPS products. [Muellerschoen et al., 2001] simulated an autonomous environment for CHAMP satellite, integrating it with this products attaining accuracies of 25 centimeters. Furthermore, the TASS system (TDRSS Augmentation Service for Satellites) is planned to continuously broadcast the GDGPS corrections to satellites up to an altitude of 1000 km [Bar-Sever et al., 2004]. These real-time products increases the attainable autonomous accuracy and opens the path to new high-precision applications.

In this thesis, the real-time GPS products have been studied in several test cases, but due to the unavailability of NASA's GDGPS products (they are only offered as a commercial service), it has been used another source for these products: a global modification of the WARTK concept, which allows a real-time estimation of the GPS clocks. This approach, still in experimental phase and tested in [Hernandez-Pajares et al., 2007a] is based in the regional WARTK ([Hernandez-Pajares et al., 2000b]) and is able to provide products with similar performance to GDGPS (more details in Chapter 2).

Space receivers technology

Several GPS receivers are available for space applications. Between others, the TopStar3000, MosaicGNSS, Viceroy, SGR-05, SGR-20, Phoenix-S and NAV2000HDCP which provides single-frequency tracking, and GRAS, Lagrange, Monarch, BlackJack, IGOR, TopStar3000G2, OEM4-G2L and PolaRx2 for dual-frequency tracking. The most used receiver is the BlackJack (and its evolution, the IGOR), which is equipped in SAC-C, CHAMP, GRACE, Jason-1, Jason-2, FORMOSAT-3/COSMIC constellation and TerraSAR-X. All missions used in the validation of algorithms of this thesis have a BlackJack/IGOR receiver. [Montenbruck et al., 2006] provides information of this receiver and does a performance analysis, showing excellent sensitivity and low noise measurements in comparison to other receivers.

More information on space receivers technology can be found on [Montenbruck et al., 2007].

Neural networks in GPS processing

Neural networks has been used in some works for GPS processing, such as [Hernandez-Pajares et al., 1997] or [Infriyatmoko et al., 2008] to take advantage of its high optimization properties for non-linear processes. In particular its applicability to LEO autonomous navigation was demonstrated on [Hernandez-Pajares et al., 2000a] and [Hernandez-Pajares et al., 1999] applying a Self-Organized Map for multipath mitigation. These works have been the starting point of this thesis, which began with the ESA funded project *Neural Networks for Radionavigation* [Vigneau et al., 2007b].

Research objectives

The main objective of the thesis is to contribute to real-time absolute LEO navigation by developing new algorithms and methods. The target is to provide accurate and continuous positions for the satellite, by emulating a real-time processing (taking into account the unavailability of future measurements, and limitations in both computational resources and access to specific data, such as postprocessed products). In order to assess the level of success of the methods, they are evaluated against data from real missions and compared to reference postprocessed trajectories.

The thesis has advanced in different axis trying to provide, as a whole, ways to allow a continuous trajectory estimation with the utmost accuracy. In this sense, different aspects have been covered:

- *Multipath and interference mitigation.* Reflections of GPS signals in the spacecraft structure cause a distress that affects the measured distance. On the other hand, some spacecraft have more than ons GPS antenna in its payload. This creates a cross-talk interference that also affects the measures. These two effects are heavily dependant on the geometry, and cannot be distinguished in the sense of how they affect the signal. The repeatability of these effects can be used to mitigate its impact into the final navigation solution. As said, the usage of Neural networks algorithms has been assessed in this work for multipath mitigation in an onboard LEO environment.

- *Dynamic force models.* The high predictability of the trajectory of Earth orbiters is used in conjunction to GPS measurements to provide a more accurate solution than GPS standalone positions. This is a widely used technique in postprocessing strategies, but has high computational requirements and needs parameters not available in real

time. The simplification of these models, along with the suppression of the parameters not available in an onboard environment is necessary to use these kind of positioning by a satellite processor in real-time conditions.

- *Maneuver handling.* Earth orbiters do not follow a fully predictable orbit, some low-order perturbations modifies its trajectory on the long term, and atmospheric drag slowly brakes the satellite, decreasing its altitude. This makes necessary a periodic correction of its trajectory. This is done by short impulses produced by the satellite propulsion systems in what is called a maneuver. When a spacecraft is in a maneuver, it no longer follows the free-flight dynamic models, so this should be taken into account in the estimation filter.

All the algorithms and methods that will be presented have been designed specifically to be able to work in an onboard environment, as they are purely sequential, do not use future data and do not make use of unavailable products for the satellite, so even though none of them have been really implemented in a real embedded satellite processor, they could all be implemented in it. This validation, which is out of the scope of this thesis, has been done by some works which were able to implement some real-time algorithms into satellite processors, such as [Muellerschoen et al., 2001], [Reichert et al., 2002], [Gill et al., 2004] or [Montenbruck and Ramos-Bosch, 2007].

Moreover, the possibility of new techniques able to provide real-time accurate GPS products (such as GDGPS or global WARTK), and the present trends to make this a feasible option, suggests that its testing could provide useful results. This makes that one of the objective of the thesis is the extensive testing of these kind of new potential products.

Methodology

The methodology used in the development of this work consisted in four phases:

1. Identification and critical assessment of a potential improvement in a LEO scenario.

2. Design of algorithms and methods implementing the enhancement.

3. Software implementation of the design.

4. Execution of tests using real data in a wide spectrum of cases for different LEO satellite missions, GPS products and measurement types, to properly assess the method.

The developed software tools were written in Fortran, C, C++, C-shell and gawk script under Linux architecture.

Thesis breakdown

This thesis work consists on four chapters distributed as:

- Chapter 1, *Multipath mitigation by using artificial neural networks*. A low computational load multipath mitigation technique using artificial neural networks for pseudorange measurements is explored and assessed for dual-frequency GPS receivers.

- Chapter 2, *Reduced dynamic orbit modeling for real-time LEO navigation*. The simplification of the models to make use of dynamic forces is explained in this chapter. Different satellites, measurement type, model complexity and GPS orbit and clock products are explored and assessed.

- Chapter 3, *Maneuver handling*. A dynamic-kinematic switch mode is explained in this chapter. It makes use of the best of both worlds: the independence of forces of the kinematic filtering and the high accuracy and precision of the dynamic model.

- Chapter 4, *Multipath mitigation in single-frequency receivers*. A multipath mitigation technique for single-frequency receivers is explained in this chapter. The computational requirements are higher than in a kinematic positioning (as in the first chapter), but the combination of dynamic models and multipath mitigation techniques improves the navigation accuracy of single-frequency receivers, which are cheaper and have less requirements of power, mass and volume.

Three appendices are available at the end of the thesis:

- Appendix A, *GPS Fundamentals*. The thesis is written assuming some a priori knowledge of GPS from the reader. This chapter provides a quick introduction to GPS, but additional background on the system can be found in [Parkinson, 1996a] and [Hernandez-Pajares et al., 2001].

- Appendix B, *Neural Networks Fundamentals.* Quick introduction to neural networks.

- Appendix C, *Main characteristics of the LEO satellites used.* Some data of the spacecraft used.

Chapter 1

Multipath mitigation by using artificial neural networks
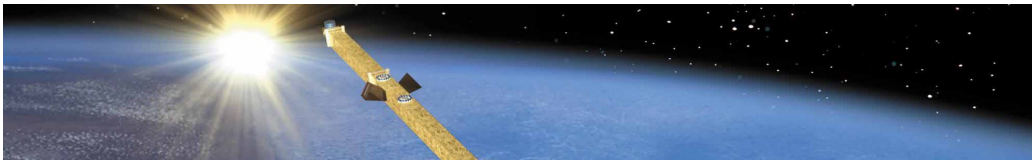
Somewhere, something incredible is waiting to be known

Carl Sagan

This chapter presents an hybrid onground-onboard method to mitigate multipath of GPS pseudorange measurements in LEO satellites. The described algorithms are based on the Artificial Neural Network theory (see for instance [Haykin, 1994]), and have been designed to be used in a spacecraft processor (onboard processing), specifically focused to keep low computing needs. The work aims for real time processing, where the satellite uses a GPS receiver to estimate its position. Firstly, the method is described, both the on-ground and onboard parts. Secondly, the algorithms are tested against real data from SAC-C and CHAMP satellites in order to assess its effectiveness.

1.1 Introduction

The signal acquired by GPS receivers are affected by several errors coming from different sources. In order to obtain an accurate positioning is necessary to correct, or at least mitigate, most of them. Dual-frequency receivers allow the use of a combination of measurements in both frequencies that removes practically all of the ionospheric term ([Hernandez-Pajares et al., 2007b]).

Heading image: Artistic image of CHAMP satellite. Focus on its tail, where magnetometers are located.

This leaves the multipath effect as one of the most significant error sources in pseudorange processing.

Multipath is an effect linked to signal reflections in the environment of the receiver (figure 1.1). These reflections affect the receiver front end, masking the real correlation peak of the signal, and causing range errors up to typically 15 m or more in extreme cases. The environment of the receiver, it's antenna cut-off angle and the correlator strategy are the most determining factors for the proper multipath minimization.

Multipath Errors
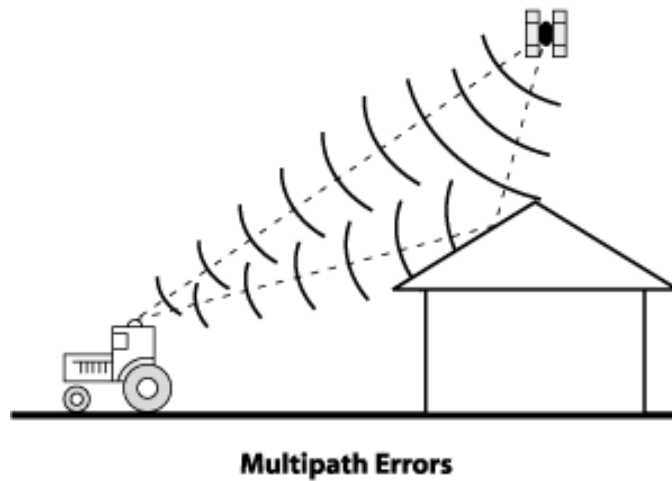
Figure 1.1: *Schematic of how the multipath affect the GPS signal. Reflected signals, with a different ray path, reach the antenna, and interfere with the direct signal.*

Depending on the specific behavior and environment of the receiver, multipath has different characteristics. Fixed ground stations have the same GPS satellite configuration repeating each sidereal day: the rays are reflected in the same structures. This makes the signal affected in the same way when the satellite is in the same position relative to the receiver. Moving ground receivers have very high multipath variability due to the constant changes in the environment.

On the other hand, spacecrafts have a multipath environment very different from ground users. On surface receivers the multipath rays comes from the surrounds of the station (or rover), but on space receivers the multipath come from the own spacecraft body. This leads to a high spatial correlation between close rays (in terms of its line of sight) so, as it occurs in fixed ground receivers, the multipath is repeatable with the geometry of rays. This is specially true in satellites, in which in general no significant reflectivity changes

are expected with the surrounding surfaces (for example, rain, snow or tree growth). Figure 1.2 shows, for SAC-C satellite, three similar multipath signatures (with an arbitrary bias) for three footprints on the antenna sky at different times for close line of sight vectors in a spacecraft reference frame. Satellites with mobile solar panels may have important differences in its incoming multipath due to the change of geometry of the panels following the sun and this will have an impact in the repeatability in some of the incoming directions of the ray.
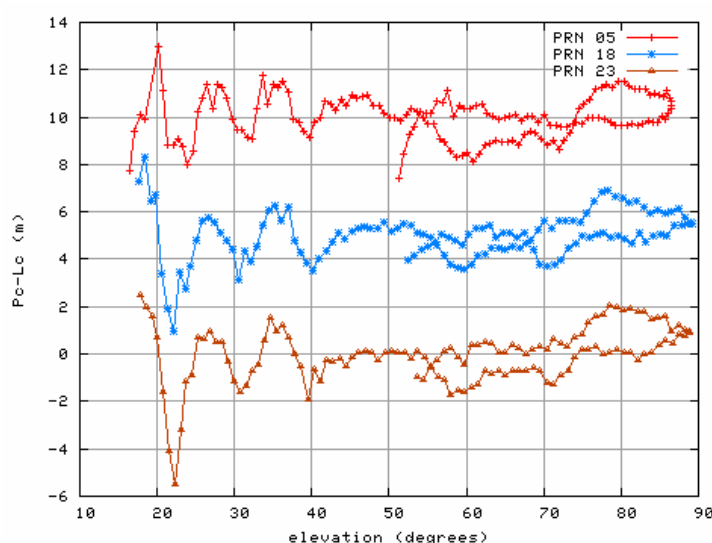
Figure 1.2: *Repeatability of multipath for different arcs and time. Ordinate axis represents the multipath in meters plus an arbitrary bias. Data processed from SAC-C satellite for day 155 of 2002.*

In this chapter a method to mitigate the multipath by taking advantage of its repeatability will be presented in order to achieve a better performance in the navigation solution. Neural networks will be used in the method to reduce the number of parameters needed to properly characterize the multipath of the satellite. The method is divided in two phases:

1. An *a priori* estimation of a multipath map (which characterizes the multipath for a set of azimuth/elevation directions) that can be computed on the ground with the data of the past few days of the LEO satellite.

2. An onboard real time multipath correction.

To assess the goodness of the corrections and its impact on the final navigation solution, they have been applied to a kinematic Least Mean Squares single point positioning. The scope of this chapter is to provide a very low cost algorithm which would not have any problem to be embedded into the satellite processor, thus it has been chosen this simple positioning instead of a dynamic orbit model, which would largely increase the computation needs of the positioning filter. The use of such kind of filter, along with some simplifications to keep the computational needs in reasonable levels, will be explored in Chapter 2.

The idea of characterizing multipath by its incoming directions can be seen in [Parkinson, 1996a], and some works have provided satellite multipath maps, such as [Reichert and Axelrad, 2001] for CRISTA-SPAS and [Montenbruck and Kroes, 2003] for CHAMP. The multipath map would also absorb other direction-dependent effects, such as interference cross-talk from other spacecraft antennas (as will be seen in the results section for CHAMP) and phase center variations. An example of this can be seen for satellite JASON-1, which has large pseudorange phase center variations as seen in [Haines et al., 2004][1].

1.2   Method

The *a priori* multipath map estimation will provide the multipath detected for a set of given directions which will be called *cell centers*. The multipath for each observation can be obtained by means of a classic observable combination that allows isolating the multipath [Parkinson, 1996b]. In this chapter, the main observable used is the ionospheric-free pseudorange combination, which is defined (as shown in Appendix A) as

$$P_c = \frac{f_1^2 P_1 - f_2^2 P_2}{f_1^2 - f_2^2} \qquad (1.1)$$

Nevertheless, with antispoofing activated, the measurements of P_1 and P_2 are, in general, much noisier than the ones of C/A (coarse acquisition code, or C_1). For this reason, this observable has been chosen instead of P_1, thus redefining P_c:

$$P_c = \frac{f_1^2 C_1 - f_2^2 P_2}{f_1^2 - f_2^2} \qquad (1.2)$$

---

[1][Haines et al., 2004] reported up to 90 cm of PCV in the ionosphere-free pseudorange combination. Nevertheless as PCV cannot be detached from the other geometry dependant errors, part of these 90 cm can probably be due to multipath.

This redefinition of P_c inserts an additional term to be taken into account, which is the Total Group Delay (TGD), the instrumental delay difference between C_1 and P_1. Note that, despite instrumental delays for the ionospheric-free combination are defined to be zero, this is only true by definition when the combination is obtained using P_1 and P_2. However, when P_c is computed using C_1 instead of P_1, the TGD term must be taken into account (this TGD is due to the difference between C_1 and P_1). See Appendix A for more details.

Equation 1.2 is the main combination used for the LEO satellite real time positioning. But, in order to isolate the multipath, M_{P_c}, in the *a priori* process, the ionospheric-free carrier phase observable must be used:

$$L_c = \frac{f_1^2 L_1 - f_2^2 L_2}{f_1^2 - f_2^2} \tag{1.3}$$

Using equation 1.2 and 1.3, the following equation is used to isolate the multipath in the *a priori* process:

$$P_c - L_c = M_{P_c} + B_c + \epsilon \tag{1.4}$$

where multipath coming from carrier-phase measurements can be neglected in front of M_{P_c} (typically more than one order of magnitude smaller), B_c is an unknown constant value for each arc, and ϵ is unmodeled noise. The value of B_c must be again estimated after each new cycle-slip of any L_1 or L_2 carriers.

Equation 1.4 provides two unknowns per pseudo-observation which need to be estimated: M_{P_C} and B_c. The second term is kept constant along an arc and the first one is different for each observation, but similar for "close" rays due to the geometric nature of multipath. This similarity of the values of multipath for close rays can be used to group multipath unknowns in the *a priori* postprocessing and estimate a map depending on the line of sight between the LEO and GPS satellites (always in a LEO body-fixed reference frame). This map is computed with a neural network (a 2D Self-Organizing Map), leading to a cell distribution adapted to multipath variations (irregular grid), with a higher center density where greater variations are detected. The algorithm (without counterpart in the classical statistics) allows the simultaneous construction of a multipath map, with spatial resolution adapted to the initial gradient, and the corresponding 2D indexing for speeding up the corresponding computations. This allows similar multipath mitigation but using much less parameters.

The onboard real time processing uses this *a priori* multipath map estimation and applies the proper corrections, i.e., the values of the cells, to

each observable, or alternatively, it can be used to update the multipath in real-time.

1.2.1   A priori multipath map estimation

The computation of the *a priori* multipath map is done on ground and is just updated from time to time due to its high stability over time. The period of time used for the estimation should allow covering most of the possible ray directions that the LEO antenna can receive. Five days of data have been proven to be a good choice. In this context, the process is divided into several steps:

1. *Preprocessing*: A few stages are done in order to prepare the data, such as cycle-slip detection and the reference frame determination (to obtain the LEO attitude and compute the azimuth and elevation of each GPS satellite with respect to the LEO body-fixed reference frame).

2. B_c *estimation*: Merging all the observations given by equation 1.4, a single matrix is created to obtain a first estimation of all the unknowns (bias and multipath unknowns grouped in cells of 5x5 degrees) solved by means of a batch estimation. The inversion of this matrix provides an estimation of B_c for all arcs and a first rough 5x5 map.

3. *Regular grid map*: The B_c estimated values are then used to recalculate the multipath of each observation, forming cells of 1x1 degrees (averaging M_{P_c} by using equation 1.4 without inverting large matrices).

4. *Multipath variation estimation*: In order to characterize the cells with more multipath variability, a value is assigned to each cell proportional to the standard deviation of the multipath values of the nearest cells (using the 1x1 map). This gives a value which reflects the variation of the multipath on the surroundings of every cell. The way to do this is to select the cells at a radius of 5 degrees and compute the standard deviation of its multipath values. This distance is calculated transforming each cell position from azimuth/elevation into a unitary vector, and doing the scalar product between vectors (to have an homogeneous and continuous metric).

5. *Monte Carlo algorithm*: This algorithm distributes thousands of directions across the sky, assigning more directions where more multipath variation was estimated. This will be the training set for the neural network. The Monte Carlo algorithm was first described in

[Metropolis and Ulam, 1949] and more information can be found on [Manno, 1999].

6. *Self-Organizing Map*: The directions generated are inserted as inputs into this step and the cell centers of the final Self-Organized Multipath Map (SOMM) are generated simultaneously to its indexation (with two index values) by means of a self-organizing map algorithm [Kohonen, 1990]. Centers are ordered in such a way that two close cells in the sky have similar indices. This is used to avoid unaffordable searches in real time LEO scenarios (see the *Real time multipath mitigation* section). In figure 1.3 the distribution of these cells is shown for a five-day test for the SAC-C satellite. The different images correspond to the different parts of the iteration process to get the final map. This map has been found to be repeatable for different selections of days.

The advantage of this irregular map in front of a regular one can be seen in figure 1.4 for SAC-C satellite, with a reduction of 50% of the centers (i.e., parameters) to get a similar navigation performance. The topological ordering of the map avoids intensive searches through all the centers for each observation.

The a priori estimation also computes the TGD differences between P_1 and C_1 for each satellite, as this information is necessary for the real time navigation. For practical purposes it is done as a simple average between P_1 and C_1 of all the days used in the map estimation.

Afterwards, the SOMM can be transmitted to the LEO satellite (along with the TGD information) and the real time process can begin. The images of a 1x1 regular grid map and a SOMM are plotted in figure 1.5 in order to see the differences between both maps.

1.2.2 Real time multipath mitigation

The real time process is split into these steps:

- *Preprocessing*: Similar to the *a priori* process, a few stages are done to prepare the data: cycle-slip detection, TGD correction, and the Line-of-Sight vector in the adopted reference frame.

- *Cell selection*: The closest cell to the direction of each observation is searched by looking at a radius of 2 indices around the previous observation of the same arc. If the time between the previous observation of the satellite and the present one is big enough, the radius is increased (up to searching through all the cell centers).
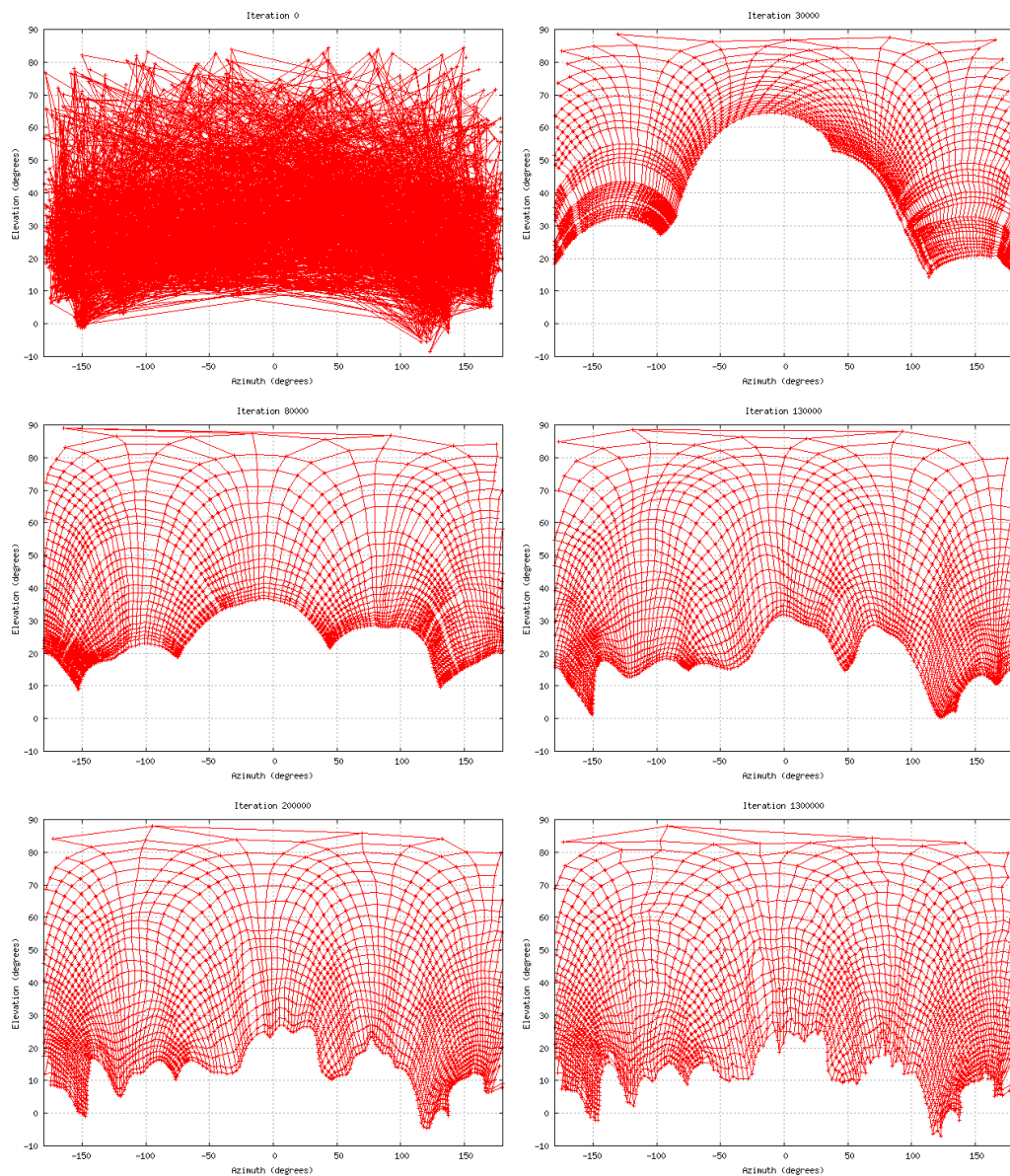
Figure 1.3: *Center distribution for the training process of a Self-Organized Multipath Map (SOMM) computed for SAC-C satellite for days 150 to 154 of 2002. Lines link neighboring indices. From left to right and top to bottom, the images represent the 0%, 2%, 6%, 10%, 15% and 100% of the total direction distribution process. At the beginning the centers are organized creating big structures, and in the last part of the algorithm they are fine tuned to their final positions.*
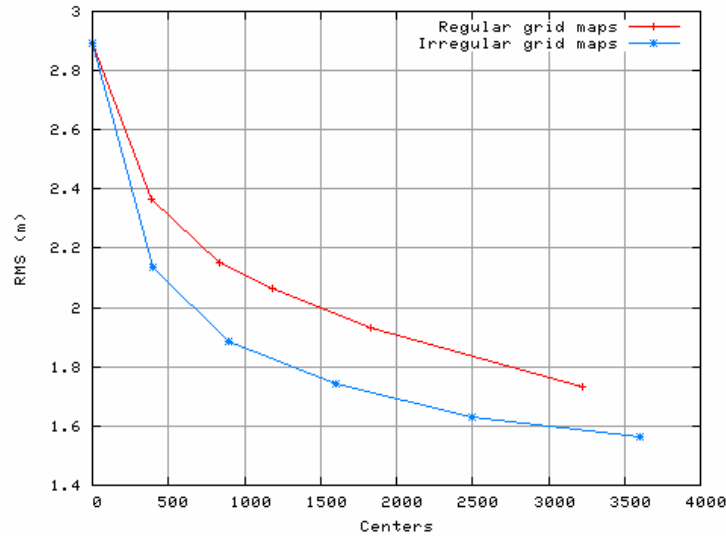
Figure 1.4: *SAC-C navigation RMS error for day 155 of 2002 using days 150 to 154 to estimate the a priori multipath map. Red and blue lines represent regular and irregular maps respectively.*
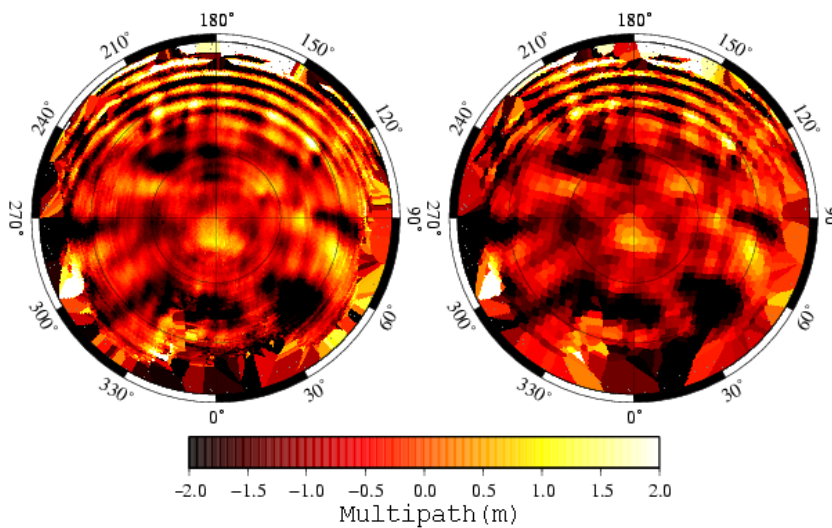
Figure 1.5: *On the left, regular grid map with 26347 centers, on the right, SOMM with 2484 centers. Map for SAC-C for days 150 to 154 of 2002.*

- *Multipath correction*: The proper multipath correction of the selected cell is applied directly to the observable. In figure 1.6 it is shown an example of the multipath of the combination before and after the correction. Another possible approach would be to use a low CPU burden neural algorithm, which has been tested in [Hernandez-Pajares et al., 2000a], to allow a real time updating of the cell values onboard the satellite. This will increase the time between map updates, and will provide a higher autonomy to the spacecraft, in line with the latest tendencies to autonomous satellite processing.

- *LEO positioning*: Navigation is performed by means of a standard least mean squares with smoothed and unsmoothed P_c to compare the results. As seen in [Montenbruck and Kroes, 2003] and [Williams et al., 2002], BlackJack GPS receivers have been reported to have anomalous measurements (such as sporadic code biases in P_1, P_2 and C_1 of 15.511 meters, and L2 ramps, where L_2 carrier-phase measurement is offset by a range rate of 6.1m/s). In order to discard these bad measurements, when there are six or more satellites available and the fitting RMS (the RMS of the residuals of the filter) is too high, all the combinations with 1 less satellite are computed and the one with lower RMS is chosen as the final position.

1.3   Flight data analysis

GPS observations in RINEX format, at a sampling rate of 0.1 Hz from two different LEO satellites, have been used: SAC-C and CHAMP, both equipped with dual-frequency BlackJack GPS receivers. The POD antennas of both satellites are zenith oriented. To assess the method, the obtained positions have been compared with the postprocessed precise orbit determination from JPL [2], which has a typical accuracy of a few centimeters.

The strategy has been tested using precise IGS clocks and orbits instead of the broadcasted ones. Clearly, this is an unrealistic situation, but is done because in this way it is possible to asses the maximum expected impact of this mitigation in the final navigation solution avoiding that the limited performance of broadcast orbits and clock errors jeopardize the results. To be able to make use of this method in a realistic environment, clocks of GPS satellites could be estimated or provided (also using predicted orbits, which have errors slightly higher than the precise ones, but on the order of a few

---

[2]Available at ftp://sayatnova.jpl.nasa.gov
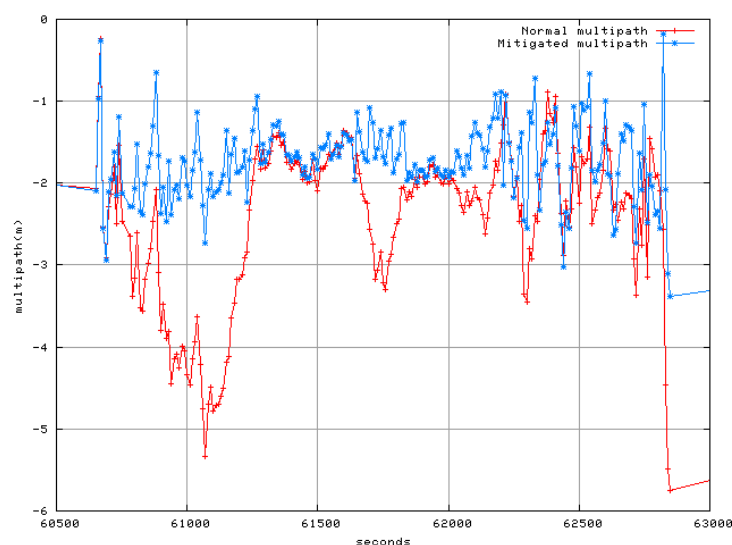
Figure 1.6: *Multipath for an arc of SAC-C satellite. In blue is shown the remaining multipath (plus thermal noise) after the mitigation.*

centimeters, so it would not have a large impact on the solution as will be seen in Chapter 2).

The 3D positioning error RMS shown in all the results corresponds to the RMS of the 95% of the observations with less error (i.e., the 5% of the total epochs with higher error are discarded, and the remaining ones are used in the RMS computation). This has been done, on one hand, to discard epochs with bad line-of-sight geometries and, on the other hand, to filter out bad measurements, which can affect the positioning with errors up to tens of meters.

Different smoothing periods have been used with similar results, gaining about 50% improvement by using the multipath correction in both smoothed and unsmoothed observables. The smoothing of the pseudorange using carrier-phase observables is done using the *Hatch Filter* [Hatch, 1982], which is commonly used in Satellite Based Augmentation Systems (SBAS), such as WAAS and EGNOS [RTCA, 2001].

In figure 1.7, the RMS error position is shown for a full 100 day period for non-smoothed, 10-sample and 50-sample smoothed observables for SAC-C and CHAMP satellites.

This multipath mitigation technique significantly improves the navigation solution with the exception of the 50 samples smoothing in CHAMP. This is

Figure 1.7: *Daily 3D positioning error RMS for period a of 100 days in SAC-C (left column, from day 155 to 255) and CHAMP (right column, from day 235 to 335) of 2002. Each point provides the RMS for all the epochs of a single day. First, second and third rows correspond to unsmoothed, 10-sample and 50-sample smoothed observables, respectively.*
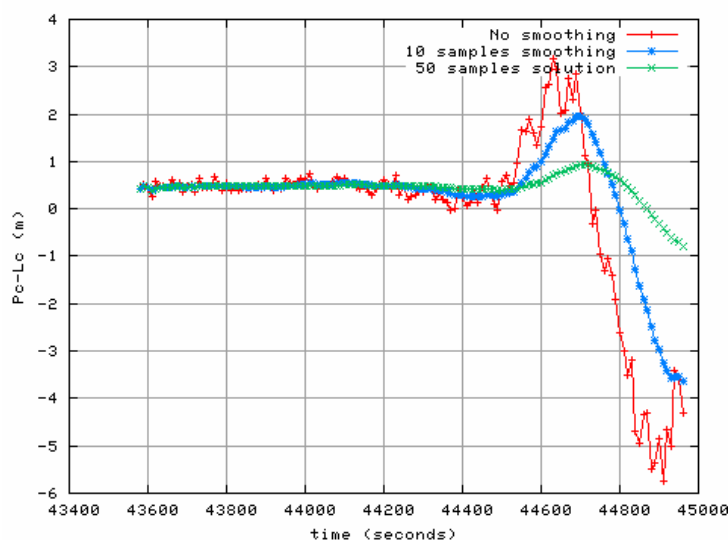
Figure 1.8: *Unmitigated multipath for a single arc with unknown bias for CHAMP satellite for day 235 of 2002. The effect of applying smoothing with different samples is shown.*

a satellite with a very low multipath environment, and, as shown in figure 1.8, the larger values of multipath are only reached in the latest part of the arc. In fact, this effect, is not due to reflection of the signal in the spacecraft structure, but due to cross-talk between the POD and occultation antennae of the receiver (as noted in [Montenbruck and Kroes, 2003]). This effect has a geometric dependence, so it is absorbed into the multipath map. As a consequence of these errors in pseudorange on the later part of the arcs, the bias between L_c and P_c (from equation 1.2) can be well estimated from the beginning of the arc with enough smoothing samples. Consequently, for this satellite, the more smoothing samples used, the less the observable is sensitive to geometric dependent errors, and therefore the correction presents a more marginal effect.

In table 1.1 the averages of the 100 processed days are shown for both satellites (a value of 1 in smoothing means, in fact, unsmoothed observables).

1.4 Onboard multipath map updating

The current approach of the method creates a map in an apriori on-ground processing, and transmits it to the LEO, which applies it until a new map is uploaded. If there is any change in the satellite, its map can be affected,

Table 1.1: *Average improvement of kinematic positioning results in the selected periods for both SAC-C and CHAMP satellites.*

Spacecraft and smoothing samples		3D RMS (m)		Position improvement
		no mitigation	mitigation	
	1	3.25	1.89	42%
SAC-C	10	2.03	1.00	51%
	50	1.76	0.92	48%
	1	1.75	1.12	36%
CHAMP	10	0.99	0.72	27%
	50	0.71	0.69	2%

thus degrading the performance. Possible changes that can occur in a LEO environment are such as aging effects, panel deployment or even the connection/disconnection of other antennas (which, is not multipath, but strongly affects the signal in the same geometric dependence, so consequently the map is able to mitigate it). In this sense, figure 1.9 shows this degradation of the performance of the multipath map along the time (for more than a year), comparing the noise and multipath of P_c without changing the map with a map update every 100 days.

The solution in the present approach would be to wait for some days, recompute the map and send it to the satellite, but as seen in [Hernandez-Pajares et al., 2000a], it is possible to use a single neuron neural network to provide a real time updating of the cells values. This onboard updating process would slightly adapt the value of the multipath cells with the new measurements. The approach would have a larger computational effort in the sense that it has to update the covariance matrix of the 2500 cells. In order to make use of this method some approximation should be done, in particular, only the values of the covariance matrix above a certain levels should be taken in consideration, and the rest would be supposed zero. This would increase the spacecraft autonomy, as it would be able to adapt its multipath map to its environment changes. Anyway, eventually it would be needed a new upload, because this real-time updating would only affect the values of the cells (the multipath correction), not its position (azimuth/elevation), so to be able to change the position of the cells a full on-ground processing would be needed. The decrease in the number of map cells that neural networks provides is of special interest in this autonomous real time updating because, the reduction of cells would be critical to treat the covariance matrix.
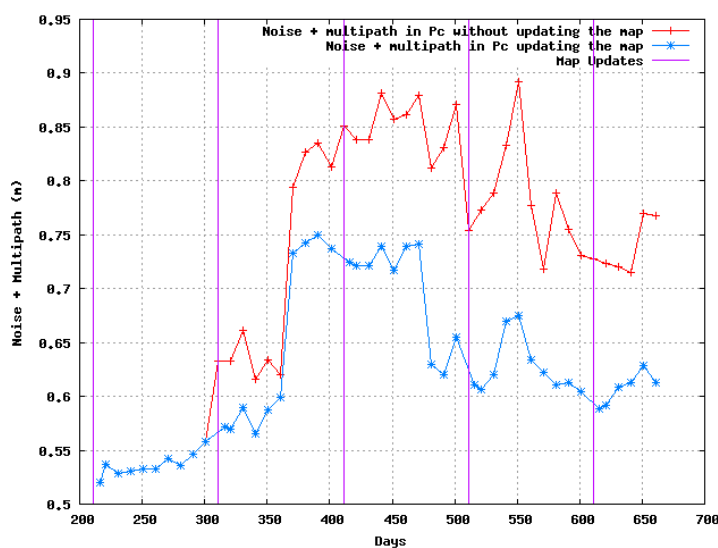
Figure 1.9: *Comparison of the noise and multipath of P_c between updating and not updating the multipath map. Data is for SAC-C from day 211 of 2002 to 300 of 2003. Vertical lines represent the computation period for the new maps.*

1.5 Conclusions and discussion

In this chapter it has been demonstrated that the application of a hybrid offline and real-time multipath mitigation technique can significantly improve kinematic navigation solutions of LEO satellites in the presence of pronounced static multipath. Multipath is linked to the spatial orientation of the satellite, thus it is impossible to distinguish between other effects also binded to the body structure (and thence, the attitude), such as interference cross-talk from other antennas ([Montenbruck and Kroes, 2003]) and PCV ([Haines et al., 2004]). The presented technique will create maps that absorb and afterwards, mitigate all these effects.

By using these maps improvements in 3D positioning accuracy of 40%-50% for SAC-C (achieving errors of about 90 cm) and of 25%-35% for CHAMP (achieving errors of about 70 cm) have been obtained in the tested periods of 100 days. The technique has low CPU and memory requirements, so it is suitable to be used in low resource environments, such as spacecraft applications.

Moreover, it should be taken into account that the results are heavily dependent on the *a priori* multipath map, so in a real environment, this es-

timation should be done frequently with special care, testing its performance before sending it to the LEO satellite. As said, it has been used precise orbits and clocks. Broadcast orbits and clocks have a typical error budget in Signal-in-Space range errors (SISRE) of about 1-1.5 m [Warren and Raquet, 2003]. In this case, these errors would be the dominant error source, but applying multipath mitigation would nonetheless enhance the navigation solution. Another option could be the usage of predicted ephemerides and clocks, which have a slightly better performance. This would need an upload of this product with a periodicity of 6 hours. The mismodelled error mainly due to orbits would decrease, thus increasing the impact of multipath mitigation. Another option would be the use of some kind of real-time clock estimation, such as JPL real-time products, which have a SISRE of about 10 cm [Bar-Sever et al., 2002]. This would lead to similar results to the ones shown in the chapter, but would need a permanent communication link to the satellite, which is still an open problem.

Satellites with moving parts, such as solar panels, would present a worse performance, as all the reflective structures would not be fixed to the spacecraft, thus compromising the assumption of repeatability. In this case, and depending on which is the main multipath source, the optimal reference frame (to get the repeatability) could be linked to the spacecraft body or the moving parts.

The following chapters will deepen into the use of different kind of GPS orbit and clock products into satellite autonomous navigation, assessing the attainable accuracies with each of them.

Chapter 2

Reduced dynamic orbit modeling for real-time LEO navigation
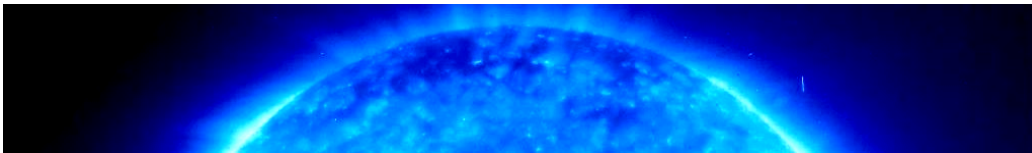
Learn from yesterday, live for today, hope for tomorrow.
The important thing is not to stop questioning.
Albert Einstein

This chapter is focused on the use of dynamic force models in the onboard satellite processor. In order to be able to use the models that are commonly accepted for postprocessing solutions, it is needed to remove all dependence on products not available in real time, and to simplify some of the models to keep the computational cost at affordable levels for spacecraft computers. The first part of the chapter will explore the algorithm selection for practical autonomous LEO navigation. The second will validate the algorithms against real data of four different satellite missions: CHAMP[1], SAC-C[1], JASON[2] and GRACE-A[3] (see info on Appendix C). Different options (such as measurements type and GPS ephemerides products) will be explored and its performance assessed.

2.1 Introduction

The application of dynamic models for satellite orbit determination is a widely used technique and well documented in astrodynamics literature (such

---

Heading image: Image of the sun captured by SOHO's EIT in the Fe IX/X 171Å line.
[1]Obtained from ftp://sayatnova.jpl.nasa.gov, courtesy of NASA
[2]Obtained from http://www.aviso.oceanobs.com, courtesy of CNES
[3]Obtained from ftp://podaac.jpl.nasa.gov, courtesy of NASA

as [Montenbruck and Gill, 2000] and [Vallado, 2001]). Most works are restricted to post-processing orbit determination solutions, mainly due to its implied computational burden and the necessity of auxiliary parameters not available in real-time. Several adaptations to real-time navigation has been done both in absolute and relative positioning as seen in the chapter *Introduction*.

The present chapter will deepen into real-time onboard navigation with dynamic models. It will make use of a reduced dynamic filter, which introduces the empirical accelerations concept. These accelerations are inserted as a way to absorb unmodeled and mismodeled effects. In this sense, we will define and assess algorithms and parametrization options (such as measurements used, GPS orbit and clocks products and gravity field order) for a set of LEO satellites in a wide altitude range (from 350 km to 1350 km). The software developed is based on the GHOST software libraries [Montenbruck et al., 2005].

To assess the effectiveness of the algorithms for LEO satellites, the real-time positions will be compared against POD reference solutions obtained in postprocess using precise GPS orbits and clocks. These solutions have an accuracy of few centimeters compared with the reference solutions given by each of the processing centers of the satellites. It has been chosen to create the own reference solution instead of using the one given by each of the centers in order to provide a consistent controlled reference solution for all of the satellites. Besides, this orbit uses the same data as the real time processing, in this way it is possible to check the difference of real time and postprocessing using the same input data. The quality of these reference orbits is assessed in table 2.2 comparing them to the orbits provided by each of the centers.

2.2 POD reference post-processing strategy

The models used for the postprocessing reference orbit are shown in table 2.1.

The process to obtain the reference orbit has been:

1. *Single Point Positioning*: As a first step a kinematic single point positioning strategy is performed using only pseudorange measurements. This is to obtain a first rough approximation of the trajectory. The accuracy of this first estimation at the level of several meters.

2. *Orbit fit*: Taking as inputs the raw spacecraft positions, an orbit is fitted using the dynamic models to obtain a better approximation of

Table 2.1: *Models used in the postprocessing precise orbit determination strategy to obtain reference orbits.*

Model/Parameter	Selection in postprocessing
Earth gravity field	GGM01S at 100x100 [Tapley et al., 2004]
Atmospheric density	J71 [Jacchia, 1971]
Planetary ephemerides	Low precision model [Montenbruck and Gill, 2000]
Earth tides	Solid, Pole and Ocean [McCarthy and Petit, 2004]
Ref. frame transformations	IERS1996/IAU1980 transformations (IGS) [Mireault et al., 1999]

the trajectory. The accuracy of the resulting positions are of a few tens of centimeters.

3. *GPS integration with dynamic models*: Using the previous trajectory as reference (mainly to discard faulty measurements), the dynamic models and the GPS measurements are combined into a batch filter to obtain the final reference orbit. The accuracy of this trajectory is in the order of few centimeters, but the exact performance depends on the specific spacecraft (see table 2.2).

In the last step the precise trajectory of the spacecraft is estimated (both in position and velocity), among its clock on each epoch, the drag and solar radiation coefficients, the carrier-phase ambiguities for each arc and the empirical accelerations at 600 seconds intervals. The empirical accelerations are considered constant values inside of each block.

2.3 Real-time orbit determination strategy

2.3.1 Navigation algorithm

The real-time positioning deserves special care in computational load and in additional data requirements (which can be unavailable for software running onboard the spacecraft). In this sense, the batch approach (all parameters solved at once) used in the POD strategy is no longer valid for an epoch

Table 2.2: *List of spacecraft used along with its nominal altitude in the selected data arcs of 2006. Last column shows an estimation of the error for the POD used as reference (compared with the reference solutions that provide each of the satellite processing centers).*

Spacecraft	Altitude	Data arcs (days)	Accuracy of reference
CHAMP	350 km	100-150	8 cm
GRACE-A	460 km	230-280	4 cm
SAC-C	700 km	230-260	7 cm
JASON	1350 km	130-150	5 cm

by epoch processing, so the Extended Kalman Filter (EKF) is used instead. The EKF is an extension of the Kalman Filter for non linear processes, but with differentiable functions (which is the case for the navigation equations) and connects the different epochs taking full profit of the stochastic nature of the unknowns.

The real-time navigation is done in a step by step basis. The parameters estimated (per epoch) are:

- Position and velocity of the spacecraft (3 positions plus 3 velocities parameters).

- Clock error (1 parameter).

- Drag and solar radiation coefficients, with a small initial standard deviation, as they have been initialized by the POD estimation of a previous day (2 parameters).

- Empirical accelerations, which are now treated as random walk variables, introducing process noise in the filter to account for its variations (3 parameters).

- Carrier-phase ambiguities (one parameter per satellite in view).

Thence, the number of parameters to be estimated each epoch are 12 + number of satellites in view.

Each of the navigation steps is divided in:

1. *Initialization of the filter*: It is done in the first epoch only to provide initial values to the filter. It uses a kinematic single point positioning

algorithm to obtain both initial position and velocity. Carrier-phase ambiguities are initialized with the pseudorange (this is repeated right after every cycle-slip), and, as said, the drag and solar radiation coefficients with the ones obtained by the POD estimation of a previous day.

2. *Time update*: Propagates the previous state vector and state transition matrix of the spacecraft to the present epoch by means of a 4th-order Runge-Kutta integrator. The covariance matrix is computed from the state transition matrix.

3. *Outlier and cycle-slip detection*: A data editing module is used to detect and discard bad measurements, and mark cycle-slips (restarting ambiguities unknowns). More details are given in the next section: *Data editing module*.

4. *Measurement update*: With the present observations, the covariance matrix prediction and the state vector, it is computed the estimation of parameters for the current epoch.

To fully characterize an EKF process, it is necessary to define the state transition matrix ($\mathbf{\Phi}$) and the process noise matrix ($\mathbf{Q}$). These two matrices provide the relationship between the previous epoch and the present one. In this sense, the state vector and covariance matrix predictions for the current epoch ($\mathbf{X}_i^-$ and $\mathbf{P}_i^-$) can be obtained by:

$$\mathbf{X}_i^- = \mathbf{\Phi}_i \mathbf{X}_{i-1}^- \tag{2.1}$$
$$\mathbf{P}_i^- = \mathbf{\Phi}_i \mathbf{P}_{i-1}^+ \mathbf{\Phi}_i^T + \mathbf{Q} \tag{2.2}$$

In the reduced dynamic navigation $\mathbf{\Phi}$ and $\mathbf{Q}$ can be defined as:

$$\mathbf{\Phi} = \begin{bmatrix} \mathbf{\Phi}_{r,v} & \mathbf{S}_{C_R} & \mathbf{S}_{C_D} & \mathbf{S}_a & 0 & 0 \\ 0 & 1 & 0 & 0 & 0 & 0 \\ 0 & 0 & 1 & 0 & 0 & 0 \\ 0 & 0 & 0 & d \cdot \mathbf{I}_{3\times3} & 0 & 0 \\ 0 & 0 & 0 & 0 & 1 & 0 \\ 0 & 0 & 0 & 0 & 0 & \mathbf{I}_{n\times n} \end{bmatrix} \tag{2.3}$$

$$\mathbf{Q} = \begin{bmatrix} 0 & 0 & 0 & 0 & 0 & 0 \\ 0 & 0 & 0 & 0 & 0 & 0 \\ 0 & 0 & 0 & 0 & 0 & 0 \\ 0 & 0 & 0 & (\sigma_a^2(1-d^2)) \cdot \mathbf{I}_{3\times3} & 0 & 0 \\ 0 & 0 & 0 & 0 & \sigma_{dt}^2 & 0 \\ 0 & 0 & 0 & 0 & 0 & 0 \end{bmatrix} \tag{2.4}$$

where:

- First column/row stands for position-velocity parameters (3+3).

- Second column/row stands for solar radiation coefficient parameter (1).

- Third column/row stands for drag coefficient parameter (1).

- Forth column/row stands for empirical accelerations parameters (3).

- Fifth column/row stands for receiver clock parameter (1).

- Sixth column/row stands for carrier-phase ambiguities (n).

and:

$\boldsymbol{\Phi}_{r,v}$, $\mathbf{S}_{C_R}$, $\mathbf{S}_{C_D}$ and $\mathbf{S}_a$ are obtained through numerical integration. d is the damping factor for empirical accelerations defined as: $d = e^{-\frac{\Delta t}{\tau}}$, and is used to keep empirical accelerations in values not far from zero (Gauss-Markov model). σ_a^2 are the process noise of empirical accelerations, which are fine-tuned for each combination of spacecraft/GPS products. σ_{dt}^2 is the clock process noise, as there is no clock information, this sigma must be high enough to allow the clock be estimated each epoch independently from the former one in a de-facto white noise random process.

2.3.2 Dynamic models

Table 2.3 summarizes the models used for the $\boldsymbol{\Phi}$ determination. The atmospheric density model J71 used in the POD reference estimation utilizes data not available in real-time (solar activity and geomagnetic index), so the simpler Harris-Priester model (based on fixed coefficients) has been chosen. The lower accuracy of this model is compensated by a small addition of process noise in the along-track component (the main affected component in drag forces). Tidal deformations of the Earth cause an acceleration of about 200 nm/s^2 at a 400 km altitude, and a simple approximation for the k_{20} solid earth tide [Rizos and Stolz, 1985] has therefore been considered.

The modeling and determination of spacecraft trajectories in the vicinity of the Earth involves two main reference frames: the International Celestial Reference Frame (ICRF), offering a natural formulation of the satellite equations of motion and position of third bodies such as the Sun and Moon; and the International Terrestrial Reference Frame (ITRF), offering an Earth-fixed system to model the gravitational acceleration affecting the spacecraft. Besides the natural reference frame of GPS is the ITRF (the GPS satellite

orbits are typically provided in this frame). The restricted real-time availability of information to properly transform coordinates between these frames suggests the difficulty to perform rigorous ICRF-to-ITRF transformations in such conditions.

In this sense, as seen in [Montenbruck and Ramos-Bosch, 2007], the solution chosen has been to use only the ITRF system and reformulate the equation of motion into this system. ITRF is not an inertial system, so two "fictitious" forces appear in this rotating reference frame: the centrifugal and the Coriolis forces. These new accelerations have to be taken into account in the dynamic filter. The centrifugal and Coriolis accelerations are given by:

$$\mathbf{a}_{centrifugal} = \omega^2 \mathbf{r}_\perp = -\boldsymbol{\Omega} \times (\boldsymbol{\Omega} \times \mathbf{r}) \tag{2.5}$$

and

$$\mathbf{a}_{Coriolis} = -2\boldsymbol{\Omega} \times \mathbf{v}_{rot} \tag{2.6}$$

Where $\boldsymbol{\Omega}$ is the angular velocity vector which has a magnitude equal to the rotation rate ω and is directed along the axis of rotation of the rotating reference frame, $\mathbf{r}$ represents the position of the satellite and $\mathbf{v}_{rot}$ its velocity as seen in the rotating reference frame. Thus the $\boldsymbol{\Delta}\mathbf{a}$ that should be included in the spacecraft acceleration computation is determined by:

$$\boldsymbol{\Delta}\mathbf{a} = \mathbf{a}_{Coriolis} + \mathbf{a}_{centrifugal} = -2\boldsymbol{\Omega} \times \mathbf{v}_{rot} - \boldsymbol{\Omega} \times \boldsymbol{\Omega} \times \mathbf{r} \tag{2.7}$$

It is not necessary to rigorously evaluate the above expressions, and an approximate rotation rate $\omega = 0.7292115 \cdot 10^{-4}$ rad/s about an axis slightly tilted relative to the Earth axis provides a good estimation for $\boldsymbol{\Omega}$. The axis transformation has been performed using the IGS EOP predicted (ultra-rapid) products. Remaining differences between this approximate and a rigorous modeling of the former effects are compensated by slightly higher values in the process noise of the empirical accelerations.

Furthermore besides the simplification of the models, it has been introduced other key contributions into the real-time navigation, which have been shown to enhance the final navigation solution. In particular:

1. An on-the-fly data editing module (part of the outlier detection as already mentioned) to discard faulty measurements (or simply measurements with a clear higher error than the expected) and mark cycle-slips.

2. The mitigation of the GPS clock errors by adding process noise in the carrier-phase ambiguity estimation in the Kalman filtering when using broadcast and predicted GPS orbits and clocks.

Table 2.3: *Models used in the real-time orbit determination strategy to obtain the autonomous orbit solution.*

Model/Parameter	Selection in real-time
Earth gravity field	GGM01S at variable degree/order [Tapley et al., 2004]
Atmospheric density	Harris-Priester [Harris and Priester, 1962]
Planetary ephemerides	Low precision model [Montenbruck and Gill, 2000]
Earth tides	k_{20} solid only [Rizos and Stolz, 1985]
Ref. frame transformations	IERS1996/IAU1980 transformations (IGS predicted)

Data editing module

Aside from a typical elevation cut-off data editing (it has been used between 0 and 5 degrees, depending on the satellite), it is possible to discard outliers by looking at the residuals of the Kalman filter. If these residuals present a large scatter, it can be a trace of a bad measurement in the input data. Applying a RAIM[4] algorithm (as shown in [Brown, 1994]) it is possible to trace and remove these bad measurements. This process is based in repeating the filter process for all the groups of one less satellite (i.e, 10 satellites in view, means 10 runs of the filter with 9 satellites in view). Unfortunately, 9 satellites in view mean a total of 21 parameters to be estimated, and in a resource limited environment (onboard processor) the iterative repetition of the filter calculus process can be unaffordable.

To overcome this issue a novel on-the-fly data editing method has been introduced in this study to detect and remove bad measurements. It is based on the comparison of the measurements with its models and is done in two stages:

1. *LEO clock determination.* The dynamic orbit modeling allows a propagation of the position of the spacecraft from the previous epoch (nec-

---

[4]RAIM algorithm (Receiver Autonomous Integrity Monitoring) is commonly used in augmentation positioning services in order to discard faulty measurements and provide integrity, but its use is not dependant on these augmentation systems and can be applied independently.

essary for the predicted value in the Kalman filter). This predicted position and the carrier-phase ambiguities estimations (also from the previous epoch) permits a precise modeling of each of the measurements, except for the LEO clock error. This step obtains an estimation of this clock error, discarding in the process the measurements with large differences (both outliers and cycle-slips).

2. *Fine screening of measurements.* Once the LEO clock error has been determined, it is used to fully model the measurements. The obtained residuals are thence sequentially compared against its expected uncertainty. If this relation is higher than a certain threshold, the measurement is flagged as faulty (for pseudorange) or a cycle-slip is marked (for carrier-phase).

This screening process is heavily leant on the dynamic modeling (for its propagation of the position) and becomes more effective as the accuracy of the positions increases after the convergence time.

For the first step (*LEO clock determination*), the modeled measurement can be computed from:

$$\rho_i^* = |\mathbf{r} - \mathbf{r}_{GPS,i}| - c\delta t_{GPS,i} + B_i \tag{2.8}$$

Where ρ_i^* is the modeled measurement for satellite i, $\mathbf{r}$ the LEO position, $\mathbf{r}_{GPS,i}$ the GPS position, $\delta t_{GPS,i}$ the GPS clock error, c the speed of light and B_i the carrier-phase ambiguity. As said, this modeled range does not account for the receiver clock and an approximation of the receiver clock for the current epoch is obtained from the difference between observed and modeled ranges weighting with the expected uncertainty of the residuals. This uncertainty $\sigma(\rho_i^*)$ is estimated from the covariance of the receiver position projected on the Line-of-Sight vector, the covariance of the carrier-phase ambiguity and the assumed standard deviation (from now on sigma) of the measurement:

$$\sigma(\rho_i^*) = \sqrt{\mathbf{e}_i^T \cdot \mathbf{P}_i^- \cdot \mathbf{e}_i + \sigma(\rho_i)^2 + \sigma(SISRE)^2} \tag{2.9}$$

Where $\sigma(\rho_i)$ is the expected standard deviation of noise of the measurement, $\sigma(SISRE)^2$ the expected SISRE of the selected GPS products, and $\mathbf{e}_i$ is a vector with zeros in all its components except the three position parameters (which will have the Line-of-Sight components) and the corresponding ambiguity (which will have a '1'). In practice the covariance matrix $\mathbf{P}_i$ is collapsed into a 4x4 matrix (with positions and the corresponding ambiguity), and the $\mathbf{e}_i$ vector into a 4 dimensions vector with the position parameters and '1' in the ambiguity.

To obtain the satellite clock estimation $c\delta t_{LEO}$ and its uncertainty $\sigma(c\delta t_{LEO})$ the following equations are used:

$$c\delta t_{LEO} = \frac{1}{\sum \frac{1}{(\sigma(\rho_i^*))^2}} \sum \frac{\rho_i - \rho_i^*}{(\sigma(\rho_i^*))^2} \tag{2.10}$$

$$\sigma(c\delta t_{LEO}) = \sqrt{\frac{1}{\sum \frac{1}{(\sigma(\rho_i^*))^2}}} \tag{2.11}$$

Where ρ_i is the measured range for satellite i. This is used to obtain the clock-free prefilter residual (χ_i) and its uncertainty:

$$\chi_i = \rho_i - \rho_i^* - \delta t_{LEO} \tag{2.12}$$

$$\sigma(\chi_i) = \sqrt{(\sigma(\rho_i^*))^2 + (\sigma(c\delta t_{LEO}))^2} \tag{2.13}$$

Here, $\sigma(\chi_i)$ was computed assuming that the contributions from $\sigma(\rho_i^*)$ and $\sigma(c\delta t_{LEO})$ were independent. This is clearly not the case, as $c\delta t_{LEO}$ was estimated from ρ_i^* and thence, are actually correlated. This is done as an approximation because it will only be used as a data editing threshold, not a navigation filter weighting, so the effect that this approximation could cause is that some cases close to the threshold are discarded or accepted when they strictly should not. This is not critical as these discarding/acceptance of near-limit measurements does not have a noticeable impact. Besides, in general, the $\sigma(\chi_i)$ will receive contributions mainly from $\sigma(\rho_i^*)$ as it will be higher than $\sigma(c\delta t_{LEO})$.

The ratio of the χ_i in relation to its uncertainty is defined as $\widehat{\chi_i}$:

$$\widehat{\chi_i} = \frac{\chi_i}{\sigma(\chi_i)} \tag{2.14}$$

The RMS of these $\widehat{\chi_i}$ (dimensionless values) is computed, if it is higher than a certain threshold (3 units), a bad measurement is suspected. In such a case, the process is repeated with subsets with one less measurement. The solution with smallest residuals is accepted, and the omitted measurement is considered to have a cycle-slip in the current epoch (the filter ambiguity is reset). This discarding process is used iteratively and can remove various observations. $c\delta t_{LEO}$ is computed using only carrier-phase measurements, this is done because the clock and orbit errors will be partially absorbed in the carrier-phase ambiguity, and pseudorange measurements will have much larger errors (and these errors will not follow a gaussian distribution). As will be seen later in the next section, when using broadcast products, the GPS clocks are partially absorbed by the ambiguity parameters. Pseudorange

measurements are fully affected by GPS clock errors, thus its error differs from a gaussian distribution, which would worsen the $c\delta t_{LEO}$ estimation.

Figure 2.1 shows histograms for a processing with broadcast and precise products, and the position of the RMS threshold. As shown it only discards the worst estimations, and most of the time it is not needed to iteratively remove observations. This RMS threshold is used only to get a proper estimation of $c\delta t_{LEO}$, once it is sufficiently well known (i.e, the scatter of $\widehat{\chi_i}$ is below the threshold of 3 units), the *Fine screening of measurements* stage is performed.

In this step, all of the computed $\widehat{\chi_i}$ are compared against another threshold (including, now, pseudorange measurements). If higher, are marked as outliers (or cycle-slip in carrier-phase measurements). The value chosen for this threshold is of 1 dimensionless unit. This second stage is the one that discard most outliers.

This method has been proven to enhance the position accuracy of the real-time positioning. Thanks to the availability of a predicted position for each epoch previous to the filter step (due to the dynamic propagation), it is able to precisely detect outliers and cycle-slips. It tries to emulate in a much lighter way the iterative process of repeating the full kalman filtering.

Mitigation of GPS broadcast ephemeris errors

The use of broadcasted products introduces an error into the modeled measurement. This error is the Signal-in-Space Range Error (SISRE) difference between the real clock and position of the GPS satellite and the one provided by the ephemerides product used. Figure 2.2 shows the difference between broadcasted and precise products in SISRE (computed as suggested in [Malys et al., 1997]). As can be seen this mismodeling error varies slowly and depends on the satellite (except the sudden jumps that appear when changing the ephemeris block used, typically every 2 hours. Once the ephemeris block is changed, the affected measurement is automatically flagged as containing a cycle-slip, to reestimate the ambiguity).

A possible option to take into account this effect would be to add an additional common parameter in pseudorange and carrier-phase measurements for each satellite, trying to model in this way the slow varying error. This new parameter should have a low process noise. This approach would have two drawbacks:

- LEO clock and this additional parameter could not be properly decorrelated in the filter without any kind of initial value for any of them (which is not available) to decorrelate them, thus creating an ambiguity that would make bad estimations of both.
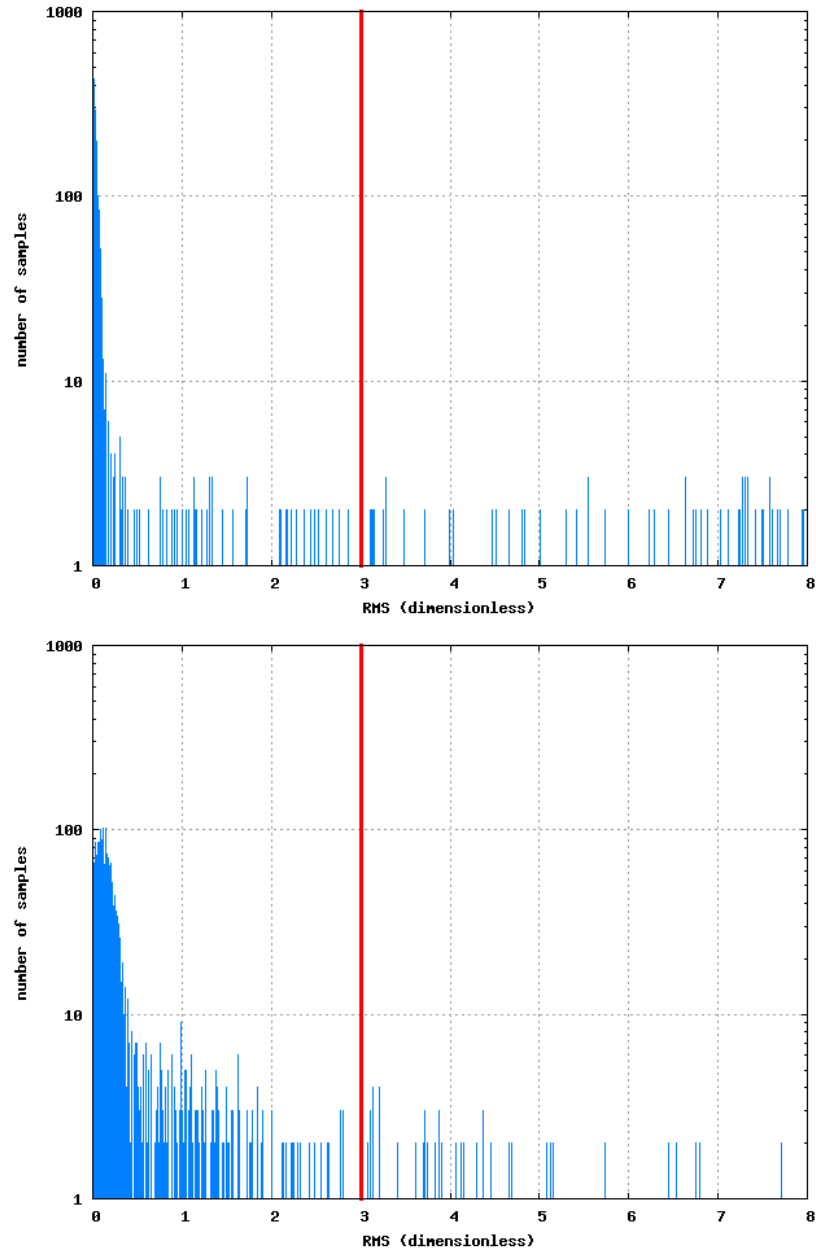
Figure 2.1: *Histograms of the RMS of $\widehat{\chi}$ values. Top plot was obtained using precise orbit and clocks and the bottom one broadcasted products. The vertical line is the 3 units threshold.*

- This approach would increase the computation needs of the filter due
  to the additional unknowns, thus increasing from 24 parameters (with
  12 satellites in view) to 36.

To avoid this situation, it has been chosen to re-use the carrier-phase
ambiguity parameter, and decrease the weight of pseudorange (in relation to
the one that has when computing with precise products). The introduction
of a small quantity of process noise in the ambiguity parameter absorbs part
of this error, thus enhancing the final navigation solution. The process noise
has only been inserted when processing with broadcasted (process noise of 2.5
mm/$\sqrt{s}$) and predicted ephemerides (0.5 mm/$\sqrt{s}$). The disadvantage of this
approach is that pseudorange measurements are affected by a mismodeling
not present in carrier-phase ones, but the solution is to decrease the weight of
the pseudorange observables in the filter, thus trusting more in carrier-phase
measurements.

Figure 2.2: *SISRE between broadcasted and precise products. In red
are shown all the satellites. Green and blue highlight PRN satellites
6 and 24 to see the slow variation tendency. Data from 30th October
of 2006.*

When using this approach, equation 2.4 becomes:

$$\mathbf{Q} = \begin{bmatrix} 0 & 0 & 0 & 0 & 0 & 0 \\ 0 & 0 & 0 & 0 & 0 & 0 \\ 0 & 0 & 0 & 0 & 0 & 0 \\ 0 & 0 & 0 & (\sigma_a^2(1-d^2)) \cdot \mathbf{I}_{3\times3} & 0 & 0 \\ 0 & 0 & 0 & 0 & \sigma_{dt}^2 & 0 \\ 0 & 0 & 0 & 0 & 0 & \sigma_b^2 \cdot \mathbf{I}_{n\times n} \end{bmatrix} \qquad (2.15)$$
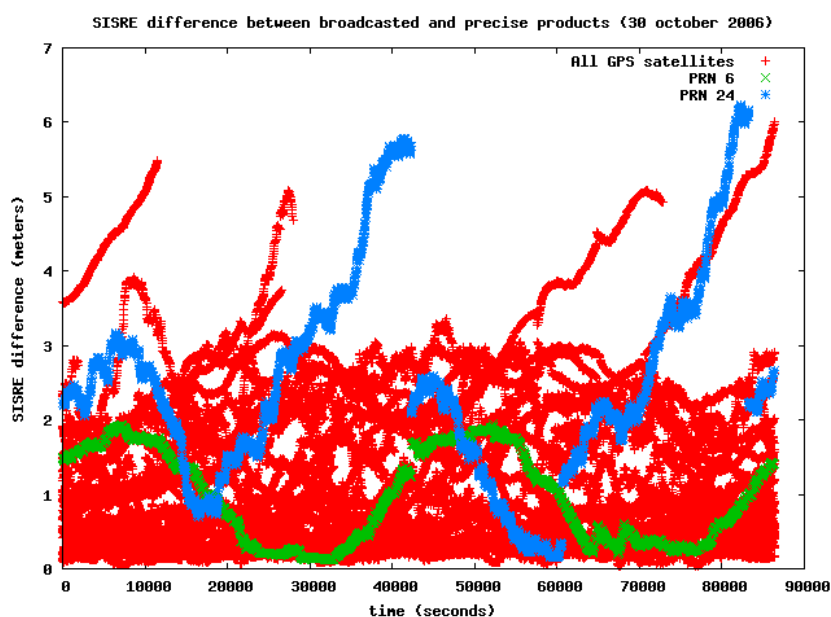
Where σ_b^2 is the process noise inserted associated to the usage of the broadcasted ephemeris to allow the absorption of the slow variation errors in carrier-phase ambiguities.

Figure 2.3 shows two different GPS arcs where it is compared the ambiguity estimation from the filter (using process noise) with the SISRE of the broadcast products (in relation to precise postprocessed products). As can be seen both quantities follow a similar pattern, thus deducing that a non-constant ambiguity allows a better absorption of the broadcast errors.

A small test has been done in order to check the benefits of the addition of process noise in the carrier-phase ambiguity. Figure 2.4 compares the attained accuracies using broadcasted products with different levels of process noise.

2.4 Flight data analysis

2.4.1 Data sets

In order to evaluate the algorithms, they have been applied to real data obtained from four different satellites: CHAMP, SAC-C, JASON and GRACE-A (equipped with dual-frequency GPS receivers). These spacecraft have orbital heights ranging from 350 to 1350 km, so they offer a broad spectrum of the different goodness of the models for different altitudes. To assess the method, the obtained positions have been compared with the postprocessed solution obtained using precise orbits and clocks. Table 2.2 specifies the data arcs (or periods), the spacecraft altitudes in these arcs, and the position difference of the generated POD reference orbit compared against the reference solutions provided by each of the satellite processing centers. Transformations between antenna phase centers have been done by attitude quaternion information for GRACE-A and JASON and nominal attitude laws for SAC-C and CHAMP (Z axis in earth direction, X in direction of flight, Y forming a right-hand system).

The data arcs chosen for the satellites span over different periods of 2006.
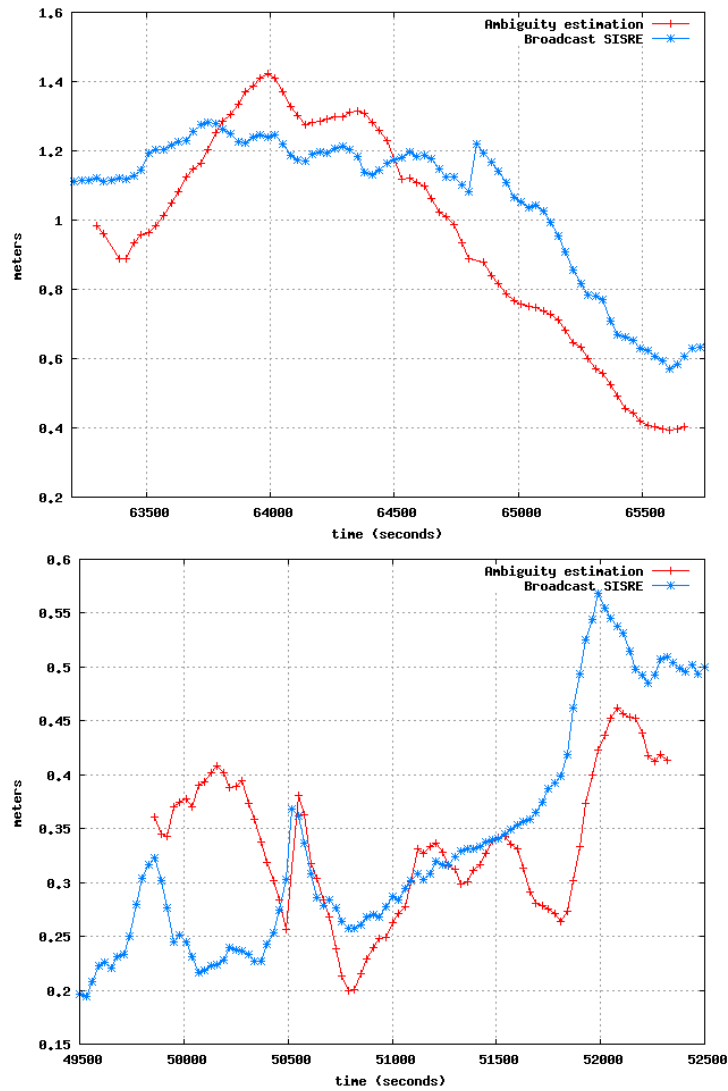
Figure 2.3: *Comparison between the estimation of an arc ambiguity by the filter using process noise, and the error of the broadcast products for the same satellite. The ambiguity has an arbitrary bias. Top and bottom plots correspond to different times for PRN 10 of SAC-C for the 28th of October of 2006.*
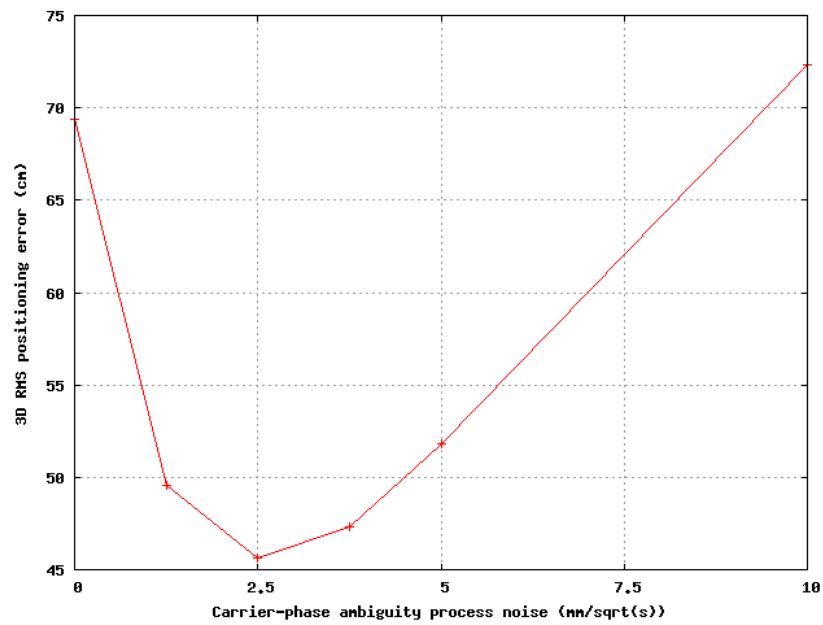
Figure 2.4: *Mean daily 3D RMS positioning error versus carrier-phase ambiguity process noise. Data obtained from processing SAC-C satellite for days 230 to 260 of 2006 using broadcast products.*

2.4.2 Analysis, processing and parametrization options

The process to evaluate the real-time positioning compares it with the computed reference orbit on a daily basis. Both processes were done with epoch steps of 30 seconds, and compared in the same points. The final result is the 3D RMS of the position error discarding the first hour, to allow the real time filter to converge into a stable solution. The step size of 30 seconds has been chosen to avoid larger errors associated with higher step sizes. Figure 2.5 shows a plot for GRACE-A satellite comparing the attained 3D RMS positioning error using different measurement intervals with precise GPS products. As it can be seen an interval of 150 seconds doubles the error of a 30 second interval.
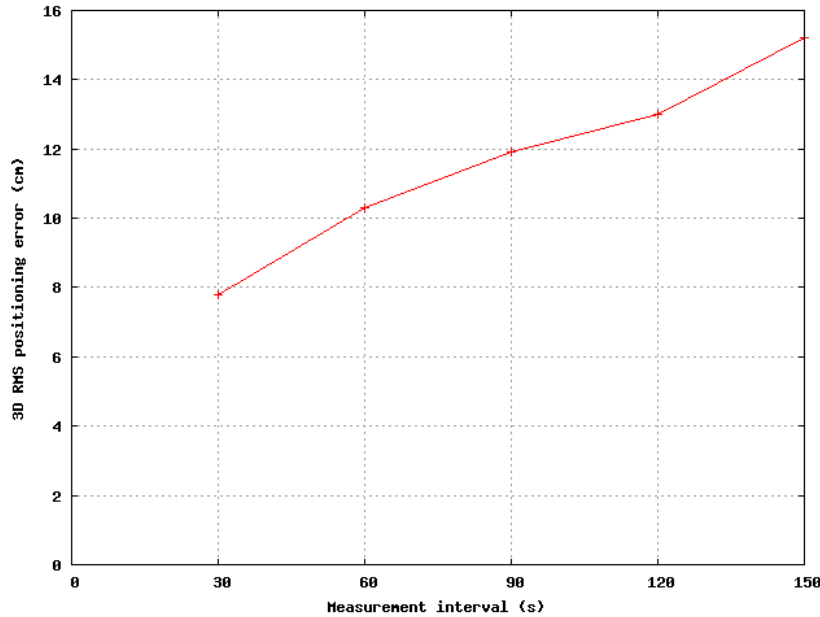
Figure 2.5: *Comparison of 3D RMS positioning error against measurement intervals. Data from GRACE-A (precise GPS orbits and clocks), day $22^n d$ of September of 2006.*

The parameters used in the filter have been adopted to achieve a good performance in relation with the reference orbits of the spacecraft. A summary of the detected typical observable noise and empirical accelerations is shown in table 2.4. As can be seen, each satellite show different values for both noise and empirical accelerations. This high variability means that each

satellite should be treated independently, with parameters optimized for each specific spacecraft. The observables noise is a measure of the sigma of each measurement, and the empirical accelerations (obtained in the POD) is a measure of the inaccuracy of the models for each satellite. The standard deviation of the residuals of the filter provides the estimation of the observable noise, though this can be unaccurate as some measurement errors can be absorbed in the parameters estimation, and systematic modelling errors may increase the residuals beyond the noise level of the data. Empirical accelerations, as expected, are higher for low altitude satellites, as models are less accurate in the lower altitude range. Empirical accelerations obtained in the real-time process are higher than the ones in the table, as it suffers from more mismodelings.

Table 2.4: *Typical (1-sigma) observable noise and empirical accelerations for each satellite. The empirical accelerations account for unmodeled (or mismodeled) forces affecting the spacecraft. These are the typical values obtained when processing the reference orbit. Empirical accelerations for the real time processing will greatly vary, as they may absorb other effects. This is specially true, for example when comparing these numbers with different values of degree and order of gravity field.*

Spacecraft	Observables noise (cm)			Empirical Acc. (nm/s^2)		
	IF-PR	IF-CP	GRAPHIC	Radial	Along	Cross
CHAMP	60	0.7	9	0.8	45	40
GRACE-A	40	0.8	12	0.3	12	8
SAC-C	150	1.7	18	0.0	3	14
JASON	80	1.0	8	0.1	1	6

Several test cases have been chosen in order to assess a wide range of options both in accuracy and implementation effort. In particular, three different items have been identified for the test cases:

- Measurements type

- Gravity field order

- GPS orbit and clocks products

2.4.3   Measurements type

All of the chosen satellites have dual-frequency receivers, and therefore are able to use different kind of combination of measurements in order to remove the ionosphere contribution to the signal. In this sense, the tested combinations have been:

- *Ionospheric free carrier-phase combination*, which is able to remove most of the ionosphere contribution to the measurements (in fact, the 99.9%, this discrepancy is due to higher orders of the ionospheric term, see [Hernandez-Pajares et al., 2007b] for more details. The remaining contribution is negligible in the scope of the current work). This is the most precise combination, but requires additional parameters in the filter in order to estimate the ambiguity inherited from the carrier-phase measurements.

$$L_c = \frac{f_1^2 L_1 - f_2^2 L_2}{f_1^2 - f_2^2} \qquad (2.16)$$

- *Ionospheric free pseudorange combination*, very similar to the previous one, but without ambiguities (simplifying the filter) and a much larger noise, mainly due to multipath and thermal noise. In particular, if P_1 and P_2 noise are uncorrelated, the noise of P_c is about three times higher than their.

$$P_c = \frac{f_1^2 P_1 - f_2^2 P_2}{f_1^2 - f_2^2} \qquad (2.17)$$

- *GRAPHIC combination*, which needs only one frequency. These results are of particular importance in space applications, as single-frequency receivers have a cost and spacecraft resource consumption much lower than dual-frequency ones. This combination is able to eliminate all the ionospheric effect, but at the cost of having an ambiguity (from the carrier-phase) and more noise than a pure carrier-phase combination (residual from the pseudorange). Most of the noise and multipath in this combination is due to C_1 (noise and multipath of L_1 is negligible in front of C_1). Chapter 4 will analyze a multipath mitigation technique for single-frequency receivers using this combination.

$$G_1 = \frac{C_1 + L_1}{2} \qquad (2.18)$$

Figure 2.6 shows the observable noise for SAC-C satellite for the ionospheric free pseudorange and GRAPHIC combination. The plot represents

$P_c - L_c$ in red and $G_1 - L_c$ in blue and allows comparing the typical noise of both measurements. Formally, the noise of P_c would be about six times the noise of G_1 (supposing comparable noises of P_1 and C_1, as P_c is the triple than P_1 and G_1 the half of C_1). More information on combinations of measurements can be found on Appendix A.
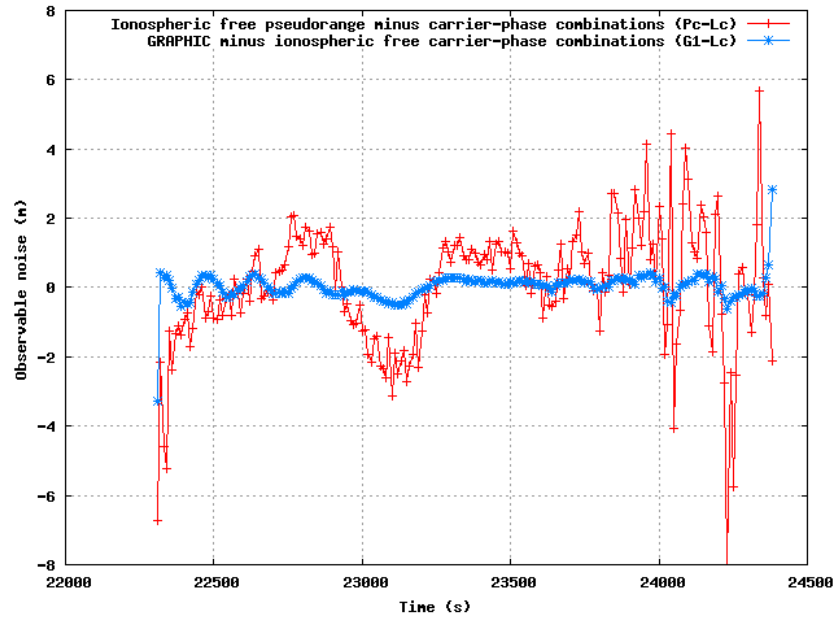
Figure 2.6: *Comparison of the typical noise of two different measurements used: ionospheric free pseudorange (red) and GRAPHIC (blue). Both $P_c - L_c$ and $G_1 - L_c$ suffer from an arbitrary bias that has mostly been removed manually to properly show the differences in noise between both combinations. Data is from 28th of August of 2006 for SAC-C satellite and GPS PRN 10.*

2.4.4 Gravity field order

One of the most critical parameters in terms of accuracy and computational burden is the order and degree of the gravitational field model used. This is specially true when the satellite is settled at low orbital altitudes. In this sense, the four spacecraft at different heights will show a broad representative spectrum for LEO satellites.

The following options will be considered (order x degree): 100x100, 70x70, 50x50 and 30x30.

2.4.5 GPS orbit and clock products

With the ionospheric errors removed by the proper combinations, the quality of the GPS orbit and clock information is the main factor for the quality of the real-time navigation accuracy. The traditional source for this information is the own GPS broadcast message with an update time of 2 hours, and a representative SISRE of about 1-1.5 m ([Warren and Raquet, 2003]), but there are other products that could be used in a space environment. The following ones have been tested:

- *Broadcast ephemeris*, with the said 1-1.5 m of SISRE. This is the already available product.

- *Predicted orbits and clocks*, with a SISRE of about 1m (mainly due to clock errors). In this work the ones generated by IGS (called IGU) have been used. These products are generated every 6 hours with a latency of 3 hours. In order to be used it would be needed some kind of periodic communications link to the satellite. In this work, the IGU products were considered updated as soon as they would be generated (with the 3 hours latency).

- *Precise orbits and clocks*, with a SISRE of few centimeters. This product is completely unavailable in real-time, but is studied for comparison purposes. It should be the "best" scenario in terms of GPS orbit and clock products. The products provided by CODE center have been used. They have a rate of 30 seconds, suitable with the chosen step size. As seen before, a higher step size is translated in a degradation of the performance.

- *Real-time orbits and clocks*, such as the JPL's GDGPS ([NASA/JPL, 2008] and [Bar-Sever et al., 2002]) or WARTK (see [Hernandez-Pajares et al., 2007a]). In this work this kind of product has been generated with the help of a global WARTK approach. This solution (still on experimental phase) based on ambiguity solving techniques thanks to the usage of accurate real-time ionospheric determination, begins from the predicted orbits of the GPS satellites (IGU) and does an estimation of the GPS clocks emulating a real time process with a set of 40 stations world-wide scattered. The results achieved with this products are of about 15cm in SISRE, and are quite equivalent to the ones obtained through JPL GDGPS. This solution would lead to another non-trivial practical problem to solve, as it would need a permanent communication channel with the LEO satellite. The scope of this work is to evaluate the results in

position enhancement that would bring this kind of solution. This could be used to judge if it is worth some investment in providing a feasible technical solution to the permanent communication channel. More information on WARTK algorithms, with its capabilities and feasibility studies, can be found on [Hernandez-Pajares et al., 2002] and [Hernandez-Pajares et al., 2004].

2.4.6 Results

Between all the different processing options, two basic configurations will be chosen:

1. Broadcasted products:

   - Measurements type: Dual-frequency receiver with ionospheric-free carrier-phase combination.
   - Gravity field order: 70x70.
   - GPS orbit and clock products: Broadcast ephemeris and clocks.

2. Precise real time orbits and clocks (global WARTK clocks):

   - Measurements type: Dual-frequency receiver with ionospheric-free carrier-phase combination.
   - Gravity field order: 70x70.
   - GPS orbit and clock products: Global WARTK products.

The rest of the test cases will be done as modifications in only one of the items, thus exploring one of the dimensions (understanding one dimension as variations of a single parameter) at a time. The obtained results are slightly better than the ones presented in [Montenbruck and Ramos-Bosch, 2007]. Although the time window is different, the results shown here have been the outcome of a fine-tuning process which have made possible further optimizing the algorithm and parameters and hence improving results. Figure 2.7 shows the sample position errors for a full day using the real-time navigation filter for GRACE-A using broadcast and WARTK ephemeris.

Filter parameters adopted in the individual test cases have been selected to achieve a good performance against the reference orbit of the satellites. For each of the cases it has been obtained the daily 3D RMS of the positioning error (discarding the first hour, to provide enough time to the filter to converge). The provided accuracy is the mean 3D RMS (in cm) of all the days. A summary of the obtained errors can be seen in the following sections and tables.
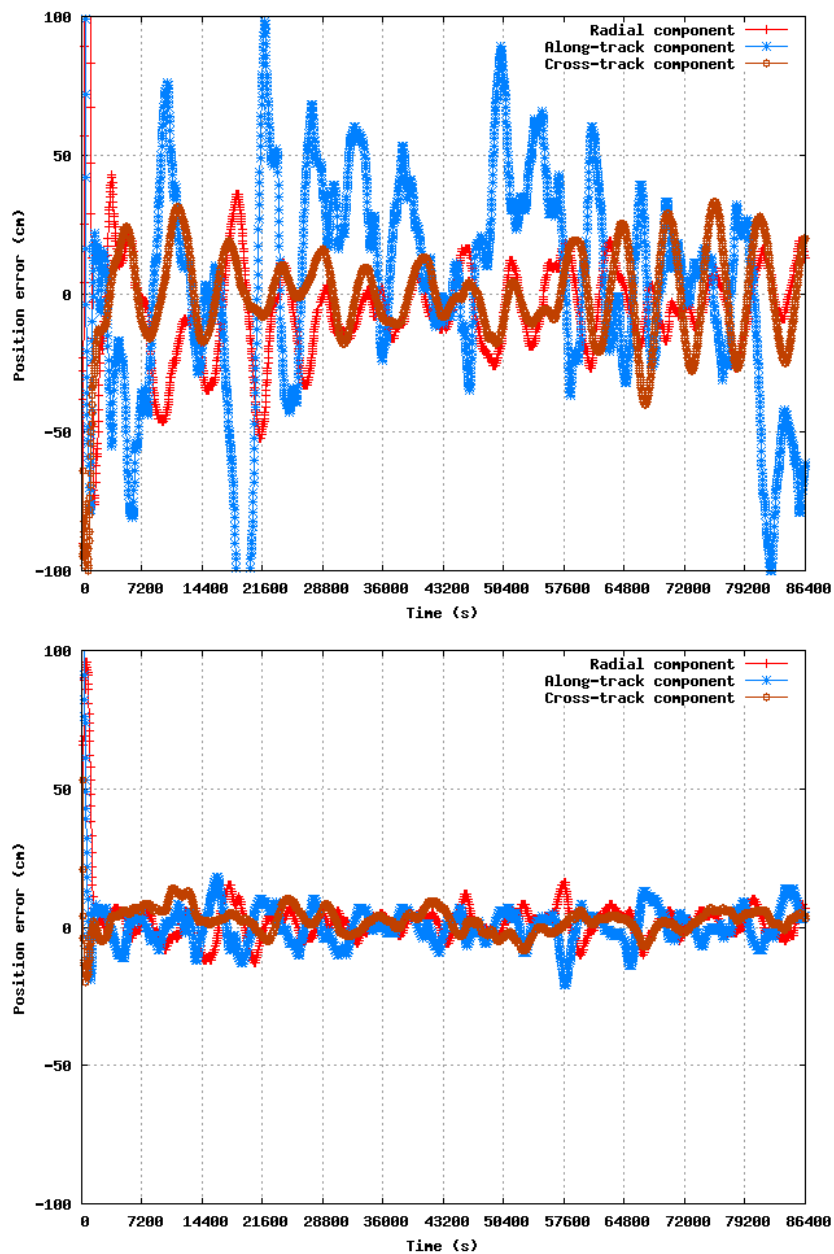
Figure 2.7: *Sample positioning errors for GRACE-A on day 250 of 2006. Top plot corresponds to broadcasted ephemeris and clocks, and the bottom one to WARTK clocks and IGU orbits.*

Measurements type

Tables 2.5 and 2.6 show performances for broadcast and WARTK products respectively. The different types of measurements are shown in columns.

The benefits of carrier-phase processing are clearly visible in these tables. Results exhibit a notable improvement both with broadcast and WARTK products in relation to pseudorange only navigation. As expected, dual-frequency carrier-phase navigation leads to the best results, but single-frequency navigation mode (GRAPHIC) also manifests a remarkable performance. This is mainly explained because the GRAPHIC combination has six times lower noise than the ionospheric-free pseudorange combination, and (as shown in table 2.4 and figure 2.6) the noise of the GRAPHIC combination is kept in the 10-20 cm range for the analyzed spacecraft.

The use of ionospheric-free pseudorange provides the lowest performance, but it has also the lower computing needs. The navigation filter does not need to account for carrier-phase ambiguities nor cycle-slip detection, so the number of parameters to be estimated is reduced from 24 to 12 (for an epoch with 12 satellites in view).

Table 2.5: *Impact of the measurement type into the navigation accuracy. The value is the 3D RMS of the positioning error in cm.* ***Broadcast*** *products and 70x70 gravity field.*

| | Measurements | | |
Spacecraft	Iono-free CP	GRAPHIC	Iono-free PR
CHAMP	61.6	67.5	97.2
GRACE-A	45.0	51.0	99.9
SAC-C	45.6	58.1	106.7
JASON	49.2	57.7	101.3

Gravity field order

A high degree and order of the gravity field model is generally required for an adequate modeling of the spacecraft trajectory, but this is also critical for the computational load of the algorithm. An effort should be done in order to keep the complexity of the gravity model as low as possible without sacrificing navigation accuracy. In tables 2.7 and 2.8 the impact of this parameter into the final navigation accuracy is assessed.

Table 2.6: *Impact of the measurement type into the navigation accuracy. The value is the 3D RMS of the positioning error in cm.* **WARTK** *products and 70x70 gravity field.*

	Measurements		
Spacecraft	Iono-free CP	GRAPHIC	Iono-free PR
CHAMP	13.7	24.0	51.2
GRACE-A	10.2	25.7	55.5
SAC-C	14.9	51.1	90.6
JASON	17.5	28.2	34.9

Table 2.7: *Impact of the gravity field order into the navigation accuracy. The value is the 3D RMS of the positioning error in cm. Numbers in brackets represent the ratio between the RMS corresponding to the cell and the RMS of the 100x100.* **Broadcast** *products and ionospheric-free carrier-phase measurements.*

	Gravity Model			
Spacecraft	100x100	70x70	50x50	30x30
CHAMP	59.5 *(1.0)*	61.6 *(1.0)*	76.7 *(1.3)*	123.6 *(2.1)*
GRACE-A	42.7 *(1.0)*	45.0 *(1.1)*	58.3 *(1.4)*	89.3 *(2.1)*
SAC-C	45.6 *(1.0)*	45.6 *(1.0)*	46.0 *(1.0)*	85.9 *(1.9)*
JASON	49.2 *(1.0)*	49.2 *(1.0)*	49.3 *(1.0)*	50.0 *(1.0)*

Table 2.8: *Impact of the gravity field order into the navigation accuracy. The value is the 3D RMS of the positioning error in cm. Numbers in brackets represent the ratio between the RMS of the cell and the RMS of the 100x100.* **WARTK** *products and ionospheric-free carrier-phase measurements.*

Spacecraft	Gravity Model			
	100x100	70x70	50x50	30x30
CHAMP	12.2 *(1.0)*	13.7 *(1.1)*	22.7 *(1.9)*	37.6 *(3.1)*
GRACE-A	9.3 *(1.0)*	10.2 *(1.1)*	15.9 *(1.7)*	24.3 *(2.6)*
SAC-C	14.9 *(1.0)*	14.9 *(1.0)*	16.2 *(1.1)*	29.9 *(2.0)*
JASON	17.5 *(1.0)*	17.5 *(1.0)*	17.5 *(1.0)*	18.1 *(1.0)*

As expected, the higher the spacecraft, the lower degradation is found when decreasing the gravity field order. Low altitude satellites are more sensitive to the the short-scale perturbations, and therefore need a large number of terms to properly model the gravity field affecting them. A reasonable trade-off should be done depending on the specific spacecraft altitude under study. In this sense, an order no higher than 70x70 would be the proper choice for the lower altitude range up to 500 km (CHAMP and GRACE-A), while a 50x50 would be enough for higher altitudes such as SAC-C at 700 km. The highest satellite, JASON, at 1350km provides good results even with the reduced 30x30 model. Low order models for low altitude satellites need great increments in empirical accelerations (up to some μm/s^2), but even so are unable to fully absorb the mismodelings of the 30x30 and present low performances worsening the navigation by a factor of two or three.

Figure 2.8 shows the obtained empirical accelerations for GRACE-A for day 250 of 2006 using WARTK products. It is possible to see the impact of the different gravity fields into the estimated accelerations. As expected, the empirical accelerations try to compensate the reduction of the order and degree of the gravity field model.

GPS orbit and clock products

Table 2.9 shows the performance of different source selection of GPS ephemerides and clocks. Broadcasted ephemeris provide the poorest accuracy, but are readily available for the spacecraft. IGS predicted (IGU) products enhance the solution, reducing the error between 20% and 40%, but would need a periodic upload to the satellite (once every 6 hours). WARTK
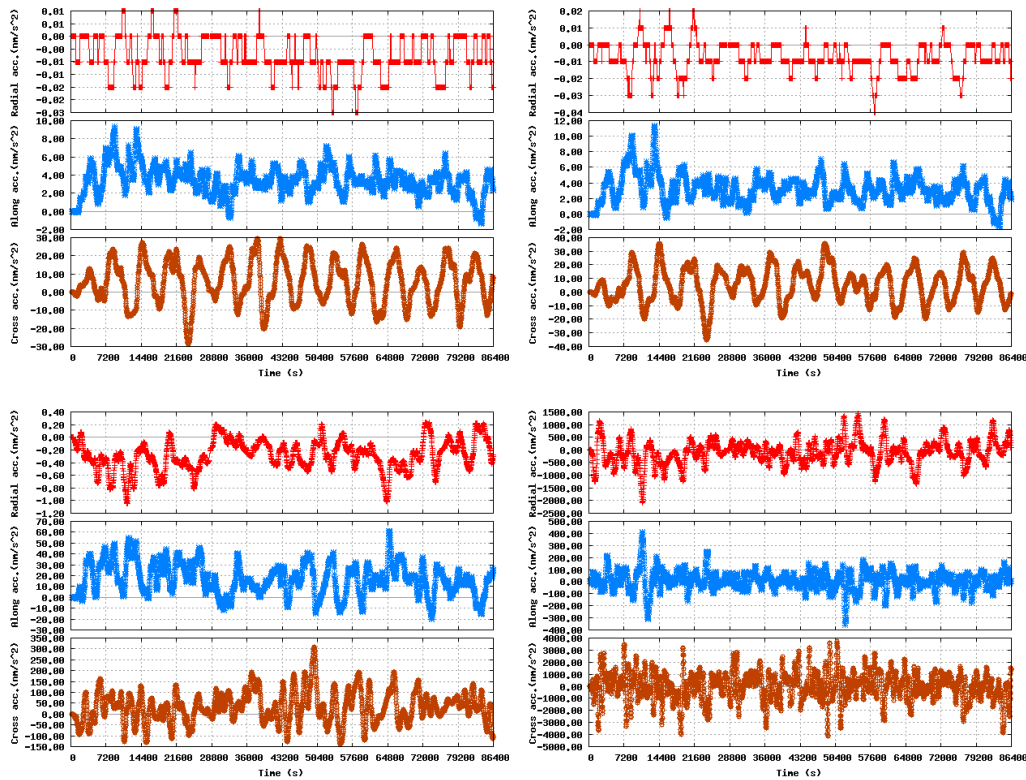
Figure 2.8: *Estimated empirical accelerations for GRACE-A for day 250 of 2006 using WARTK products. Different gravity models can be seen: 100x100 (top-left block of 3 plots), 70x70 (top-right), 50x50 (bottom-left) and 30x30 (bottom-right) where each block of 3 plots represent the evolution in time of radial, along-track and cross-track empirical acceleration components. As the order and degree of the gravity model is reduced the accelerations tend to increase to compensate the mismodeling introduced.*

products are generated in real-time, so its use would be restricted to the availability of a permanent communication channel with the spacecraft, but its existence would greatly enhance the solution, reducing the error up to 80%, and attaining a decimetric accuracy. Final CODE products are completely unavailable in real-time and are only included for comparison purposes (real-time WARTK products only degrade the accuracy in relation to final CODE ones by between 5% and 30%).

Table 2.9: *Impact of the GPS orbit and clock products into the navigation accuracy. The value is the 3D RMS of the positioning error in cm. Ionospheric-free carrier-phase measurements and 70x70 gravity field.*

	GPS ephemeris and clocks			
Spacecraft	**Broadcast**	**IGU**	**WARTK**	**CODE**
CHAMP	61.6	46.6	13.7	10.1
GRACE-A	45.0	28.4	10.2	8.3
SAC-C	45.6	29.7	14.3	13.6
JASON	49.2	40.7	17.5	14.9

2.5 Conclusions and discussion

The chapter has explored a set of options for the use of dynamic models into an autonomous LEO onboard navigation in the 350-1350 km altitude range. The results show the suitability of the models and strategies used (carrier-phase process noise and data editing module).

Accuracies of 50-60 cm have been attained with the already available broadcast ephemeris, and 15 cm with a dedicated world wide network of stations transmitting corrections to the spacecraft with a permanent communication link (using WARTK or GDGPS). As said, this would lead to an open problem of how to provide this link, but the scope of this chapter is restricted to assess the accuracy that could be reached with this kind of link. A possible option could be the use of geostationary satellites to act as transponders, as NASA/JPL TASS system (TDRSS Augmentation Service for Satellites), which is planned to continuously broadcast the GDGPS corrections to satellites up to an altitude of 1000 km [Bar-Sever et al., 2004].

Another relevant aspect covered is the difference between single- and dual-frequency receivers. The L_1 GRAPHIC combination results are only mod-

erately worse than the ones obtained with the ionospheric-free carrier-phase combination (that needs both frequencies). This is of particular importance as single-frequency receivers would contribute to notable resource savings in the spacecraft, specially for low-budget and small satellites (with stricter requirements of volume, mass and power consumption).

The order and degree of the gravity field is a key parameter in computational load, and it should be chosen with care. The orbital altitude of the spacecraft should determine a reasonable option.

Chapter 3
Maneuver handling
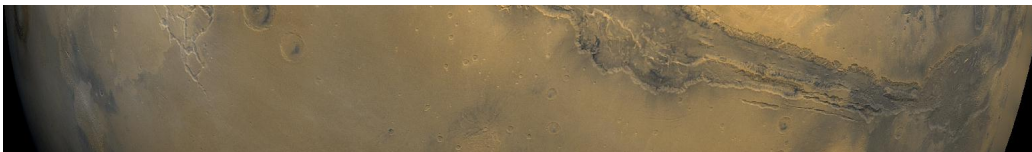
There is no harm in doubt and skepticism,
for it is through these that new discoveries are made.
Richard Feynman

Following the path of satellite autonomous navigation, this chapter is focused on maneuver handling. When a spacecraft begins a maneuver, its trajectory starts to diverge from the one that would have followed if it was only affected by the external forces taken into account in the previous chapter. The chosen approach has been to introduce a dual switch mode between dynamic and kinematic positioning. The first part of the chapter will explore the technique, providing details on how to do the switch. The second will validate the method for a set of selected maneuvers of GRACE mission.

3.1   Introduction

Once Earth orbiters have reached its nominal orbit, they follow it for some time, but orbital perturbations cause the satellite to drift from this original trajectory and suffer from orbit decay. Thence, it becomes necessary a way to compensate these perturbations and keep the satellite in its mission nominal orbit. This task is called *stationkeeping* and is accomplished by the onboard thruster system. These orbital maneuvers are very short in relation to the orbital period, and as such, can be treated as an instantaneous velocity increment Δv, or as a continuous thrust. For longer maneuvers a more detailed model has to be applied taking into account the variation of mass

---

Heading image: Mars surface. Detail of Valles Marineris.

along the burn (such as orbital transfers with large boosts that are applied to reach the final spacecraft orbit).

This velocity increment, delta-v is a measure of the requirements of propellant for propulsive tasks and orbital maneuvers over the phases of a space mission. Table 3.1 shows the typical delta-v needs for several kind of maneuvers.

Table 3.1: *Typical delta-v needs for several kind of maneuvers.*

Maneuver	delta-v
LEO launch	9.5 km/s
LEO drag compensation at 400-500 km	<100 m/s per year max
LEO drag compensation at 500-600 km	<25 m/s per year max
LEO drag compensation at >600km	<7.5 m/s per year max
LEO to GEO transfer orbit	4.2 km/s
GEO station-keeping	50-55 m/s per year

3.2 Spacecraft propulsion

The purpose of a propulsion system is to change the velocity of a spacecraft in order to achieve the delta-v goal for a specific maneuver. Since delta-v goal is harder to attain in more massive spacecraft, it is used the platform independent measure of impulse (with units of force by time). So the goal of a propulsion method is to create an impulse.

The efficiency of a propulsion system is given by the specific impulse, which is defined as the impulse per unit of weight-in-Earth (designated as I_{sp}). The unit for this value is seconds and the higher it is, the more efficient the propulsion system is. A spacecraft with high specific impulse can achieve the same impulse with lower propellant consumption. Tsiolkovsky rocket equation [Tsiolkovsky, 1903] relates delta-v with specific impulse:

$$\Delta v = -I_{sp}g_0 ln(\frac{m_0}{m_1}) \tag{3.1}$$

where g_0 is the gravitational acceleration on Earth's surface, m_0 the initial total mass including propellant used and m_1 the final total mass. If the delta-v requirements are too demanding, there will be a high need of propellant mass, thus increasing the total spacecraft mass and decreasing the

relationship payload to total mass. Thrusters with good specific impulse will need less propellant for the same delta-v, and thus increase mass efficiency.

Table 3.2 provides information on different kind of propulsion methods. Stationkeeping tasks are usually accomplished by highly efficient (high I_{sp}) thrusters, such as the Ion thruster or the HET.

Table 3.2: *List of various propulsion methods, its I_{sp} and the thrust that can achieve expressed in Newtons.*

Propulsion method	I_{sp} (s)	Thrust (N)
Solid thruster	100-400	10^3-10^7
Hybrid thruster	150-430	<0.1-10^7
Monopropellant thruster	100-300	0.1-100
Bipropellant thruster	100-480	0.1-10^7
Resistojet thruster	200-600	10^{-2}-10
Hall effect thruster (HET)	820-5000	10^{-3}-10
Ion thruster	150-8000	10^{-3}-10

3.3 Method

As said, when a spacecraft begins a maneuver a new unmodeled force appears. The delta-v will be inserted into its velocity, thus changing its orbit to a new one. Taking as basis the algorithms described in Chapter 2 a new method to allow autonomous satellite navigation in maneuvers using GPS measurements has been designed and tested. Even though the lack of bibliography available on using GPS measurements to track LEO satellite maneuvers, the method seemed a reasonable approach, and provided promising results. The steps in which it is based are:

1. Before the maneuver, the satellite navigates using the full potential of dynamic models. As seen in Chapter 2 it is possible to reach 45 cm RMS real-time positioning error with broadcast ephemeris, and 10 cm with WARTK real-time clocks (values for GRACE-A, but they are similar for the overall of analyzed spacecraft).

2. When the maneuver begins, the Kalman filter switches to a kinematic mode, where dynamic forces are not taken into account, and only GPS measurements are used in the position, and the position and velocity

propagation are replaced by an initialization with a SPP (velocity by means of Doppler measurements). This step makes use of the well determined carrier-phase ambiguities that have been obtained in the dynamic processing. The filter needs some kind of information about when the maneuver begins, though it is not necessary to have very precise timing, as it should be necessary only to activate the kinematic mode before the maneuver. It would also be possible to implement an automatic maneuver detector, which could compare a dynamic solution with a pure kinematic one, and mark as starting time the epoch when both start diverging. However the approach was tested just assuming an a priori knowledge of the starting time of the maneuver (feasible in an operational scenario).

3. Once the maneuver ends, the spacecraft starts again to behave as models predict, switching to the former dynamic mode.

The dynamic-kinematic connection (in both senses dyn-kin and kin-dyn) must be done with special care to minimize the lose of information, optimizing the achievable accuracy in the maneuver and afterwards. In this sense, the EKF in the dynamic navigation makes use of the state transition matrix ($\mathbf{\Phi}$) and process noise matrix ($\mathbf{Q}$) seen in equations 2.3 and 2.15:

$$\mathbf{\Phi} = \begin{bmatrix} \mathbf{\Phi}_{r,v} & \mathbf{S}_{C_R} & \mathbf{S}_{C_D} & \mathbf{S}_a & 0 & 0 \\ 0 & 1 & 0 & 0 & 0 & 0 \\ 0 & 0 & 1 & 0 & 0 & 0 \\ 0 & 0 & 0 & d \cdot \mathbf{I}_{3\times3} & 0 & 0 \\ 0 & 0 & 0 & 0 & 1 & 0 \\ 0 & 0 & 0 & 0 & 0 & \mathbf{I}_{n\times n} \end{bmatrix} \tag{3.2}$$

$$\mathbf{Q} = \begin{bmatrix} 0 & 0 & 0 & 0 & 0 & 0 \\ 0 & 0 & 0 & 0 & 0 & 0 \\ 0 & 0 & 0 & 0 & 0 & 0 \\ 0 & 0 & 0 & (\sigma_a^2(1-d^2)) \cdot \mathbf{I}_{3\times3} & 0 & 0 \\ 0 & 0 & 0 & 0 & \sigma_{dt}^2 & 0 \\ 0 & 0 & 0 & 0 & 0 & \sigma_b^2 \cdot \mathbf{I}_{n\times n} \end{bmatrix} \tag{3.3}$$

A pure kinematic navigation would have more simple $\mathbf{\Phi}$ and $\mathbf{Q}$ definitions:

$$\mathbf{\Phi} = \begin{bmatrix} 0 & 0 & 0 \\ 0 & 1 & 0 \\ 0 & 0 & \mathbf{I}_{n\times n} \end{bmatrix} \tag{3.4}$$

$$\mathbf{Q} = \begin{bmatrix} \sigma_{r,v}^2 \cdot \mathbf{I}_{6\times6} & 0 & 0 \\ 0 & \sigma_{dt}^2 & 0 \\ 0 & 0 & 0 \end{bmatrix} \tag{3.5}$$

where first column/row are position parameters, second, clock parameter, and third, carrier-phase ambiguities parameters. The new term $\sigma_{r,v}^2$ stands for the process noise of the positions and velocities. Normally, an approximate position and velocities are available (computed from Single Point Positioning), and $\sigma_{r,v}^2$ corresponds to a measure of their goodness.

Switching to kinematic navigation mode should be done with special care to take profit of the well determined parameters that the dynamic filter has provided. In this sense, the maximum information possible should be kept in the filter. Equations 3.6 and 3.7 corresponds to the kinematic mode after the switch (the changes in relation to dynamic equations 3.2 and 3.3 are highlighted in red):

$$\mathbf{\Phi} = \begin{bmatrix} \mathbf{0} & \mathbf{0} & \mathbf{0} & \mathbf{0} & 0 & 0 \\ 0 & 1 & 0 & 0 & 0 & 0 \\ 0 & 0 & 1 & 0 & 0 & 0 \\ 0 & 0 & 0 & d \cdot \mathbf{I}_{3\times3} & 0 & 0 \\ 0 & 0 & 0 & 0 & 1 & 0 \\ 0 & 0 & 0 & 0 & 0 & \mathbf{I}_{n\times n} \end{bmatrix} \tag{3.6}$$

$$\mathbf{Q} = \begin{bmatrix} \boldsymbol{\sigma_{r,v}^2} \cdot \mathbf{I}_{6\times6} & 0 & 0 & 0 & 0 & 0 \\ 0 & 0 & 0 & 0 & 0 & 0 \\ 0 & 0 & 0 & 0 & 0 & 0 \\ 0 & 0 & 0 & (\sigma_a^2(1-d_i^2)) \cdot \mathbf{I}_{3\times3} & 0 & 0 \\ 0 & 0 & 0 & 0 & \sigma_{dt}^2 & 0 \\ 0 & 0 & 0 & 0 & 0 & \mathbf{0} \end{bmatrix} \tag{3.7}$$

As can be seen the terms depending on the dynamic propagation, $\mathbf{\Phi}_{r,v}$, $\mathbf{S}_{C_R}$, $\mathbf{S}_{C_D}$ and $\mathbf{S}_a$, have disappeared. The position will not be propagated, but estimated epoch by epoch. A Single Point Positioning will be used to provide a first raw position (as in the pure kinematic mode) and velocity approximation. The new term $\boldsymbol{\sigma_{r,v}^2}$ stands for the process noise of position and velocity and, as before, is a measure of the goodness of the SPP estimation. The process noise in the carrier-phase ambiguity has also been removed. This has been done because that approach allowed a better GPS clock and orbit error absorption (in broadcast ephemeris), but was based in the dynamic filter smoothed position. With the kinematic approach it is preferable to have a more robust filter disconnecting this process noise during a short time span.

This kinematic switch makes use of the well determined carrier-phase ambiguities to provide better results than a pure kinematic one. In the long term, this mode will behave exactly as the pure one, because as satellite tracks are lost, and new ones are acquired, the well determined ambiguity values are slowly faded in the filter. Nevertheless the maneuvers are short compared to the GPS arcs: 10-15 minutes at most against about 40 minutes.

When the maneuver is finished, the filter switches again to a dynamic force model approach. If the maneuver has been short enough, the ambiguities would be more or less the same, empirical accelerations would show an increased sigma and the position and velocities states can be reestimated again after a convergence time. The data editing module explained in the former chapter, which provided a good way to discard faulty measurements, can not be used in the kinematic mode, as it is leant in the dynamic position estimations.

3.4 Flight data analysis

The aforementioned method has been tested with the GRACE mission, which consists on a pair of satellites (A and B) in a polar orbit at an altitude of 500 km at the beginning of its mission and at 300 km after 5 years. They are kept at a nominal distance of 220 km and its main objective is to improve the knowledge on the Earth's gravity field, and enhance the higher order parameters of the models. In order to keep the distance between both spacecraft in the mission requirements of $\pm$ 50 km [Case et al., 2004], periodic maneuvers have to be done, usually executed by GRACE-B. The SOE (Sequence of Events) file[1] records the change of state of each of both satellites, including thrusters. This file has been used to identify the days on which maneuvers took place. Table 3.3 provides the list of maneuvers that have been analyzed.

As said, Doppler measurements can be used to compute the velocity estimate with the SPP, but this measurements were not available in the GRACE receiver logged files. Instead of Doppler, in order to estimate the velocity it has been used the three previous carrier-phase measurements to compute a range rate as:

$$RR_i = \frac{11 * L_i - 18 * L_{i-1} + 9 * L_{i-2} - 2 * L_{i-3}}{6 * \Delta t} \tag{3.8}$$

Where RR_i is the range rate for epoch i, L_{i-n} is the ionospheric-free carrier-phase measurement of the n-th previous epoch, and Δt is the time increment between epochs (in particular, 30 seconds). Equation 3.8 was

---

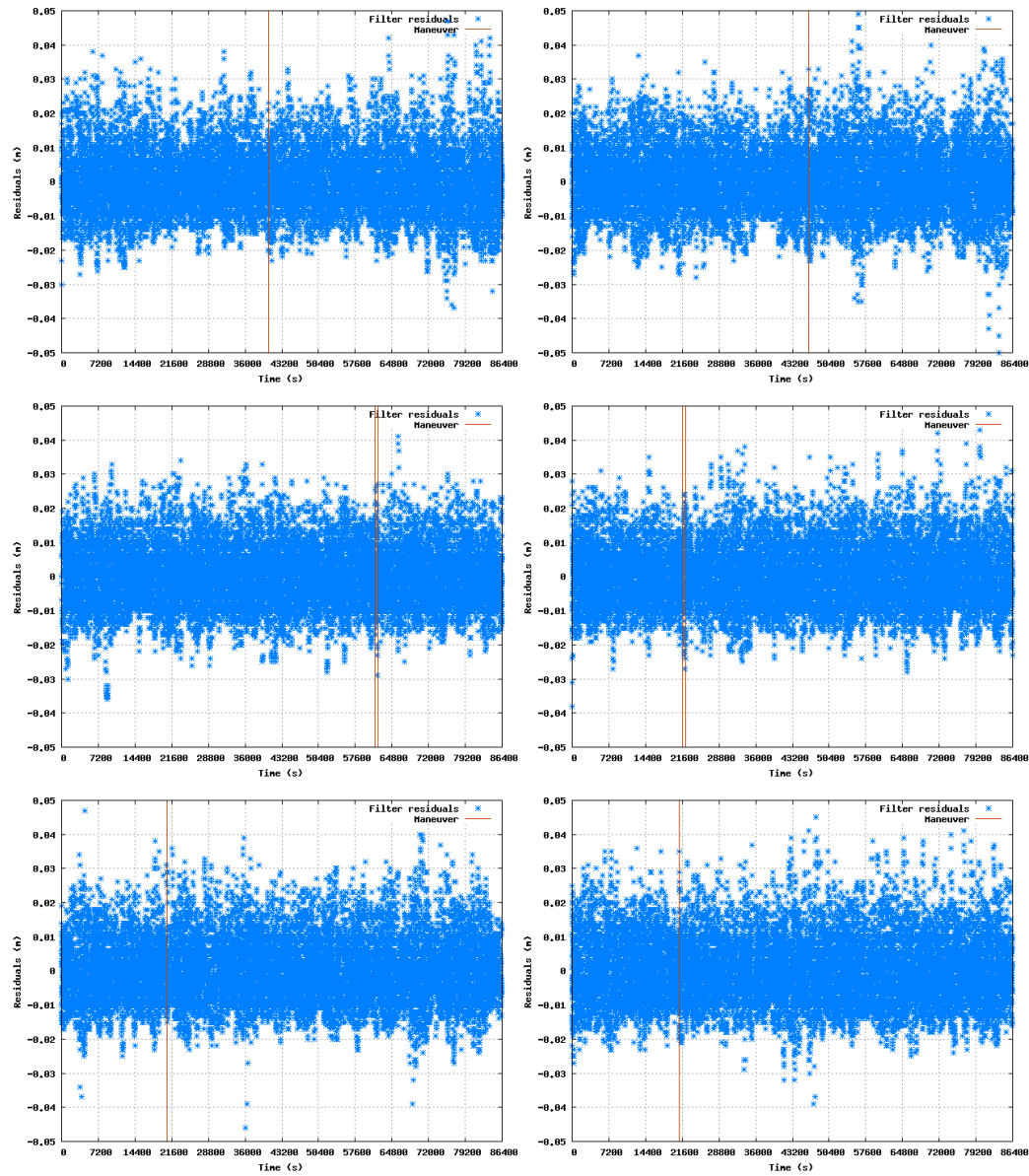[1]Available at ftp://podaac.jpl.nasa.gov/pub/grace/doc/TN-01_SOE.txt

Figure 3.1: *POD filter residuals for the different maneuvers listed in table 3.3. All the residuals are in the 2-3 cm range. Plots correspond to maneuver #1 (top-left), #2 (top-right), #3 (middle-left), #4 (middle-right), #5 (bottom-left) and #6 (bottom-right).*

Table 3.3: *List of maneuvers analyzed for GRACE-B. Timetags are given in GPS time.*

#	Year/Day	Maneuver window	Duration	Approx. delta-v
1	2007/004	11:15:35 - 11:17:01	86 s	6.5 mm/s
2	2006/011	12:52:50 - 12:53:42	52 s	8.5 mm/s
3	2005/346	17:05:44 - 17:15:55	611 s	100 mm/s
4	2005/337	05:59:35 - 06:11:03	688 s	110 mm/s
5	2005/158	05:45:10 - 05:45:38	28 s	4 mm/s
6	2005/096	05:49:20 - 05:51:29	129 s	11 mm/s

obtained deriving an equation obtained by a Lagrange interpolation of points L_i, L_{i-1}, L_{i-2} and L_{i-3} in the time corresponding to epoch i.

In order to compare the trajectory obtained with the explained method, it has been necessary to generate reference postprocessed trajectories that would take into account the maneuvers. The batch POD strategy explained in Chapter 2 has been used. Maneuvers have been included as a delta-v increment during the time the thrusters are active. For this, a fine-tuning process had to be done to put proper initial times and maneuver durations, and the delta-v is treated as an additional parameter set. Figure 3.1 shows the filter residuals of the positioning. As can be seen, they are quite stable with 8-10 mm of RMS, thus the maneuver has been properly tracked.

The maneuvers will be processed with the afore mentioned method. Two different kind of GPS orbit and clocks will be used: broadcast products and WARTK real-time clocks (plus IGU predicted orbits).

3.4.1   Results with broadcasted products

Figure 3.2 shows a day without a maneuver, but a dynamic-kinematic-dynamic switch is applied as if it existed (emulating a 10 minutes maneuver). This is used to allow comparing the position difference of the switch mode against a pure dynamic (that can be computed due to the absence of a maneuver) and is a measure of how the switch degrades the position in relation to the pure dynamic approach. The figure shows the 3D positioning error of both modes compared to the POD postprocessed positioning and the difference between both modes. As can be seen the position is slightly worsened and once the maneuver is finished the position converges again to the pure dynamic solution. The maximum difference is in the order of 80 cm and is
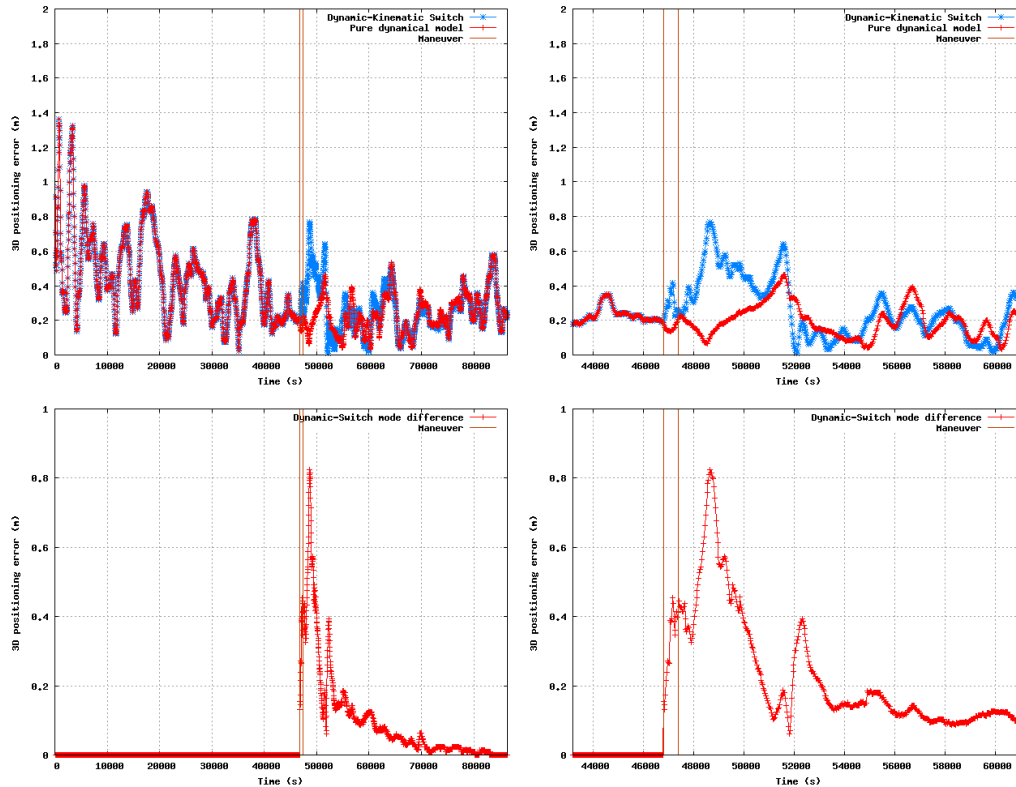
Figure 3.2: *Sample of how the switch mode behaves compared to a pure dynamic solution using broadcasted products. The data is from GRACE-B, day 10 of 2006. The marked maneuver in fact did not exist, but emulates a 600 seconds maneuver from 13:00:00 to 13:10:00. Top images are the 3D positioning error for the full day of both modes (full day -left- and zoom -right-), and bottom ones, are the difference of positions between both modes.*

kept in the range of the dynamic accuracy solution. After 5000 seconds the difference drops to values lower than 20 cm.

Figure 3.3 shows the 3D position error of the six identified maneuvers. As can be seen, the error after the maneuver is slightly increased (a peak arises just after the maneuver), but the error is kept in the general precision of the dynamic mode. As an approximation, comparing the error before and after the maneuver it is possible to limit the additional error to a maximum difference of about 1 meter.

3.4.2   Results with WARTK real-time products

In order to evaluate its use in maneuvers, WARTK real-time products have also been used in the same set of maneuvers. As expected, the results are better than with broadcast products, reaching the point that the maneuver has no noticeable impact on the positioning accuracy. Figure 3.4 shows, as in the broadcast case, a forced switch, emulating a maneuver, and compares it with the pure dynamic filter. Using these products the difference between both modes is less than 10 cm (compared to the 80 cm with broadcasted ones), which is lower than the expected accuracy attained, so the maneuver has been properly tracked by the navigation filter. The convergence time has also been reduced, up to about 4000 seconds.

Figure 3.5 shows the 3D position error of the six identified maneuvers. As can be seen, the error after the maneuver has no noticeable difference compared with the previous values.

3.5   Conclusions and discussion

This chapter has explored the handling of maneuvers by introducing a new concept of switch modes between dynamic and kinematic filters. A way to connect both modes is presented and assessed with real data from maneuvers from GRACE-B satellite for both broadcast and WARTK real-time products. The results show the suitability of the approach achieving reasonable errors for broadcast ephemeris (in relation to the normal position accuracy) during and after the maneuver (up to 1 meter), and a very good behavior for WARTK products (about 5 cm worse).

This method would not need any kind of information about the maneuver, although in the present study the beginning and end times of the maneuver are used for simplicity: this information can be approximate as far as the declared start and end times of the maneuvers are before and after the real ones. As it was said above, even an automatic maneuver detector could be

Figure 3.3: *3D positioning errors of the maneuvers using broadcasted products. In red is represented the positioning error of a pure dynamic filter, which as expected has a big leap in position error when the maneuver begins, these errors can reach several hundreds of meters. In blue, the switch mode shows its behavior under maneuvers. A small peak can be identified after the maneuvers, which is due to the degradation of the accuracy, but the error is kept in the general precision of the dynamic mode.*
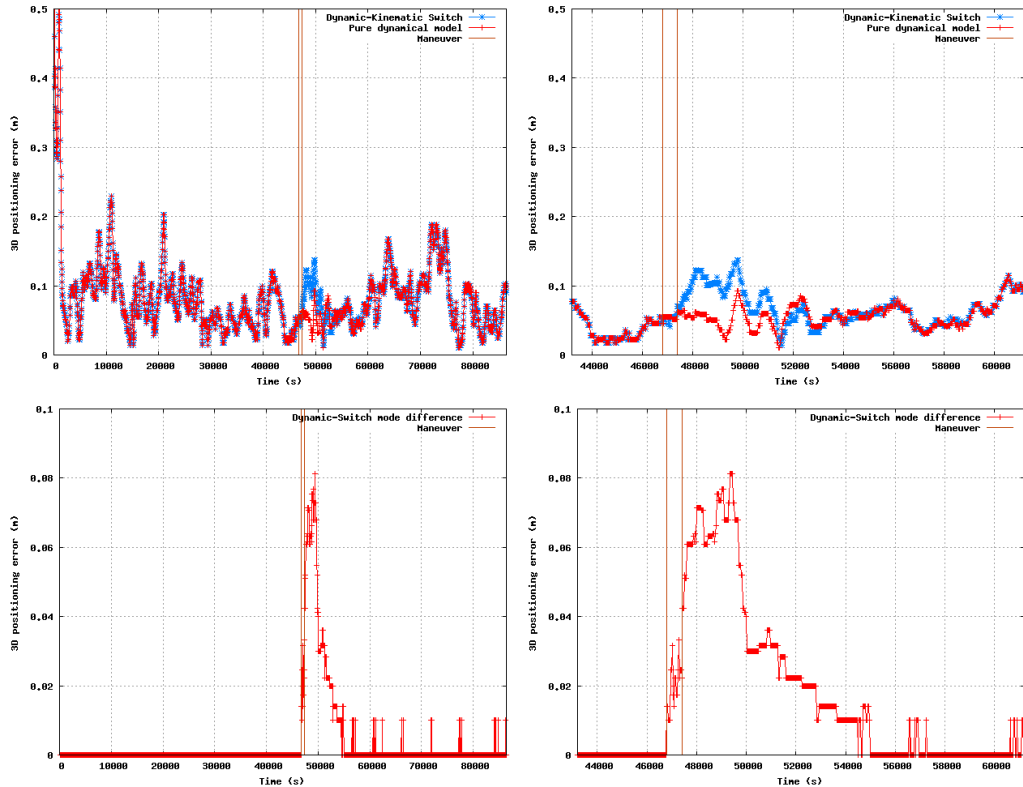
Figure 3.4: *Sample of how the switch mode behaves compared to a pure dynamic solution using WARTK real-time products. The data is from GRACE-B, day 10 of 2006. The marked maneuver in fact did not exist, but emulates a 600 seconds maneuver from 13:00:00 to 13:10:00. Top images are the 3D positioning error for the full day of both modes (full day -left- and zoom -right-), and bottom ones, are the difference of positions between both modes.*
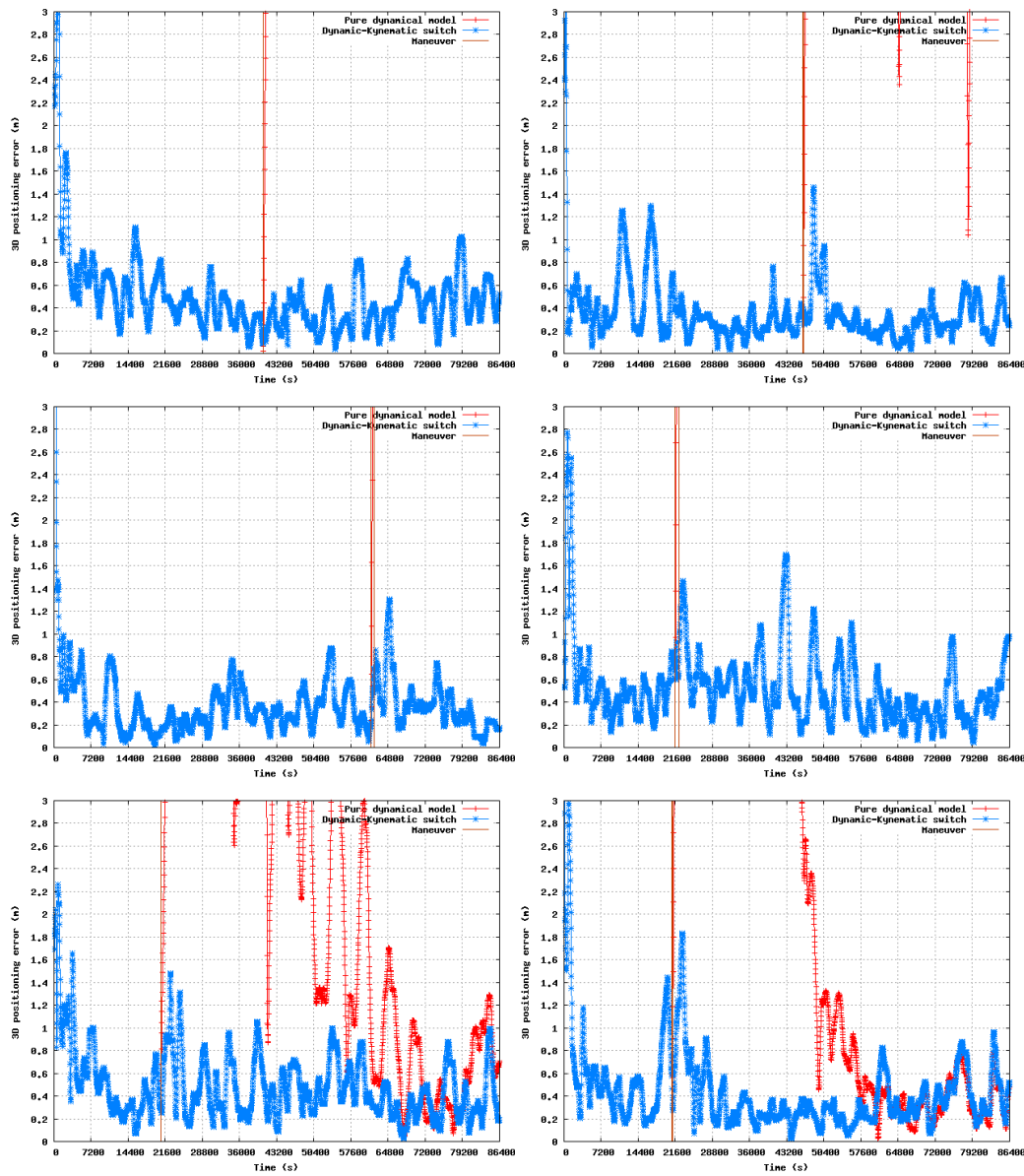
Figure 3.5: *3D positioning errors of the maneuvers using WARTK real-time products. In red is represented the positioning error of a pure dynamic filter, which as expected has a big leap in position error when the maneuver begins, these errors can reach several hundreds of meters. In blue, the switch mode shows its behavior under maneuvers.*

implemented, making it fully independent from any kind of external infor-
mation.

   Another possible approach to handle maneuvers is to keep the dynamic
mode active during the maneuver and introduce a new set of parameters: the
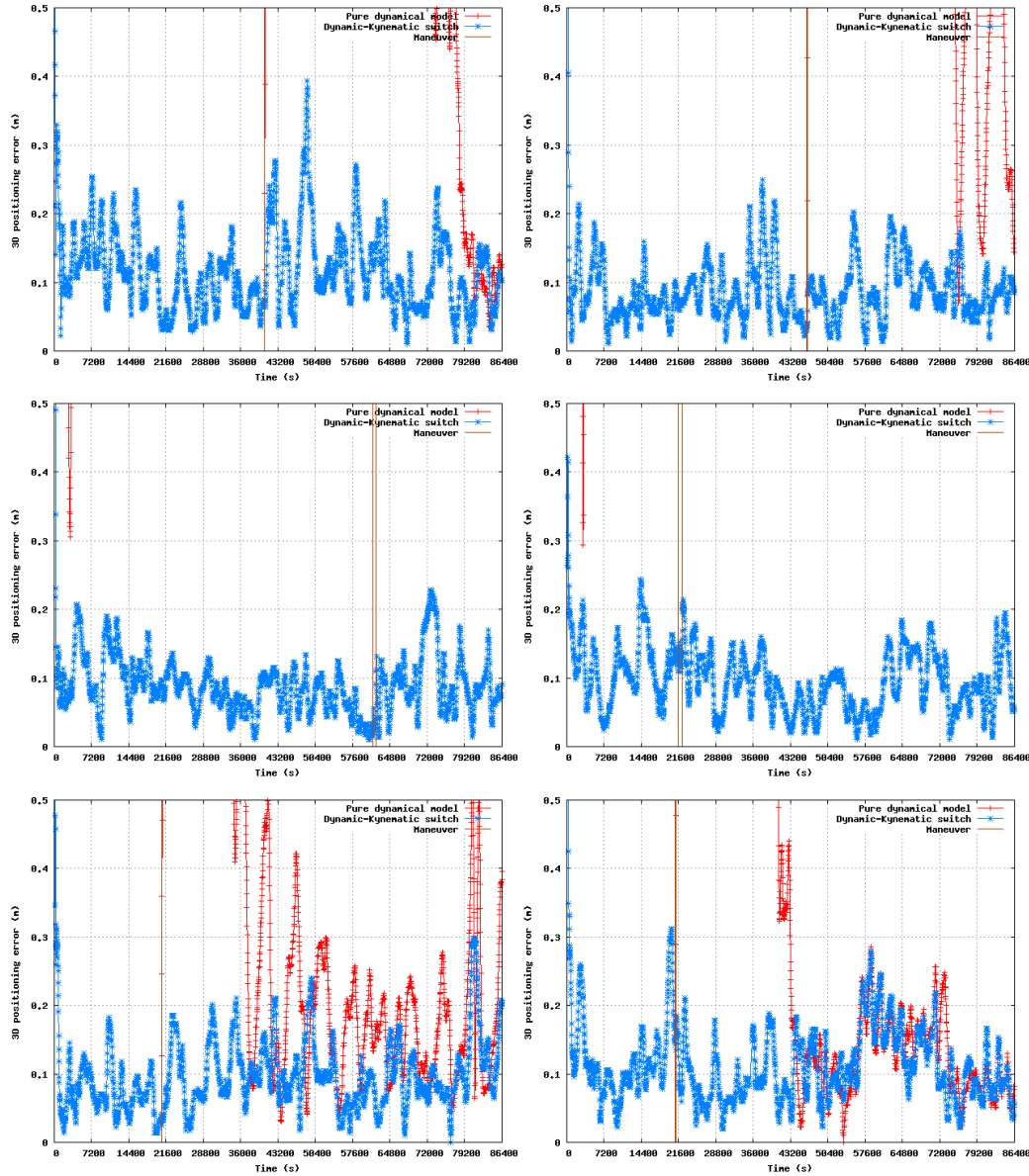delta-v components (three unknowns). This will allow to keep the dynamic
data editing module and enhance the measurement selection in the maneuver.
This will need a good knowledge of the maneuver, in particular starting and
ending times, and a good approximation of delta-v. This approximation is
needed because the delta-v would be highly correlated with the empirical
accelerations, thus needing a tighten initial value, which would be corrected
with the measurements. This approach can provide an enhancement on the
broadcast navigation reducing the peak after the maneuver at the cost of
needing additional information about it.

Chapter 4

Multipath mitigation in single-frequency receivers
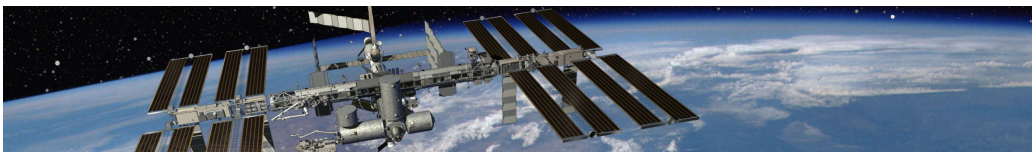
We build too many walls and not enough bridges

Isaac Newton

The benefits of multipath mitigation in spaceborne receivers has been shown in Chapter 1. Chapter 2 has been devoted to explore the benefits of dynamic modeling along with the needed simplifications to make it feasible for onboard computers. Following this line, the present chapter will investigate the benefits of multipath mitigation techniques into dynamic models. It will be shown that the technique is suited for single-frequency receivers. The first part of the chapter will provide details on the method proposed, and the second will assess its performance with real data from different missions.

4.1   Introduction

Single-frequency receivers present a more limited environment than dual-frequency ones. They are only able to use C_1 and L_1 measurements (and P_1 the military receivers), and consequently, the ionospheric-free combinations P_c and L_c cannot be formed. On the other hand, in view of the pronounced resource needs and cost of present dual-frequency receivers for space applications, the utilization of single-frequency GPS receivers in autonomous navigation may contribute to notable resource saving. This is of particular relevance in the incoming expected GNSS configuration where several satellite constellations may be available (GPS, GALILEO, modernized GLONASS...),

---

Heading image: International Space Station artistic image.

and it could be more desirable tracking more satellites using only one frequency. Besides, nano and picosatellites (with strict requirements of volume, mass and power consumption) would greatly benefit from a precise single-frequency navigation. On the other hand, the International Space Station (ISS) is equipped with two single-frequency GPS receivers. The exclusion of dual-frequency receivers was not due to any technological reason, but because the ISS partners rejected the use of semicodeless tracking of the encrypted military signal ([Gomez, 2002]). More details on the ISS will be commented in the section 4.4.

The GRAPHIC combination G_1 is specially well suited for single-frequency receivers, as it is able to remove the ionospheric effect with the drawback of using a measurement with an unknown ambiguity (from L_1) and much more noise than L_c (from C_1):

$$G_1 = \frac{C_1 + L_1}{2} \tag{4.1}$$

Chapter 2 presented the application of dynamic models for both single- and dual- receivers. The first ones provided moderately worse results than the second ones because the additional noise affecting the GRAPHIC combination degraded the final positioning results. One important contribution of this noise is the multipath and interference effect. As seen in Chapter 1, the application of multipath maps in real time LEO pseudorange navigation lead to good improvements in position accuracy with very low computational requirements, but this technique required dual-frequency measurements.

The present chapter will explore the application of multipath mitigation techniques adapting it to single-frequency receivers.

4.2 Method

Equivalently to Chapter 1, the technique consists on two steps:

- The computation of an a priori multipath map estimation of C_1.

- To perform the real-time navigation after correcting GRAPHIC observables with the estimated map.

The a priori estimation map provides a characterization of the multipath in the Coarse/Acquisition pseudorange measurements (C_1) for a set of given directions in a spacecraft fixed reference frame (cell centers). For dual-frequency receivers, it is possible to isolate multipath by means of a

combination of C_1 and the carrier-phase measurements of both frequencies (similar to 1.4) with:

$$C_1 + \frac{f_2^2 + f_1^2}{f_2^2 - f_1^2} \cdot L_1 - \frac{2f_2^2}{f_2^2 - f_1^2} \cdot L_2 = MP_{C_1} + B \tag{4.2}$$

where f_1 and f_2 are the frequencies of both signals, L_1 carrier-phase measurements on f_1, L_2 on f_2, and B stands for the ambiguity, which receives contributions from both L_1 and L_2. Carrier-phase multipath has been neglected in front of MP_{C_1}.

The ambiguity is kept constant along each arc while no cycle-slip appear, but multipath (which strictly would be different for each measurement) can be grouped for close rays viewed in a LEO fixed reference frame due to its geometric nature (in fact, it is assigned to the closest cell center). As seen in Chapter 1, by using a batch filter it is possible to estimate these parameters.

Single-frequency receivers cannot lean on this as they do not have access to L_2. In this sense, the GRAPHIC combination is the natural option to remove the ionosphere, but this combination does not isolate multipath from the rest of the parameters (geometry, clocks...), so in single-frequency receivers the former approach is no longer possible. In this case, the map is obtained by a POD estimation using G_1. Gathering the filter residuals and grouping them by azimuth/elevation it is possible to obtain a single-frequency map. This map will absorb all geometric dependant errors, such as: multipath, interferences coming from other antennas, or even phase center variations.

When the map is finished, it is uploaded to the satellite. The onboard real time processing uses G_1 and the a priori multipath map estimation, applying the proper correction to each measurement (i.e. depending on the incoming direction of the ray).

As explained in Chapter 1 this map will absorb not only multipath errors, but also interferences from cross-talk with other GPS antennas anchored to the spacecraft, and even Phase Center Variations.

4.2.1 A priori multipath map estimation

The process to obtain the multipath map with single-frequency measurements can be divided in different steps:

1. POD estimation using G_1 for a long set of days (30 to 50) with a reduced dynamic model approach using precise GPS products. This attains an accuracy of about 10-20 centimeters depending on the satellite (details on table 4.1). Next section will provide details on the POD strategy.

2. Each daily processing provides the filter residuals of each G_1 measurement and the elevation and azimuth of its incoming directions.

3. The residuals of all the days (which can be mainly interpreted as multipath related signatures) are merged and grouped by elevation/azimuth forming the cell centers, with a resolution of 1x1 degrees.

4. For each cell center the residuals mean and standard deviation values are computed. The mean value will form directly the multipath map and the standard deviation map. This second map, is in fact used in the filter as weights for each observation (weight map). This weighting approach has shown to further improve the positioning accuracy, as it provides an estimation for the filter of the goodness of the multipath correction. If the receiver provides CN_0 data, this weight map could be used to calibrate the relationship between CN_0 and noise level for each measurement, and use this calibration for weighting instead of the full map.

The use of the filter residuals to extract the map makes this kind of estimation very affected by the positioning accuracy (contrary to the dual-frequency one, which is completely independent as the multipath is isolated from the range measurements and clock errors). Part of the multipath information shall be partially absorbed by the filter parameters, mainly the GRAPHIC ambiguity, which will be the same for each GPS arc (consequently if multipath does not have zero mean in the arc, its effect will be partially absorbed by the ambiguity). As the real time processing also uses G_1, the effect of this kind of correlation will be reduced, because it will also be necessary to compute an ambiguity parameter. This map should be used with special care into a pseudorange only filtering (no ambiguity in the measurements used).

When the 1x1 map is obtained it is possible to create, through a Self-Organizing Neural Network, an adapted map with less centers. This map use less parameters to properly characterize the multipath environment and make feasible a real time map updating. This will increase the autonomy of the satellite, as the map can last longer, and would even allow to adapt the map to changes in the connection and disconnection of other GPS antennas, which brings variations to the interference affecting the measurements (more details can be found in Chapter 1).

As a way to check the goodness of this method, figure 4.1 shows one associated map obtained in the described process against one obtained by using observations in both frequencies for SAC-C. This satellite has a BlackJack
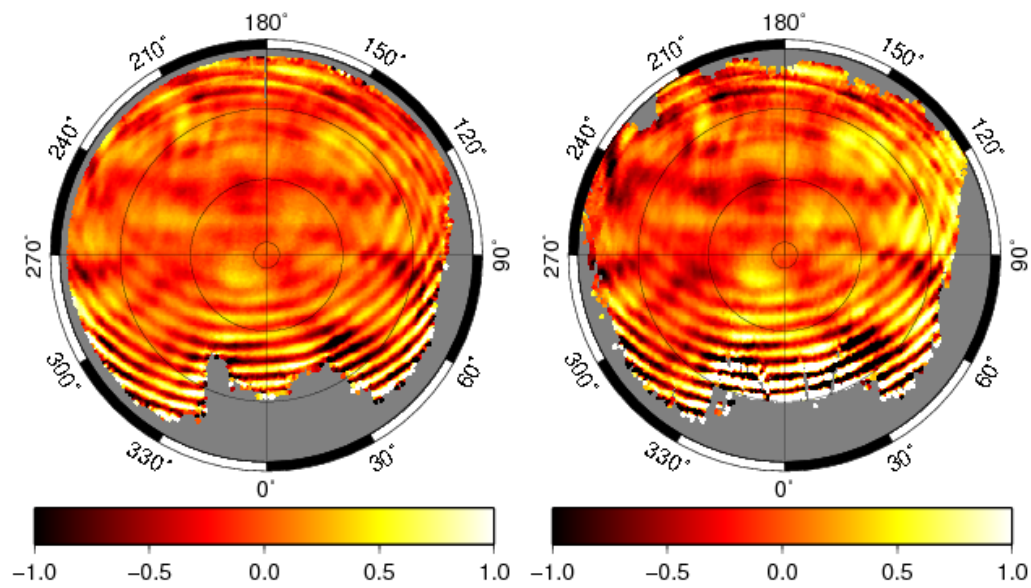
Figure 4.1: *C_1 multipath maps for SAC-C satellite using the two different techniques: single-frequency POD residuals (left) and dual-frequency batch geometric-free (right). First map is obtained by processing days 180 to 229 of 2006, and second one 220 to 224 of 2006. Both maps show clear similarities, but the first one seem to have slightly lower values, which comes from the fact that the nature of the method means that a certain part of the multipath is absorbed by G_1 ambiguity and the other navigation parameters.*

dual-frequency GPS receiver, thus allowing both kind of processing for validation purposes. It can be seen that both maps are quite equivalent, but the first one seems smoother, with lower peak values. This is probably due to the above mentioned correlation, which makes the other parameters of the filter absorb part of the multipath. It has to be taken into account that the corrections to G_1 are the half of the values shown in the map (which directly represents C_1 multipath).

4.2.2   POD strategy

The strategy followed to obtain the POD to extract the maps is very similar to the one explained in Chapter 2, but using only L_1 and C_1 measurements. In this sense, ionosphere-free pseudorange measurements have been changed to C_1 and ionosphere-free carrier-phase measurements to G_1. The observables sigma has been increased to better match the expected C_1 and G_1 noise. This increased the error compared to external references, but allowed to create a fully single-frequency postprocessing strategy.

4.2.3   Real time multipath mitigation

The followed real time strategy is explained in Chapter 2. Additionally, taking into account the spacecraft's attitude, the observables are corrected using the multipath map. The weight map is used to provide weights to the measurements in the filter when using precise GPS orbit and clocks (WARTK and final CODE). IGU and broadcast processing do not use the weight map, as the main source of error is not the multipath, so the weights are kept constant.

The weight map slightly improves the results with no additional computational load, for example SAC-C satellite obtained 35 cm of 3D RMS error positioning without using the weight map, and 30 cm using it with WARTK products; and GRACE-A results showed a RMS of 24 cm without map, and 18 cm with map. Figure 4.2 shows the corresponding sigma values for SAC-C satellite (the weight applied in the filter is computed by $W = 1/\sigma^2$).

Figure 4.3 shows an example of multipath mitigation for a carrier-phase continuous arc. G_1 minus L_c represents multipath plus an unknown ambiguity. The two lines compares the noise of G_1 before and after correcting it from multipath. The scatter of the points are reduced from a sigma of 20 to 14 cm. This improvement is expected to be translated to the positioning.
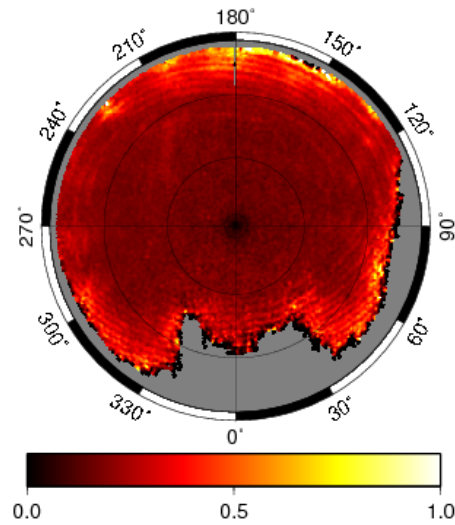
Figure 4.2: C_1 *weight map for SAC-C satellite. The values must be divided by two when using G_1 observables. The cells colored in black (representing a sigma of 0 m) are not taken into account when assigning weights in the filter. In this case, a nominal weight is used (15 cm for SAC-C). Scale is in meters.*

4.3 Flight data analysis

The method discussed above has been assessed with real data of four different satellites in order to test its effectiveness: CHAMP, GRACE-A, SAC-C and JASON satellites. Table 4.1 shows the nominal altitude of the satellites and the selected data arcs chosen for the test. All results are compared against a dual-frequency postprocess POD with precise GPS orbit and clocks at 30 seconds rate.

As in former chapters, different kinds of orbit and clock GPS products have been used: broadcasted ephemeris, IGS ultrarapid predicted, real time GPS clock estimation (WARTK) and precise final products.

For each of the satellites and products there are three different runs:

- Dual-frequency carrier-phase L_c navigation.

- Single-frequency unmitigated G_1 navigation.

- Single-frequency multipath mitigated G_1 navigation.

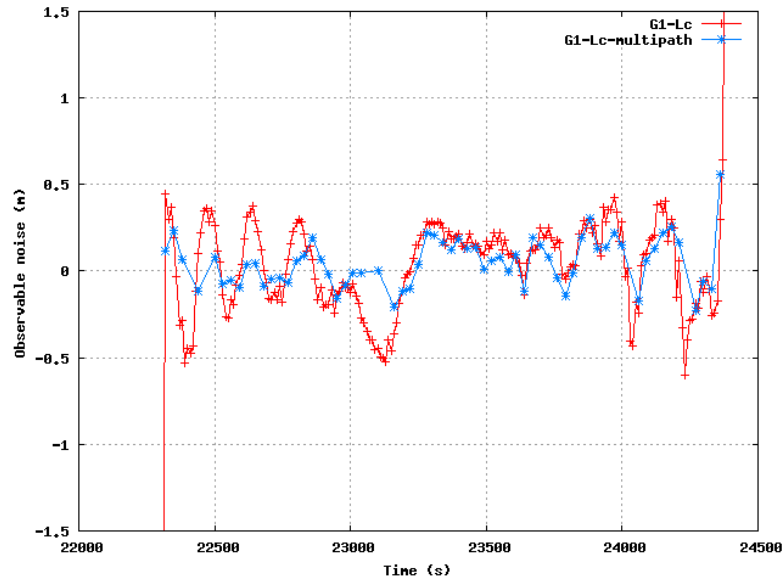**Figure 4.3:** *Comparison of the noise in G_1 for a GPS arc. The sigma of the arc is reduced from 20 to 14 cm when using the multipath map. Data is from 28th of August of 2006 for SAC-C satellite and GPS PRN 10.*

Dual-frequency carrier-phase navigation is computed for comparison purposes, because the maximum expected accuracy that could provide the mitigation of multipath would be the one given by this dual-frequency.

Figure 4.4 shows the C_1 multipath maps computed for each satellite. As said, the corresponding G_1 correction will be the half of these values. The maps are quite similar to the ones obtained by [Montenbruck and Kroes, 2003] for CHAMP and [Kroes, 2005] for CHAMP and GRACE-B (with great similarities to GRACE-A). Table 4.2 gives the 3D RMS positioning errors obtained comparing the different runs corresponding to dual-frequency carrier-phase navigation (first column), single-frequency G_1 navigation (second column) and single-frequency multipath mitigated G_1 navigation (third column). The improvement percentage of using multipath mitigated observables in relation to unmitigated ones is shown in forth column. The second percentage (fifth column) is the improvement of multipath mitigation in relation to the dual-frequency solution, i.e. taking into account that the maximum accuracy is given by the L_c navigation (no pseudorange multipath). A 100% in this column would mean that single-frequency multipath mitigated G_1 navigation behaves exactly as a dual-frequency carrier-

Table 4.1: *List of spacecraft used along with its nominal altitude. Multipath data column lists the days that were used to generate the multipath and weight maps. Navigation data arcs lists the days that the real time algorithm was applied to. Last column shows an estimation of the error for the single-frequency POD used to compute the map (compared to the dual-frequency POD reference solution). All data arcs are from 2006.*

| Spacecraft | Altitude | Data arcs (days of year) | | Accuracy of |
		Multipath	Navigation	single-freq POD
CHAMP	350 km	50-99	100-150	14 cm
GRACE-A	460 km	180-229	230-280	10 cm
SAC-C	700 km	180-229	230-260	10 cm
JASON	1350 km	100-129	130-150	12 cm

phase positioning.

Different levels of success in 3D position enhancements have been achieved depending basically on the multipath (and interference) environment of the satellite and on the GPS products used. In this sense, broadcasted products are, in general, the main error source, as can be seen in its results. Only SAC-C satellite had noticeable improvements when using these products with a 13% improvement (after the correction all satellites where between 50cm and 65cm of 3D RMS error) comparing to single-frequency G_1 unmitigated positioning. When using real-time WARTK clocks, the multipath became an important factor, and the improvement increased to a range between 9% and 40% (obtainin gbetween 15cm and 30cm of 3D RMS error).

4.4 International Space Station

A specially well suited environment to test the method presented in the chapter is the GPS receivers mounted in the International Space Station (ISS). The two ISS GPS receivers (located in the U.S. lab) are connected to four different antennas (see figure 4.5) and receive very high multipath contributions due to the large metallic structures that surrounds them, such as various solar panels, thermal radiators, communications antennas, and many attached payloads. [Gaylor et al., 2003] studied through simulations the multipath and signal blockage on the ISS and showed multipath errors of up to 20 m in pseudorange and 2 cm in carrier-phase measurements. Besides,
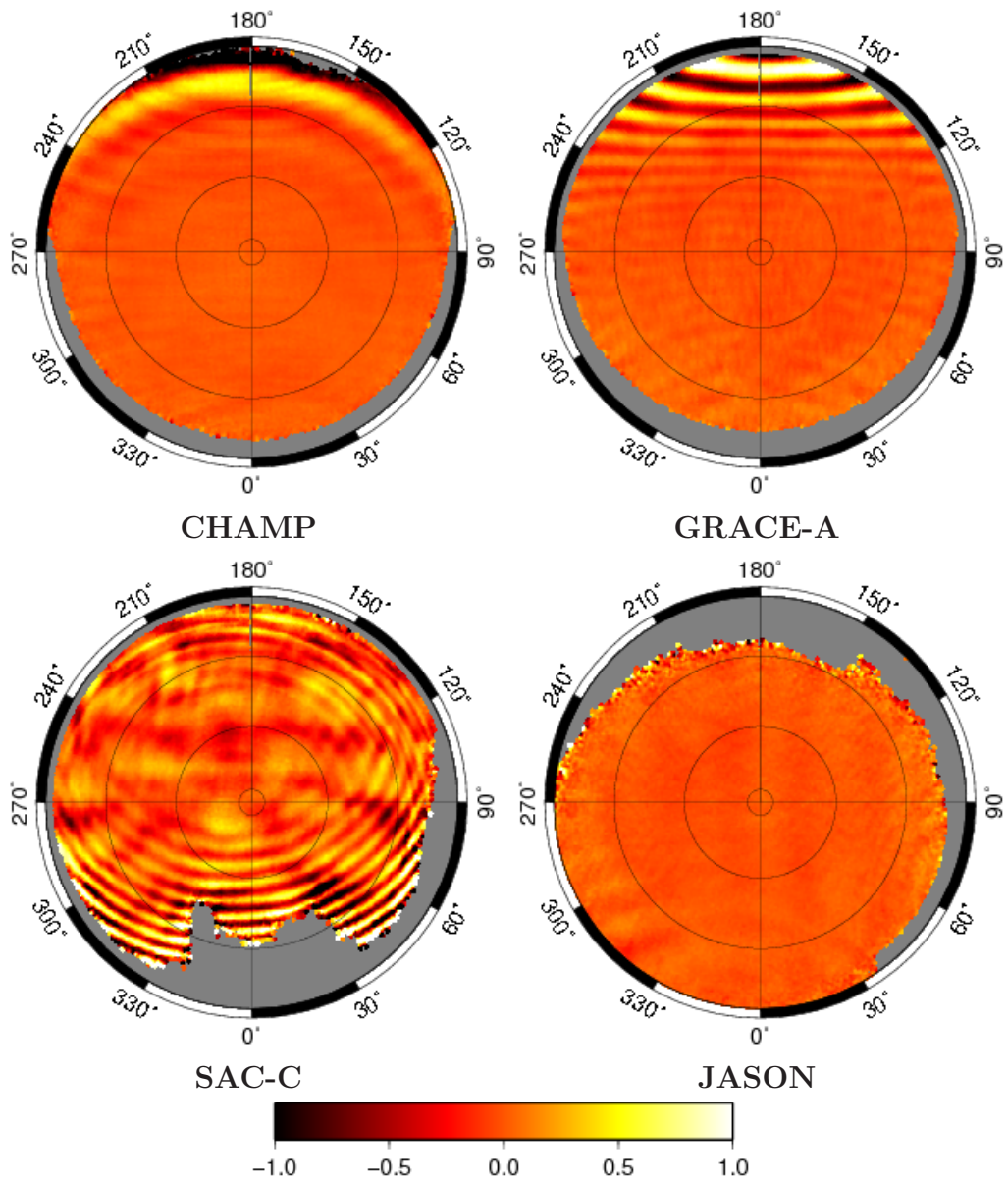
Figure 4.4: C_1 *multipath and interference maps obtained using the single-frequency method for all satellites. The waves are due to interference cross-talk between other GPS antennas. Scale is in meters.*

Table 4.2: *Summary table for the achieved accuracies in 3D RMS positioning errors for all the satellites, GPS products and combinations used. First column (2F) are the results using the full capabilities of dual-frequency receivers, second (1F) using only the first frequency, third (1F MM) using the first frequency and applying the multipath and weight maps, forth (MM %) is the improvement percentage of 1F MM versus 1F, and fifth (MM %-2F) is the improvement percentage of 1F MM taking into account that the maximum attainable accuracy is given by 2F. S/C stands for spacecraft.*

S/C	Orbit & clock products	3D RMS positioning error (cm)				
		2F	**1F**	**1F MM**	**MM %**	**MM %-2F**
CHAMP	Broadcast	61.6	67.5	**66.6**	**1.3%**	15.3%
	IGS predicted	46.6	52.5	**51.8**	**1.3%**	11.9%
	RT WARTK	13.7	24.0	**20.5**	**14.6%**	14.9%
	CODE	10.1	21.5	**18.3**	**14.9%**	28.1%
GRACE	Broadcast	45.0	51.0	**50.0**	**2.0%**	16.7%
	IGS predicted	28.4	36.4	**35.5**	**2.5%**	11.3%
	RT WARTK	10.2	25.7	**17.9**	**30.4%**	50.3%
	CODE	8.3	23.7	**15.9**	**32.9%**	50.7%
SAC-C	Broadcast	45.6	66.7	**58.0**	**13.0%**	41.2%
	IGS predicted	31.0	60.7	**45.5**	**25.0%**	51.2%
	RT WARTK	14.9	51.1	**30.4**	**40.5%**	57.2%
	CODE	12.8	49.9	**29.5**	**40.9%**	55.0%
JASON	Broadcast	49.2	57.7	**57.5**	**0.4%**	2.4%
	IGS predicted	40.7	45.9	**44.9**	**2.2%**	19.2%
	RT WARTK	17.5	28.2	**25.6**	**9.2%**	24.3%
	CODE	14.9	26.7	**24.2**	**9.4%**	21.2%

ISS partners rejected the usage of the semicodeless tracking of the encrypted
military signal and required to use a single-frequency receiver. That would
make the ISS a perfect target for assessing the method, unfortunately ISS
GPS data is not available to general public, and efforts were made to obtain
some data of the station but none of the attempted ways were successful.
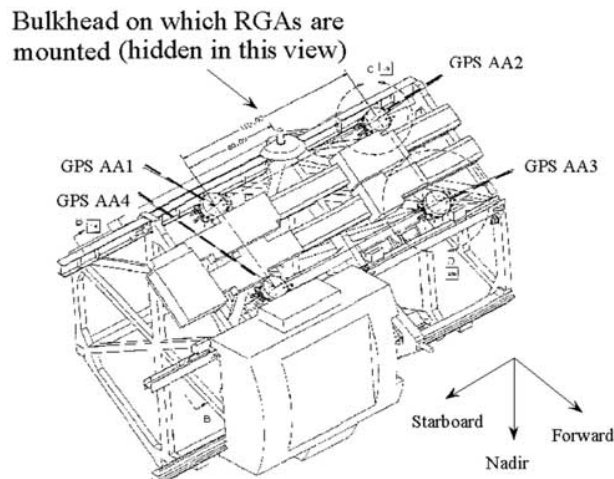More details on the GPS onboard the ISS can be found on [Gomez, 2002].

Figure 4.5: *View of the GPS antennas on the ISS.*

4.5 Conclusions and discussion

This chapter has presented a technique to enhance single-frequency satellite
autonomous navigation by means of a multipath/interference map, approach-
ing its position accuracy to the one that a dual-frequency GPS receiver can
reach. The method has been assessed with four different satellites with dif-
ferent levels of success. Broadcasted products have already very similar per-
formances processing with one or two frequencies, as the main error source
is the quality of the GPS orbits and clocks. In this case, there is very little
room for improvement, attaining only noticeable results for SAC-C satel-
lite, which has an important multipath/interference environment (up to 13%
of improvement, in relation to unmitigated navigation, and reaching almost
half-way between the accuracy of dual- and single-frequency navigation).

   Remarkable results are found when the more precise RT-WARTK prod-
ucts are used (or equivalently, other similar real time GPS clock estimations,
such as JPL GDGPS). Enhancements of 40% have been reached in the noisy

environment of the SAC-C satellite (57% comparing to dual-frequency "maximum attainable accuracy"), and even 9% in the low multipath environment found on JASON (25%). Mid range GRACE-A and CHAMP obtained quite good results of 30% and 15% respectively (50% and 30% compared to dual-frequency).

Unfortunately the availability of GDGPS products is still an open problem in a space environment, as it would need a permanent communication link with the satellite. Nevertheless, this method could also be usable in near real time orbit determinations, where the satellite downlinks every 2-3h its receiver collected data, and a ground station can obtain a quick estimation of the satellite positions. In this case, the permanent communication link would not be necessary.

Conclusions

> *It is difficult to say what is impossible,*
> *for the dream of yesterday is the hope of today*
> *and the reality of tomorrow*
> Robert Goddard

This doctoral thesis has proposed different algorithms and methods to be used in a LEO satellite autonomous real time GPS navigation. Most of the current works dealing with LEO positioning are restricted to postprocessing solutions. Onboard space applications must take special care with computational requirements and dependence on external data, which may be unavailable for the satellite. The thesis has tackled the problem in different "dimensions" trying to provide, as a whole, an entire feasible solution allowing a continuous trajectory estimation with the utmost accuracy. The particular covered aspects in the thesis have been the following ones:

- Multipath and interference mitigation.

- Dynamic force models.

- Maneuver handling.

Key points, a summary of the achieved navigation accuracies and final conclusions are discussed in the following sections.

Heading image: Sunrise over the pacific ocean. Picture taken from the ISS.

Multipath and interference mitigation

Chapter 1 shown the feasibility for real-time navigation of multipath and interference mitigation techniques based on a hybrid approach:

- *A priori* on ground multipath map estimation.

- Real time navigation correcting the pseudorange observables with the expected multipath by selecting the proper cell in the map.

Improvements in the 3D RMS positioning accuracy of 40%-50% for SAC-C (achieving errors of about 90 cm) and of 25%-35% for CHAMP (achieving errors of about 70 cm) were obtained in real data flight tests using precise GPS clock and orbits.

Neural networks allowed to decrease the number of parameters to characterize the multipath environment of the satellite. This reduction of parameters would be of special interest to allow a real time updating of the map. Adapting the map to new changes in the satellite, such as a connection/disconnection of the occultations antenna (consequently changing the interference figure), or aging effects that could slowly modify the structure reflections over time.

The work presented in Chapter 1 is mainly based in [Hernandez-Pajares et al., 2000a] and has been partially done in the frame of the ESA project *Neural Networks for Radionavigation* [Vigneau et al., 2007b]. The research done in the elaboration of this chapter has lead to:

- Two journal publications: [Ramos-Bosch et al., 2007b] and [Ramos-Bosch et al., 2007a].

- Two conference proceedings: [Ramos-Bosch, 2006] and [Vigneau et al., 2007a].

- Two awards (for [Ramos-Bosch, 2006]), a *Best Presentation Award* and a *Student Paper Sponsorship*.

Dynamic force models

Chapter 2 studied the use of dynamic models in the navigation by means of an Extended Kalman Filter. This approach increased significantly the resource requirements compared to the first one, but special care was taken to keep it in affordable levels. Besides, all the models used are not dependant

on external postprocessed products thus allowing its use in a real onboard environment.

The precision of the dynamic models are highly dependant on the spacecraft altitude (sensitive in particular to the accuracy of the gravitational model), so the selection of missions to assess the method have been splitted in a wide altitude range between 350 and 1350 km: CHAMP (350km), GRACE-A (460km), SAC-C (700km) and JASON (1350km). Moreover, several test cases have been chosen in order to explore the different processing options of the algorithms. The chosen parameters have been:

- *GPS orbit and clock products.* Broadcast, IGS predicted, real time clocks (RT-WARTK) and precise postprocessed (CODE). The readily available, broadcasted products achieved accuracies of 50-60 cm. IGS predicted ones increased the accuracy to the 30-45 cm range, at the cost of needing a periodic satellite update every 6 hours. WARTK real time clocks provided the best attainable solution with about 15 cm of error, but the trade-off is a permanent communication link to the spacecraft continuously providing GPS clocks. Final CODE products are unavailable in real time and were used for comparison purposes, attaining between 5% and 30% best results than WARTK products (10-15 cm range).

- *Measurement types.* Dual-frequency ionosphere-free pseudorange (P_c) and carrier-phase (L_c) combinations, and single-frequency GRAPHIC combination (G_1) are the main observation types considered. The benefits of carrier-phase navigation were shown in these tests. Pseudorange only filtering avoid the estimation of the carrier-phase ambiguities, but the error is greatly increased. The achieved accuracy greatly varies in terms of the satellite observable noise and multipath, and the selected GPS products. It is interesting to compare single- versus dual-frequency carrier-phase results, as G_1 processing obtains only moderately worse results than L_c (10-20% worse for broadcast products, and 40-70% for WARTK). This is of special relevance, as single-frequency receivers have lower requirements of volume, mass and power consumption, and these kind of receivers are specially well suited for small satellites with tight requirements.

- *Complexity of the gravity field model.* Decreasing the degree and order of the gravity field model reduces the computation needs, but the navigation error is increased as a function of the altitude. The closer the spacecraft to the Earth is, the more the gravity field will move away

from a perfect central force, and higher order and degree must be considered for the proper modelling of the gravitational acceleration. The lower altitude range satellites (CHAMP and GRACE-A) offer good results with a 70x70 gravity field degree and order, while a 50x50 model is enough for the mid range SAC-C. The highest orbit satellite, JASON, show excellent results with the reduced 30x30 model.

A novel data editing module to discard faulty measurements and detect cycle-slips was also implemented and tested, providing excellent outlier detection capabilities with low computational requirements. The data edition is based in studying the residuals before the filter, estimating a first approximation of the receiver's clock, and discarding the measurements with large deviations. This data editing is strongly leant to the dynamic filtering, as it makes use of a predicted position for each epoch.

In order to reduce the GPS clock and orbit errors of broadcast and IGS predicted products, a small quantity of process noise was introduced in the Kalman filter for the carrier-phase ambiguities. This increased the accuracy by about 30-40% by absorbing part of the slow varying errors of the GPS clock and orbits.

Chapter 4 joined the benefits of dynamic models with multipath and interference mitigation algorithms. The combination of techniques allowed that single-frequency receivers approached their behavior to dual-frequency ones, reaching almost half-way between single- and dual-frequency navigation accuracies. In relation to unmitigated G_1 positioning, the use of the maps decreased the 3D RMS positioning error by up to 13% for the multipath-affected SAC-C satellite using broadcast ephemeris, and up to 40% for WARTK real time clocks.

The research presented in Chapter 2 and Chapter 4 has lead to a journal publication [Montenbruck and Ramos-Bosch, 2007] and a poster presentation [Ramos-Bosch et al., 2008] respectively.

Maneuver handling

Chapter 3 focused on the positioning of spacecraft while carrying out a maneuver. The ignition of satellite thrusters inserts an additional acceleration not taken into account in the dynamical models. The satellite trajectory will thence diverge from its original one. The proposed technique was to mix the benefits of both kinematic and dynamic approaches, obtaining the independence of forces of the first one, and the increase of accuracy of the second one. In this sense, a kinematic-dynamic switch mode was developed and tested.

This mode operated using the dynamic approach when the spacecraft thrusters were disconnected, switched to kinematic mode when the maneuver began, and switched back to dynamics when it finished. Special care was taken to keep the maximum information possible in the state vector and covariance matrix of the filter. The technique was assessed with maneuvers from GRACE-B satellite, obtaining a slight degradation of the positioning in the maneuver and up to 5000 seconds after when using broadcast products. Errors up to 1 meter appeared just after the maneuver in relation to before, but the general positioning error did not exceed the typical errors for broadcast navigation. When using the more precise WARTK real-time products unnoticeable errors were obtained during and after the maneuver (up to 8 cm of difference).

Final summary and discussions

The scope of this doctoral thesis has been to contribute to satellite autonomous navigation. The optimal configuration for a spacecraft would greatly depend on several characteristics, such as its altitude mission, the available resources, the required accuracy and its computational capabilities.

Besides, several kind of GPS products have been analyzed. For spacecraft with high requirements in position accuracy, a sort of real time clock estimations from a network of ground stations would be needed. A possible option to achieve this could be by means of a network of High Earth Orbiters consisting of GEOs covering the mid latitude range, and high elliptical satellites covering the poles. This network of satellites could act as transponders for the ground corrections, providing a global communication coverage for almost any kind of LEO orbit. In fact, JPL GDGPS orbit and clocks provide these data at a rate of 352 bps, which would be suitable for broadcasting it from a space platform.

Appendix A

GPS fundamentals

Advances are made by answering questions.
Discoveries are made by questioning answers.
Bernhard Haisch

This appendix describes the fundamentals of the Global Positioning System, which is the most extended satellite navigation system used so far. More information on the GPS system can be found at [Hernandez-Pajares et al., 2001] and [Parkinson, 1996a].

System description

GPS is divided in three blocks:

- *Space segment:* Consists of at least 24 satellites distributed in 6 orbital planes, with an inclination of 55 degrees referred to the equator. The satellites are orbiting at about 20000 km from the Earth's surface, and have a period of 12 sidereal hours. These satellites are passive emissors of the signals which are used afterwards by any GPS receiver to estimate its position.

- *Control segment:* Consists of a network of ground stations, whose functions are:

  - Control and keep the status and configuration of the satellite constellation.
  - Predict satellites ephemeris and onboard clock evolution.

Heading image: Detail of a GPS satellite belonging to block IIF.

– Keep the GPS time scale.

– Periodical update of the navigation message broadcasted by the satellites.

• *User segment:* Consists of all the users of the system. The GPS receivers gather the GPS signal from the satellites and solve the navigation equations in order to obtain its own coordinates and clock error.

GPS observables and modeling

The observables are the direct measurements of the GPS system, there are five different observables which are sent in two different frequencies (f_1 at 1.57542 GHz and f_2 at 1.2276 GHz, with $\lambda_1 \approx 19.03cm$ and $\lambda_2 \approx 24.42cm$):

• *Coarse/Acquisition code (CA):* Also known as civil code, it is sent on the first carrier at f_1 and is available for all the receivers. It is a direct measure of the apparent distance between the receiver and the transmitter. Due to political decisions (mainly due to the appearance of new GNSS constellations), some GPS satellites are being launched with the CA code also available in the second carrier at f_2. The first of these satellites was deployed the 26th of September of 2005.

• *Precision codes (P_1 and P_2):* The precision code (called P_1 the one sent in f_1, and P_2 the one in f_2) is restricted to militar use only and is more precise than the CA code. Anyway, present GPS receivers are able to measure indirectly estimates of P_1 and P_2 pseudoranges, which are anyway noisier than the originals.

• *Carrier signal phase (L_1 and L_2):* This observable is, basically, the integrated observed doppler effect on the measured carrier since the time-of-lock of the given satellite. This measurement is much more accurate than the CA, P_1 and P_2, but has an ambiguity (the pseudorange at the time of lock).

Pseudorange measurements

Pseudorange measurements are: CA, P_1 and P_2. They are obtained measuring the travel time of the signal and multiplying it by the speed of light. These provide an apparent range between the satellite and the receiver that does not fit perfectly with its geometric distance due to several factors, such as: synchronism errors between receiver and satellite clocks, ionospheric and

tropospheric delays on the signal, relativistic effects on the satellite clock... Taking into account the most important terms, the pseudorange can be written as (where P represents CA, P_1 or P_2):

$$P_i^j = \rho_i^j + c(dt_i - dt^j) + rel_i^j + T_i^j + \alpha_f I_i^j + K_i^j + M_{P,i}^j + \epsilon_{P,i}^j$$

being,

- ρ_i^j is the geometric range between the satellite j and the receiver i at emission and reception time, respectively ($\sim$20000Km).

- c is the speed of light (299792458 m/s is the standard in GPS system).

- dt_i is the offset of the receiver i from GPS time ($<$300Km).

- dt^j is the offset of the satellite j from GPS time ($<$300Km).

- rel_i^j is the relativistic effect ($<$13m).

- T_i^j is the tropospheric effect (2-10m).

- I_i^j is the ionospheric effect, which can be expressed in first order (more than 99.9% of the total effect) as: $\alpha_f = 40.3/f^2$ (2-50m).

- K_i^j is the satellite and receiver instrumental delays, also called Total Group Delay or TGD ($<$2m).

- $M_{P,i}^j$ is the effect of multipath ($<$15m).

- $\epsilon_{P,i}^j$ is the thermal noise and other unmodeled sources of errors (3m).

Carrier-phase measurements

Carrier-phase measurements are: L_1 and L_2. Can be written as (where L represents L_1 or L_2):

$$L_i^j = \rho_i^j + c(dt_i - dt^j) + rel_i^j + T_i^j - \alpha_f I_i^j + B_i^j + w_L + m_{L,i}^j + \epsilon_{L,i}^j$$

Where, among the notation introduced in the previous expression:

- w_L is a term due to the relative rotation of the transmiting and receiving antennas. Known as wind-up, the direct consequence of this effect is that spinning the antenna is understood by the receiver as an apparent variation of distance between satellite and receiver ($<$20cm).

- B_i^j is the ambiguity term, including the carrier-phase instrumental delays ($\sim$20000Km), this value is kept constant while the receivers keeps track of the GPS satellite.

- $m_{L,i}^j$ is the effect of multipath. This effect is much smaller than pseudorange multipath ($<$2cm).

- $\epsilon_{L,i}^j$ is the thermal noise and other unmodeled sources of errors. Also much smaller than pseudorange $\epsilon_{P,i}^j$ ($<$1cm).

Observable combinations

Starting from the basic measurements it is possible to define a set of linear combinations between them, which present certain advantages:

Ionospheric free combinations

First order ionospheric effect (describing more than 99.9% of the total effect) depends on the square of frequency ($\alpha_i = 40.3/f_i^2$). This allows its cancellation by means of these combinations:

$$P_c = \frac{f_1^2 P_1 - f_2^2 P_2}{f_1^2 - f_2^2}$$
$$L_c = \frac{f_1^2 L_1 - f_2^2 L_2}{f_1^2 - f_2^2}$$

Obtaining:

$$P_{ci}^j = \rho_i^j + c(dt_i - dt^j) + rel_i^j + T_i^j + M_{Pc,i}^j + \epsilon_{Pc,i}^j$$
$$L_{ci}^j = \rho_i^j + c(dt_i - dt^j) + rel_i^j + T_i^j + Bc_i^j + w_L c + m_{Lc,i}^j + \epsilon_{Lc,i}^j$$

These combinations do not have a K_i^j term, as the instrumental delays (TGD) of P_1 and P_2 are designed to be cancelled in these combinations. Anyway, P_c could also be obtained by means of C_1 instead of P_1, and thus the TGD Term would appear again:

$$P_c' = \frac{f_1^2 C_1 - f_2^2 P_2}{f_1^2 - f_2^2}$$

Obtaining:

$$P_{ci}^{j\prime} = \rho_i^j + c(dt_i - dt^j) + rel_i^j + T_i^j + M_{Pc',i}^j + \epsilon_{Pc',i}^j + K_i^j$$

The Ionospheric free combinations are frequently used in navigation, because they allow to cancel practically all the ionospheric effect (which is difficult to model).

Narrow-lane and Wide-lane combinations

These combinations gives an observable with a wavelength of 86.2cm, four times bigger than L_1 or L_2, which makes it very valuable for cycle-slips detection (a cycle slip is when a receiver losses temporary the track of a satellite, and consequently the ambiguity of the carrier-phase measurements changes).

$$P_\delta = \frac{f_1 P_1 + f_2 P_2}{f_1 + f_2)}$$
$$L_\delta = \frac{f_1 L_1 - f_2 L_2}{f_1 - f_2)}$$

Obtaining:

$$P_{\delta i}^j = \rho_i^j + c(dt_i - dt^j) + rel_i^j + T_i^j + \alpha_\delta I_i^j + M_{P\delta,i}^j + \epsilon_{P\delta,i}^j$$
$$L_{\delta i}^j = \rho_i^j + c(dt_i - dt^j) + rel_i^j + T_i^j + \alpha_\delta I_i^j + B\delta_i^j + w_L \delta + m_{L\delta,i}^j + \epsilon_{Lc,i}^j$$

Ionospheric combinations

These combinations cancel out the geometric part of the measurement, leaving as main term the ionospheric effect. It is mainly used in cycle-slip detection as well as for ionospheric determination.

$$P_I = P_2 - P_1$$
$$L_I = L_1 - L_2$$

Obtaining:

$$P_{Ii}^j = \alpha_I I_i^j + K_{Ii}^j + M_{PI,i}^j + \epsilon_{PI,i}^j$$
$$L_{Ii}^j = \alpha_I I_i^j + B\delta_i^j - B2_i^j + m_{LI,i}^j + w_L I + \epsilon_{LI,i}^j$$

GRAPHIC combination

These combinations use the fact that the ionospheric term affects carrier-phase measurements with the opposite sign than pseudorange ones. This

allows a cancellation of this term by doing a mean of both measurements. In this sense:

$$G_{C_1} = \frac{C_1 + L_1}{2}$$
$$G_{P_1} = \frac{P_1 + L_1}{2}$$
$$G_{P_2} = \frac{P_2 + L_2}{2}$$

Where C_1 is the Coarse/Acquisition code.

Navigation equations

In order to determine the receiver position and clock error (regarding to GPS system) the navigation equations must be solved, requiring at least four satellites.

Least Mean Squares

If we dispose of dual-frequency receivers, taking only pseudorange measurements, we can form the P_c combination (to remove the ionosphere term), modeling all the components affecting the signal at the level of the measurement noise, thus obtaining:

$$P_{ci}^j - \rho_i^{*j} = \rho_i^j + cdt_i + \epsilon_i^j$$

Where,

- ρ_i^{*j} is all the modeled effects.

- ρ_i^j is the distance between receiver i and satellite j, $\rho = \sqrt{(x_i - x^j)^2 + (y_i - y^j)^2 + (z_i - z^j)^2}$.

- cdt_i is the receiver's clock offset multiplied by the speed of light.

- ϵ_i^j is the thermal noise, unmodeled terms and missmodeling errors.

This is a non linear system, and its resolution technique usually consists on linearizing the distance ρ_i^j in the neighborhood of a point (x_0, y_0, z_0) corresponding to a raw approximate position of the receiver. Thus it is obtained:

$$\rho_i^j = \rho_{0i}^j + \frac{x_{0i} - x^j}{\rho_{0i}^j} dx_i + \frac{y_{0i} - y^j}{\rho_{0i}^j} dy_i + \frac{z_{0i} - z^j}{\rho_{0i}^j} dz_i$$
$$dx_i = x_i - x_{0i} , \; dy_i = y_i - y_{0i} , \; dz_i = z_i - z_{0i}$$

Them P_c can be written as:

$$P_{c_i}^j - P_{c_{modelled,i}}^j = \frac{x0_i - x^j}{\rho 0_i^j} dx_i + \frac{y0_i - y^j}{\rho 0_i^j} dy_i + \frac{z0_i - z^j}{\rho 0_i^j} dz_i + cdt_i + \epsilon_i^j$$

Being, $P_{c_{modelled,i}}^j = \rho_i^{*j} + \rho 0_i^j$.

This is what is known as the prefit and the system to be solved is:

$$
\begin{bmatrix}
P_{c_i}^1 - P_{c_{modelled,i}}^1 \\
\vdots \\
P_{c_i}^n - P_{c_{modelled,i}}^n
\end{bmatrix}
=
\begin{bmatrix}
\frac{x0_i - x^1}{\rho 0_i^1} & \frac{y0_i - y^1}{\rho 0_i^1} & \frac{z0_i - z^1}{\rho 0_i^1} & 1 \\
\vdots & \vdots & \vdots & \vdots \\
\frac{x0_i - x^n}{\rho 0_i^n} & \frac{y0_i - y^n}{\rho 0_i^n} & \frac{z0_i - z^n}{\rho 0_i^n} & 1
\end{bmatrix}
\begin{bmatrix}
dx_i \\
dy_i \\
dz_i \\
cdt_i
\end{bmatrix}
$$

This is an overdimensionated system, and can be expressed as:

$$Y = AX$$

Where,

- Y is the prefits vector.

- A is known as the design matrix.

- X is the parameters vectors to estimate (dx, dy, dz and cdt).

The solution minimizing the mean square error is:

$$\widehat{X} = (A^t A)^{-1} A^t Y$$

Weighted Least Mean Squares

If W is a weight matrix for the observations vector Y in the form of:

$$
W =
\begin{bmatrix}
w_1 & 0 & \cdots & 0 \\
0 & w_2 & & 0 \\
\vdots & & \ddots & \vdots \\
0 & 0 & \cdots & w_n
\end{bmatrix},
$$

then the least mean square solution is given by:

$$\widehat{X} = (A^t W A)^{-1} A^t W Y$$

The weights w_i are usually assigned as $1/\sigma_{y1}^2$, where σ_{y1}^2 is the variance of the observations minus model noise which is typically fiven by the

observation noise assuming a proper modeling. In this case, $W = P_Y^{-1}$ and the covariance of the estimation is:

$$P_{\widehat{X}} = (A^t W A)^{-1}$$

Kalman filtering

Kalman filtering is a more complete estimation algorithm, which connects the different epochs to take full profit of the stochastic nature of the unknowns. It uses the previous estimations of the parameters to provide an enhanced estimation for the current epoch. If $\widehat{X}(n-1)$ is the obtained estimation for the (n-1)-th epoch, a prediction of the vector $X(n)$ will be done for the following epoch $\widehat{X}^-(n)$, according to the model,

$$\widehat{X}^-(n) = \phi(n-1)\widehat{X}(n-1)$$
$$P_{\widehat{X}(n)}^- = \phi(n-1)P_{\widehat{X}(n-1)}\phi(n-1)^T + Q(n-1)$$

Where,

- ϕ is the transition matrix, which defines how the parameters are propagated each epoch.

- Q is the noise matrix, which defines how accurate is the propagation model.

With these new predictions $\widehat{X}^-(n)$, it is possible to extend the observation equations:

$$\begin{bmatrix} Y(n) \\ \widehat{X}^-(n) \end{bmatrix} = \begin{bmatrix} A(n) \\ I \end{bmatrix} X(n) \; ; \; W = \begin{bmatrix} P_{Y(n)} & 0 \\ 0 & P_{\widehat{X}(n)}^- \end{bmatrix}^{-1}$$

The proper determination of ϕ and Q allows to improve the estimations. For instance, we can consider:

- *Static positioning:* This is to determine the position of fixed stations, where the vector (x, y, z) of the receiver is kept constant along the time. In this particular case we have only process noise for the receiver clock offset (σ_{dt}^2) which should be higher than 1 ms per epoch:

$$\phi(n) = \begin{bmatrix} 1 & 0 & 0 & 0 \\ 0 & 1 & 0 & 0 \\ 0 & 0 & 1 & 0 \\ 0 & 0 & 0 & 0 \end{bmatrix} \; ; \; Q(n) = \begin{bmatrix} 0 & 0 & 0 & 0 \\ 0 & 0 & 0 & 0 \\ 0 & 0 & 0 & 0 \\ 0 & 0 & 0 & \sigma_{dt}^2 \end{bmatrix}$$

- *Kinematic positioning:* The receiver is moving, so its position is modeled as the clock:

$$\phi(n) = \begin{bmatrix} 0 & 0 & 0 & 0 \\ 0 & 0 & 0 & 0 \\ 0 & 0 & 0 & 0 \\ 0 & 0 & 0 & 0 \end{bmatrix} \; ; \; Q(n) = \begin{bmatrix} \sigma_{dx}^2 & 0 & 0 & 0 \\ 0 & \sigma_{dy}^2 & 0 & 0 \\ 0 & 0 & \sigma_{dz}^2 & 0 \\ 0 & 0 & 0 & \sigma_{dt}^2 \end{bmatrix}$$

These ϕ and Q correspond to a pure kinematic positioning, in which position is treated as a random walk (typically white noise when a large process noise is considered).

Appendix B

Neural networks fundamentals
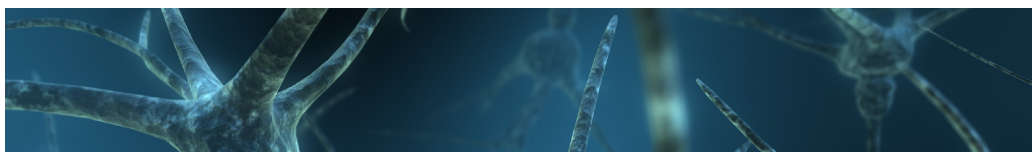
As long as we do science,
some things will always remain unexplained
Fritjof Capra

This appendix describes very briefly the fundamentals of neural networks. More information on this issue can be found for instance in [Haykin, 1994].

Introduction

In its most general description, a neural network is an algorith which is designed to model (in a very crude approximation) the way in which the brain performs a particular task or function of interest. To accomplish this task it makes use of artificial neurons, which try to emulate the biological ones in a very simplified way. The artificial neurons are connected together (with weights) typically distributed in several layers.

Neural networks are particularly fault tolerant, and one of its most powerful features is its ability to learn and generalize from input data. The algorithm adapts the weights of the connections between neurons to provide an optimal output.

The artificial neuron

An artificial neuron, as shown in figure B.1, consists of some basic components:

- *Input vector:* That are all the different inputs to the neuron.

Heading image: Artistic drawing of a net of neurons.

- *Synaptic weights:* Each x_n is multiplied by its corresponding weight. These are the parameters which represent the connection intensity between neurons, making possible the learning process.

- *Summing junction:* It combines all the inputs in the following way:

  $u = \sum_{i=1}^{n} w_i x_i$

- *Activation function:* This function gives the final output y from u. The selection of the activation function is very important in neural network applications. There are different kinds of activation functions, from a linear one, to the sigmoid function (the most common). To solve nonlinear problems, the activation function should be nonlinear. The sigmoid function is defined as:

  $\psi(x) = \frac{1}{1+e^{-x}}$

- *Threshold:* This is the magnitude offset that affects the activation node output as follows (ψ is the activation function):

  $y = \psi(u - t)$

- *Output:* This is the final product of the artificial neuron.
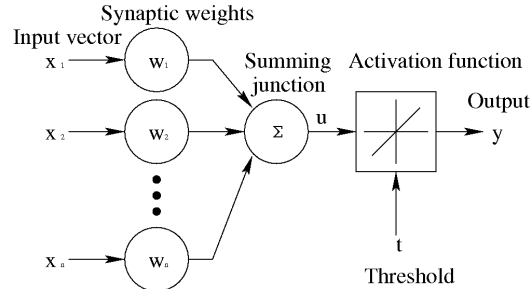

Figure B.1: *Basic elements of an artificial neuron.*

Supervised learning

The supervised learning is based on an apriori knowledge of a set of input-output patterns, thus for each input vector the values of the desired output vector are specified and the goal of the network is to minimize the error function between the output pattern and its own output. To train a network, every input vector is applied to the network and the outputs are calculated and compared with the target output vector with the error obtained back-propagated through the network to adapt the weights and minimize the error.

Single layer perceptron

The single layer perceptron (SLP) is the simplest form of a neural network used for the classification of a special type of patterns said to be linearly separable (patterns that lie on opposite sides of a hyperplane of the input space), it consists of a set of neurons (as shown in figure B.1) with adjustable weights and thresholds.

Multi-layer perceptron

The multi-layer perceptron (MLP) is a supervised learning form of multi-layered networks. The MLP is a network of connected neurons distributed in layers with no connections between neurons of the same layer (see figure B.2). Each layer can be processed in a computing step.
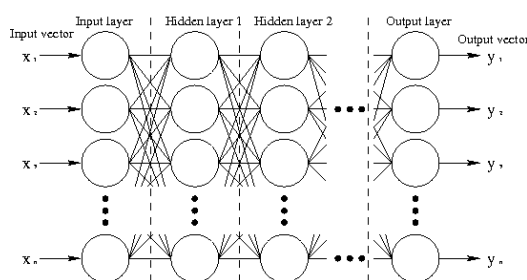

Figure B.2: *Typical multi-layered neural network.*

The components of the network consists on:

- *Input vector:* Input values given to the network.

- *Input layer:* A layer of neurons that receives the input vectors and passes this information to the network for processing.

- *Hidden layer:* A hidden layer of neurons that receives the information from the previous layer and computes it forwarding the output to an additional layer.

- *Output layer:* The last layer receives the processed information and outputs it.

- *Output vector:* Output values given by the network.

An MLP can solve much more complex problems than the single layer perceptron, such as non-linear ones. The hidden layers, which are not part

of the input or output of the network, enable it to learn complex tasks by extracting progressively more meaningful features from the input patterns. It has been demonstrated in [Funahashi, 1989] that an MLP with one single hidden layer is enough to allow any generalization.

The back-propagation (weight updating by means of a backward pass through all the filter) is done after the input pattern has been processed and the output obtained. To perform the back-propagation algorithm it is important that the activation function has derivative function, as the weight updating follows the gradient of the error (non-derivable functions can also be used, but the gradient needs to be estimated in a brute-force method, by a recursive application of small increments to weights). For this reason the nonlinear function known as sigmoid is normally used.

The step-by-step training process of a neural network is:

- Select of a training input/output pair from the training set, applying the input vectors to the network input.

- Calculate network output using a forward pass, applying all weights and activation functions.

- Compute the difference between network output and the desired target value from the training pair output value.

- Update network weights to minimize the error (back-propagation).

Unsupervised learning

The unsupervised learning does not have an apriori output knowledge, and the own network learns to self-organize itself from its own classifications to produce required outputs without external help. To do this, it is assumed that the input vectors share some common features, and that the network is able to identify these features across the range of input patterns.

There are two different kinds of unsupervised neural networks:

- *Unsupervised competitive network:* This networks are based on competitive learning, in which all neurons compete amongst themselves in order to be activated, with the result that only one is activated at any one time. This winning neuron inhibits the rest of the output neurons and its own weights are strengthened. The result is that the neurons

are forced to organize themselves. For obvious reasons, such a network is called a *Self Organizing Map (SOM)*.

- *Unsupervised hebbian network:* This network can have several output neurons activated at once and the weight updating is based on the Hebb learning rule [1].

The Kohonen network

One kind of SOM is the widely known Kohonen network. This SOM has a feed-forward structure with a single computational layer arranged in rows and columns (with two indices). Each neuron is fully connected to all the source nodes in the input layer, as seen in figure B.3.
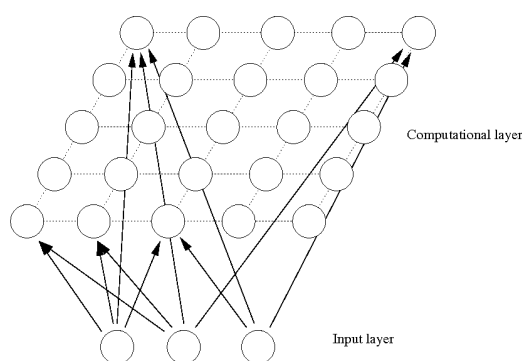

Figure B.3: *Kohonen network scheme. All neurons of input layer are connected with all neurons of computational layer.*

The Kohonen network involves four steps:

- *Initialization:* All connection weights are initialized with small random values.

- *Competition:* For each input pattern, all neurons compete themselves by computing the distance between the input vector and its correspondent weights. The one with less distance is declared as "winner".

- *Cooperation:* The wining neuron determines the spatial location of a topological neighborhood of excited neurons.

---

[1]The Hebb learning rule modifies the weights proportional to the product of the input j by the output i of the neuron multiplied by a factor ϵ (known as learning rate): $\triangle w_{ij} = \epsilon y_i x_i$

- *Adaptation:* The excited neurons modify their individual weight values in relation to the input pattern, to make them more similar. The scale factor of weights modification is proportional to the distance to the winning neuron.

This process makes the output space to follow the patterns of the input space, creating also a topological ordering, where close neurons (in the matrix computational layer arrangement of rows and cells) have similar weights (are close in the input space).

Appendix C

Main characteristics of the LEO satellites used
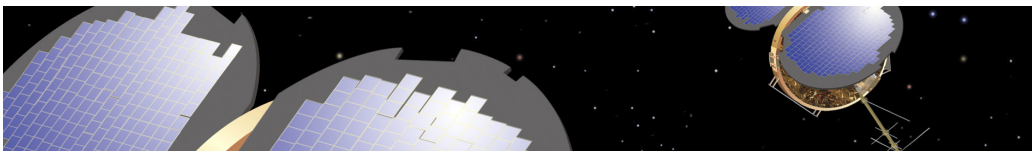
Heavier-than-air flying machines are impossible
Lord Kelvin, 1892

This appendix provides general information on the different Low Earth Orbit satellites used in the thesis and some technical data about them. More information on the satellites can be found on these web pages:

- **CHAMP**: http://www-app2.gfz-potsdam.de/pb1/op/champ/

- **GRACE**: http://op.gfz-potsdam.de/grace/index_GRACE.html

- **SAC-C**: http://www.conae.gov.ar/sac-c/

- **JASON**: http://topex-www.jpl.nasa.gov/mission/jason-1.html

---

Heading image: Artistic image of the FORMOSAT-3/COSMIC constellation.
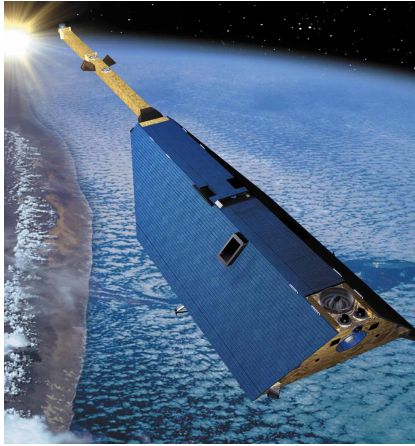
CHAMP SATELLITE

|	
Nominal altitude:	350 km
Mass:	400 kg
Launch date:	July 15th, 2000
Space Agency:	GFZ
Designed life-time:	5 years
Receiver pseudorange noise:	60 cm
Receiver carrier-phase noise:	7 mm
Receiver GRAPHIC noise:	9 cm
Typical empirical accelerations	
Radial:	0.8 nm/s^2
Along-track:	45 nm/s^2
Cross-track:	40 nm/s^2
Antenna phase center:	(-1.488,0.0,-0.393)m

Payload: Magnetometer, accelerometer, Star sensor, GPS receiver, Laser retro reflector and Ion drift meter

The CHAllenging Mini-Satellite Payload (CHAMP) is a German small satellite mission for geoscientific and atmospheric research and applications, managed by GFZ. The main objectives of the mission are generation of highly precise gravity and magnetic field measurements over a five years period. This will allow to detect besides the spatial variations of both fields also their variability with time.

GRACE SATELLITES (A & B)

Nominal altitude:	460 km
Mass:	432 kg
Launch date:	May 17th, 2002
Space Agency:	NASA/GFZ
Designed life-time:	5 years
Receiver pseudorange noise:	40 cm
Receiver carrier-phase noise:	8 mm
Receiver GRAPHIC noise:	12 cm
Typical empirical accelerations	
Radial:	0.3 nm/s^2
Along-track:	12 nm/s^2
Cross-track:	8 nm/s^2
Antenna phase center:	(0.0,0.0,-0.414)m

Payload: K-Band ranging system, accelerometer, Star sensor, GPS receiver, Laser retro reflector, CESS, Ultra Stable Oscillator and Center of Mass Trim Assemly
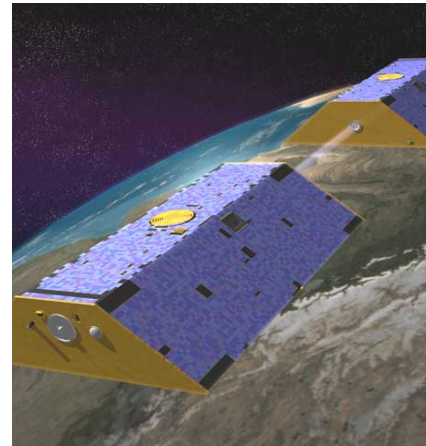
The GRACE mission is a joint project between the National Aeronautics and Space Administration (NASA) and the Deutsches Zentrum für Luft- und Raumfahrt (DLR). The primary mission of GRACE mission is to provide high accurate estimates of the global high-resolution models of the Earth's gravity field for a period of up to five years. The secondary science mission of the mission is to provide several hundreds of daily Radio Occultation (RO) measures providing vertical information of the ionosphere.

SAC-C SATELLITE

Nominal altitude:	700 km
Mass:	475 kg
Launch date:	November 21th, 2000
Space Agency:	NASA/CONAE
Designed life-time:	4 years
Receiver pseudorange noise:	150 cm
Receiver carrier-phase noise:	17 mm
Receiver GRAPHIC noise:	18 cm
Typical empirical accelerations	
Radial:	0.0 nm/s^2
Along-track:	3 nm/s^2
Cross-track:	14 nm/s^2
Antenna phase center:	(-0.345,-0.0294,-0.811)m

Payload: Scalar Helium Magnetometer, Mulitspectral Medium Resolution Scanner, Star sensor, GPS receiver, High Resolution Technological Camera and HCS

SAC-C (Satélite de Aplicaciones Científicas) is an international cooperative mission between NASA, the Argentine Commission on Space Activities (CONAE), Brazil and some european partners (Italy, Denmark and France). Its mission is to provide multispectral imaging of terrestrial and coastal environments. The spacecraft will study the structure and dynamics of the Earth's atmosphere, ionosphere and geomagnetic field. SAC-C will seek to measure the space radiation in the environment and its influence on advanced electronic components. The satellite will determine the migration route of the Franca whale and verify autonomous methods of attitude and orbit determination.

JASON SATELLITE

Nominal altitude:	1350 km
Mass:	500 kg
Launch date:	December 7th, 2001
Space Agency:	NASA/CNES
Designed life-time:	5 years
Receiver pseudorange noise:	80 cm
Receiver carrier-phase noise:	10 mm
Receiver GRAPHIC noise:	8 cm
Typical empirical accelerations	
Radial:	0.1 nm/s^2
Along-track:	1 nm/s^2
Cross-track:	6 nm/s^2
Antenna phase center:	(1.434,-0.218,-0.504)m

Payload: Altimeter, microwave radiometer, GPS receiver and Laser retro reflector array

Developed jointly by CNES and NASA, JASON-1 is the follow-on of Topex-Poseidon. JASON-1 is a mini-satellite, based on the Proteus multimission spacecraft bus. All its instruments derive from Topex/Poseidon but limiting their weight and their consumption of energy. Its unchanged orbit, compared to that of Topex/Poseidon allows a continuous acquisition of measurements and thus, further our understanding of many ocean phenomena on the long term. The follow-on of this satellite, JASON-2, was launched the 20th of June of 2008.

Bibliography

[Bar-Sever et al., 2002] Bar-Sever, Y., Muellerschoen, R., Reichert, A., Vozoff, M. and Young, L., The development and demonstration of NASA's Global Differential System. ESTEC 2002, Pasadena, USA, 2002.

[Bar-Sever et al., 2004] Bar-Sever, Y., Young, L., Stocklin, F. and Rush, J., NASA's Global Differential GPS System and the TDRSS Augmentation Service for Satellites. NAVITEC 2004, Noordwijk, The Netherlands, 2004.

[Brown, 1994] Brown, R., GPS RAIM: Calculation of thresholds and protection radius using Chi-square methods - A geometric approach. RTCA 491-94/SC159-584, 1994.

[Case et al., 2004] Case, K., Kruizinga, G. and Wu, S., GRACE Level 1B Data Product User Handbook. Jet Propulsion Laboratory, 2004.

[CNES, 2006] CNES, OSTM/Jason-2 science and operations requirements. Centre National d'Études Spatiales, TP3-J0-SP-188-CNES, 2006.

[Drinkwater and Rebhan, 2007] Drinkwater, M. and Rebhan, H., Sentinel-3: Mission requirements document. European Space Agency, EOP-SMO/1151/MD-md, 2007.

[Ebinuma et al., 2003] Ebinuma, T., Bishop, R. and Lightsey, E., Integrated hardware investigations of precision spacecraft rendezvous using the Global Positioning System. Journal of Guidance, Control and Dynamics 26(3), pp. 425–433, 2003.

[Edward, 2003] Edward, G., Integrated GPS/INS navigation system design for autonomous spacecraft rendezvous. PhD thesis, 2003.

[Funahashi, 1989] Funahashi, K., On the approximate realization of continuous mappings by neural networks. Neural Networks 2, pp. 183–192, 1989.

[Gaylor et al., 2003] Gaylor, D., Lightsey, E. and Key, K., Effects of multipath and signal blockage on GPS navigation in the vicinity of the

International Space Station (ISS). ION GNSS 2003, Portland, USA, 2003.

[Gill et al., 2001] Gill, E., Montenbruck, O. and Kayal, H., The BIRD satellite mission as a milestone toward GPS-based autonomous navigation. Journal of Navigation 48(2), pp. 69–76, 2001.

[Gill et al., 2004] Gill, E., Montenbruck, O., Arichandran, K., Tan, H. and Bretschneider, T., High-precision onboard orbit determination for small satellites - The GPS-based XNS on X-SAT. 6th Symposium on Small Satellites Systems and Services, La Rochelle, France, 2004.

[Gomez, 2002] Gomez, S., Flying High: GPS on the International Space Station and Crew Return Vehicle. GPS World 13(6), pp. 12–16, 2002.

[Haines et al., 2004] Haines, B., Bar-Sever, Y., Bertiger, W., Desai, S. and Willis, P., One-centimeter orbit determination for Jason-1: New GPS-Based strategies. Marine Geodesy 27, pp. 299–318, 2004.

[Harris and Priester, 1962] Harris, I. and Priester, W., Time-dependent structure of the upper atmosphere. Goddard Space Flight Center, NASA TN D-1443, 1962.

[Hatch, 1982] Hatch, R., Synergism of GPS code and carrier measurements. Proceedings of the Thirs Internations GEodetic Symposium of Satellite Doppler Positioning, New Mexico, USA, 1982.

[Haykin, 1994] Haykin, S., Neural Networks, a comprehensive foundation. Macmillan College, 1994.

[Hernandez-Pajares et al., 1997] Hernandez-Pajares, M., Juan, J. and Sanz, J., Neural network modeling of the ionospheric electron content at global scale using GPS data. Radio Science 32(3), pp. 1081–1089, 1997.

[Hernandez-Pajares et al., 1999] Hernandez-Pajares, M., Juan, J. and Sanz, J., GPS code multipath detection and mitigation with the carrier phase in a LEO scenario: assessment of Neural Network detection algorithms, Final report. ADM-HT/SMP/SB/8.3/252, 1999.

[Hernandez-Pajares et al., 2000a] Hernandez-Pajares, M., Juan, J. and Sanz, J., GPS code multipath detection and mitigation in a LEO scenario using neural networks. ESA WPP, ISSN 1022-6656 173, pp. 594–622, 2000a.

[Hernandez-Pajares et al., 2001] Hernandez-Pajares, M., Juan, J. and Sanz, J., GPS data processing: code and phase. gAGE/UPC, Barcelona, Spain, 2001.

[Hernandez-Pajares et al., 2007a] Hernandez-Pajares, M., Juan, J. and Sanz, J., 3D ionospheric VTEC and STEC reference datasets (N. P173003), Final ESA Report. ESTEC, 2007a.

[Hernandez-Pajares et al., 2000b] Hernandez-Pajares, M., Juan, J., Sanz, J. and Colombo, O., Application of ionospheric tomography to real-time GPS carrier-phase amiguities resolution, at scales of 400-1000 km and with high geomagnetic activity. Geophysical Research Letters 27(13), pp. 2009–2012, 2000b.

[Hernandez-Pajares et al., 2002] Hernandez-Pajares, M., Juan, J., Sanz, J. and Colombo, O., Improving the real-time ionospheric determination from GPS sites at very long distances over the equator. Journal of Geophysical Research 107(A10), pp. 1296–1305, 2002.

[Hernandez-Pajares et al., 2007b] Hernandez-Pajares, M., Juan, J., Sanz, J. and Orus, R., Second-order ionospheric term in GPS: Implementation and impact of geodetic estimates. Journal of Geophysical Research 112(B08417), pp. doi:10.1029/2006JB004707, 2007b.

[Hernandez-Pajares et al., 2004] Hernandez-Pajares, M., Juan, J., Sanz, J., Orus, R., Garcia-Rodriguez, A. and Colombo, O., Wide Area Real Time Kinematics with Galileo and GPS signals. Proceedings of the Institute of Navigation, Long Beach, California, 2004.

[Infriyatmoko et al., 2008] Infriyatmoko, A., Kang, T., Jae, Y., Jee, G., Beom, Y. and Kim, J., Artificial neural networks for predicting DGPS carrier phase and pseudorange correction. GPS Solutions (DOI 10.1007/s10291-008-0088-x), 2008.

[Jacchia, 1971] Jacchia, L., Revised static models of the thermosphere and exosphere with empirical temperature profiles. SAO Special Report 332, Cambridge, 1971.

[Kohonen, 1990] Kohonen, T., The self-organizing map. Vol. 78, IEEE, pp. 1464–1480, 1990.

[Kroes, 2005] Kroes, R., Precise relative positioning of formation flying spacecraft using GPS. PhD thesis, 2005.

[Leung and Montenbruck, 2005] Leung, S. and Montenbruck, O., Real-time navigation of formation-flying spacecraft using Global-Positioning-System measurements. Journal of Guidance, Control and Dynamics 28(2), pp. 226–235, 2005.

[Malys et al., 1997] Malys, S., Larezos, M., Gottschalk, S., Mobbs, S., Winn, B., Feess, W., Menn, M., Swift, E., Merrigan, M. and Mathon, W., The GPS accuracy improvement initiative. ION GNSS 1997, Kansas City, USA, pp. 375–384, 1997.

[Manno, 1999] Manno, I., Introduction to the Monte Carlo method. Akademiai Kiado, Budapest, Hungary, 1999.

[McCarthy and Petit, 2004] McCarthy, D. and Petit, G., IERS Conventions 2003. Verl. des Bundesamtes fur Kartogr. und Geod., Frankfurt am Main, Germany, IERS Technical Note 32, 2004.

[Metropolis and Ulam, 1949] Metropolis, N. and Ulam, S., The Monte Carlo method. Journal of the American Statistical Association 44(247), pp. 335–341, 1949.

[Mireault et al., 1999] Mireault, Y., Kouba, J. and Ray, J., IGS Earth Rotation Parameters. GPS Solutions 3(1), pp. 59–72, 1999.

[Montenbruck and Gill, 2000] Montenbruck, O. and Gill, E., Satellite Orbits. Springer, 2000.

[Montenbruck and Kroes, 2003] Montenbruck, O. and Kroes, R., In-flight performance analysis of the CHAMP BlackJack GPS receiver. GPS Solutions 7(2), pp. 74–86, 2003.

[Montenbruck and Leung, 2002] Montenbruck, O. and Leung, S., GPS Operations on the PCsat Microsatellite. ION GNSS 2002, Portland, USA, 2002.

[Montenbruck and Ramos-Bosch, 2007] Montenbruck, O. and Ramos-Bosch, P., Precision real-time navigation of LEO satellite using Global Positioning System measures. GPS Solutions (DOI 10.1007/s10291-007-0080-x), 2007.

[Montenbruck et al., 2006] Montenbruck, O., Garcia-Fernandez, M. and Williams, J., Performance comparison of semicodeless GPS receivers for LEO satellites. GPS Solutions 10, pp. 249–261, 2006.

[Montenbruck et al., 2007] Montenbruck, O., Markgraf, M., Garcia-Fernandez, M. and Helm, A., GPS for microsatellites - Status and perspectives. 6th IAA Symposium on Small Satellites for Earth Observation, Berlin, Germany, 2007.

[Montenbruck et al., 2005] Montenbruck, O., van Helleputte, I., Kroes, R. and Gill, E., Reduced dynamic orbit determination using GPS code and carrier measurements. Aerospace Science and Technology 9(3), pp. 261–271, 2005.

[Muellerschoen et al., 2001] Muellerschoen, R., Reichert, A., Kuang, D., Heflin, M., Bertiger, W. and Bar-Sever, Y., Orbit determination with NASA's high accuracy real-time Global Differential GPS System. ION GNSS 2001, Salt Lake City, USA, 2001.

[NASA/JPL, 2008] NASA/JPL, The NASA Global Differential GPS System. http://www.gdgps.net/ Accessed July 17, 2008.

[Parkinson, 1996a] Parkinson, B. W., Global Positioning System: Theory and Applications. American Institute of Aeronautics and Astronautics, 1996a.

[Parkinson, 1996b] Parkinson, B. W., Global Positioning System: Theory and Applications. Vol. 1, American Institute of Aeronautics and Astronautics, chapter 14, Multipath Effects, pp. 547–568, 1996b.

[Ramos-Bosch, 2006] Ramos-Bosch, P., Real time GPS positioning of LEO satellites mitigating pseudorange multipath through neural networks. ION GNSS 2006, Student Fellowship and Best Paper Award, Fort Worth, USA, 2006.

[Ramos-Bosch et al., 2007a] Ramos-Bosch, P., Hernandez-Pajares, M., Juan, J. and Sanz, J., Mitigacion de multipath de codigo mediante redes neuronales. Mapping Interactivo (119), pp. 10–13, 2007a.

[Ramos-Bosch et al., 2007b] Ramos-Bosch, P., Hernandez-Pajares, M., Juan, J. and Sanz, J., Real time GPS positioning of LEO satellites mitigating pseudorange multipath through neural networks. Journal of the Institute of Navigation 54(4), pp. 309–315, 2007b.

[Ramos-Bosch et al., 2008] Ramos-Bosch, P., Hernandez-Pajares, M., Juan, J., Sanz, J. and Aragon-Angel, A., Autonomous LEO navigation with single-frequency GPS receivers: Application of multipath mitigation techniques. EGU General Assembly, Vienna, Austria, 2008.

[Reichert and Axelrad, 2001] Reichert, A. and Axelrad, P., Carrier-phase multipath corrections for GPS-based satellite attitude determination. Journal of the Institute of Navigation 48(2), pp. 77–88, 2001.

[Reichert et al., 2002] Reichert, A., Meehan, T. and Munson, T., Toward decimeter-level real-time orbit determination: A demonstration using the SAC-C and CHAMP spacecrafts. ION GNSS 2002, Portland, USA, 2002.

[Rizos and Stolz, 1985] Rizos, C. and Stolz, A., Force modelling for GPS satellite orbits. Vol. 1, 1st International symposium precise positioning with GPS, Rochville, USA, pp. 87–98, 1985.

[RTCA, 2001] RTCA, Minimum Operational Performance Standards for Global Positioning System / Wide Area Augmentation System Airborne Equipment. RTCA Inc., 2001.

[Tapley et al., 2004] Tapley, B., Bettadpur, S., Watkins, M. and Reigber, C., The gravity recovery and climate experiment: Mission overview and early results. Geophysical Research Letters 31(9), pp. L09607, 2004.

[Tsiolkovsky, 1903] Tsiolkovsky, K., The investigation of space by means of reactive devices (in Russian). Nauchnoe Obozrenie 5(3), 1903.

[Vallado, 2001] Vallado, D., Fundamentals of astrodynamics and applications, Space Technology Library. McGraw Hill, Kluwer, Dordrecht, 2001.

[Vigneau et al., 2007a] Vigneau, W., Benghouzi, F., Nouvel, O., Manzano-Jurado, M., Carrascosa-Sanz, C., Abdulkader, H., Roviras, D., Hernandez-Pajares, M., Ramos-Bosch, P., Macabiau, C. and Holsters, P., Neural networks algorithms prototyping to mitigate GNSS multipath for LEO positioning applications. 3rd ESA Workshop on Satellite Navigation. User Equipment Technologies, Noordwijk, Netherlands, 2007a.

[Vigneau et al., 2007b] Vigneau, W., Nouvel, O., Carrascosa-Sanz, C., Manzano-Jurado, M., Roviras, D., Juan, M., Ramos-Bosch, P. and Macabiau, C., Neural networks for radionavigation, Final report. M3S/TN/Neural/FR, 2007b.

[Warren and Raquet, 2003] Warren, D. and Raquet, J., Broadcast vs. precise GPS ephemerides: a historical perspective. GPS Solutions 7(3), pp. 151–156, 2003.

[Williams et al., 2002] Williams, J., Lightsey, E., Yoon, S. and Schutz, R., Testing of the ICESat BlackJack GPS receiver engineering model. ION GNSS 2002, Portland, USA, 2002.

[Zhou and Feng, 2002] Zhou, N. and Feng, Y., Short-arc batch estimation for GPS-based onboard spacecraft orbit determination. Journal of Global Positioning Systems 1(2), pp. 106–112, 2002.